LBL-21128

Lawrence Berkeley Laboratory
UNIVERSITY OF CALIFORNIA

SEM AND X-RAY MICROANALYSIS OF CELLULAR DIFFERENTIATION IN SEA URCHIN EMBRYOS: A FROZEN HYDRATED STUDY

S.B. Klein
(Ph.D. Thesis)

December 1985

Biology & Medicine Division

Prepared for the U.S. Department of Energy under Contract DE-AC03-76SF00098

LBL--21128

DE86 009080

SEM and X-ray Microanalysis of Cellular Differentiation in Sea Urchin Embryos: A Frozen Hydrated Study

Susan Beth Klein

Donner Laboratory, Lawrence Berkeley Laboratory, University of California, Berkeley, CA 94720

Acknowledgements

Supported by the Director, Office of Energy Research, Office of Health and Environmental Research of the U.S. Department of Energy, under Contract DE-AC03-76SF00098 and by National Institutes of Health 5T32 GM07379.

SEM and X-ray Microanalysis of Cellular Differentiation in Sea Urchin Embryos: A Frozen Hydrated Study

by

Susan Beth Klein

SEM and X-ray Microanalysis of Cellular Differentiation in Sea Urchin Embryos -- A Frozen Hydrated Study

Susan Beth Klein

Abstract

Quantitative studies of major chemical element distribution amoung individual differentiating cells were attempted using a new method of scanning electron microscope (SEM) specimen state and calibration standards. Frozen hydrated embryos of the sea urchin Strongelocentrotus purpuratus were examined with an SEM equipped with a low temperature stage and characteristic x-ray analytic capability. Three stages: blastula, mesenchyme blastula, and early gastrula were examined. The morphology of these embryos closely resembled dehydrated embryos with two notable exceptions. First the blastocoel matrix contained large beads of approximately 1 μm diameter. Second, the cells of the archenteron lacked well defined cell boundaries. Characteristic levels of beam damage and charging provided structural information. The primary mesenchyme cells within the blastocoel were particularly susceptible to both effects. Damaging effects were noted in material stored in liquid nitrogen longer than three months. Ice crystal growth, shrinkage, elemental shift, density changes and charge accumulation may take place in these stored specimens. In addition to secondary electron imaginng, x-ray microanalysis was

performed upon fully hydrated, frozen, fractured embryos at all three stages to test for elemental shifts associated with development. Elongating cells of the blastula (the vegetal pole and oral plate) presented similar elemental content, as did the mesenchyme blastula ectoderm, and the thin, equatorial cells of the early gastrula. As suggested in previous experiments, sulfur was implicated in the ingression and migration of the primary mesenchyme, as well as the elongation of the oral plate and vegetal pole. The high Ca and K readings from the cells surrounding the archenteron pore suggested that they may be responsible for primary invagination. Conversion of the x-ray peak to background (P/B) ratios to concentration have been considered, as well as the variation in P/B ratios between individual cells and organisms. The applicability of non-coated, conducting calibration standards for reference in conversion of P/B ratios to elemental concentration is discussed.

TABLE OF CONTENTS

Acknowledgements

The completion of this project and the writing of this thesis were accomplished to a large degree because of the assistance of a number of wonderful people. Tom Hayes, Patrick Echlin, and Greg Finch provided scientific guidance and support without which this work would not have been completed. Fred Wilt generously gave of his time, advice and laboratory space. Marylin Nichols, Dulcinea Wilson and Dorothy Sprague assisted with secretarial labors above and beyond the call of duty. May McKoon is remembered for her diligent and loving tutelage. My family, Stan, Calla and Joanne Klein, all supported and encouraged me in their own manner. Most of all, I wish to acknowledge the love and patience of James A. Musser.

Introduction

Differentiation and Cellular Communication

The development of a complex organism from a single cell requires temporal and spatial regulation which produces predictable, coordinated cellular behavior. Intercellular coordination involves several components amoung which are regulation of the extracellular matrix (ECM) and ion transfer. For example, Grinnell (1978) noted in his review on cell adhesion that fibroblasts spread onto a substratum in serum free medium from the point of contact (an adsorptive spreading), whereas cells supplied with serum formed protrusions which developed contact origins (separate foci from which contact spread). This "active spreading" occurred on particular matrices, containing collagen, glycoprotein binding moeties (Kleinman et al., 1981), and specific glycosaminoglycans (GAGs) (Hay, 1981, Kujawa and Tepperman, 1983). GAGs, in the form of hydrated proteoglycans, occupy as much as half of the ECM volume and have various carbohydrate compositions, degrees of sulfation, types of linkage, and lengths (Hascall and Hascall, 1981). In general, migrating embryonic cells move through an environment rich in hyaluronic acid (HA) (Toole, 1981). Sulfated GAGs, such as chondroitin sulfate (CS) and heparan sulfate (HS), may also mediate adhesion of cells to the ECM (Laterra et al., 1983, and Kujawa and Tepperman, 1983, Fibbi et al., 1983). However, changes in adhesion (for example,

Becker 1975, and Grinnell, 1978), are not necessarily a reflection of cellular differentiation. Fibronectin added to a transformed culture causes cells to flatten but when the fibronectin is removed, they return to an rounded morphology. No new extracellular products can be identified as a result of adding fibronectin to the culture medium. Nonetheless, a number of experiments establish that certain cells placed on particular matrices respond by altering their cell surface and extracellular biochemistry (Teng et al., 1977). For example, chick limb bud chondrocytes cultured in a hyaluronate rich matrix supress chondroitin sulfate synthesis (Solursh et al., 1980). Nathanson (1983) reported that hyaluronate prevented the dedifferentiation of skeletal muscle into chondrocytes. Morishita et al. (1983) noted that several GAGs (heparin, chondroitin sulfate A, B, and C, dextran sulfate, and hyaluronate) block stimulation of a polyamine responsive protein kinase in Morris hepatoma cells. Bissell et al. (1983) demonstrated the effects of ECM on cytoskeleton, polarity and morphogenesis.

Ion transfer is a second component of intercellular coordination. Revel et al. (1973), identified gap junctions in the early chick embryo, indicating intercellular ion transfer in developing systems. Extracellular calcium has been implicated in initiating cyclic nucleotide cascades (Kurth et al., 1981, etc.), neuromuscular synapse function

(Altura and Altura, 1981), and the formation of the hyalin membrane in sea urchin eggs (Steinhardt et al., 1977, McCarthy and Spiegel, 1983). Intracellular calcium regulation of motility, contractility, endo- and exocytosis, organelle translocation, and mitochondrial function has been well documented (for review see Cheung, 1980). Furukawa and Bhavanandan (1983) found that exogenous GAG's can enter cell nuclei and affect DNA synthesis. Because diffusible substances and the ECM are important to cellular differentiation and embryonic morphogenesis, this investigation is specifically designed to examine a developing system, in situ, with minimal artifacts in elemental chemistry or morphology.

The Biological Material

The sea urchin embryo system offers a number of advantages for this experiment. The embryos are readily available, are hardy, develop externally, and mitosis is relatively synchronous. Figure 1 schematically depicts the morphogenesis of the sea urchin embryo from fertilized egg to late gastrula. At the fourth division, asymmetrical mitosis produces four micromeres (solid black) and four macromeres (striped). The cells then begin dividing asynchronously (Grinnell, 1978), but after two more complete rounds of division, a blastocoel begins to form. At the end of ten divisions, the blastula is complete. Tight junctions bind the epithelial cells at their apices; a basal lamina anchors

the basal tips. The progeny of the micromeres, macromeres and mesomeres are represented by the established coding in the early blastula of figure 1. As the blastula matures and hatches from its fertiliztion membrane, the progeny of the macromeres elongate and the lower mesomeres, labeled "animal II," become noticably thinner. At a slightly later time the upper mesomeres, labeled "animal I," elongate to form the oral plate with which the archenteron tip will later fuse. The progeny of the micromeres then begin pulsatile behavior (Gibbins, et al., 1969). These presumptive primary mesenchyme (PM) cells pass through the basal lamina and pile up at the vegetal end of the blastocoel. The rounded PM cells elaborate various forms of pseudopodia (Gufstafson and Wolpert, 1967) and begin actively to translocate around the inside of the blastocoel. As the archenteron rises, the PM cells gather at three rather precise locations at the edge of the invagination, forming a ring. Their filopodia entwine, form syncitial cables, and lay down the larval skeleton (Inoue and Okazaki, 1977). Secondary mesenchyme cells at the tip of the archenteron extend filopodia, reach toward the oral plate (and in fact often detach from the tip of the archenteron), attach themselves to the oral plate and appear to pull the two structures together. The remainder of the development to pluteus is accompanied by the growth of the skeleton.

The intra- and extracellular sulfur content of sea urchin embryos is critical to the differentiation of the

blastula. In 1972, Sugiyama investigated the location of sulfur in sea urchin embryos by light microscopy, using both ^{35}S label and various sulfur sensitive stains. He found that the presumptive PM cells and rim cells of the blastula incorporated sulfur into compounds secreted into their intercellular spaces. Karp and Solursh (1974) detected the uptake of sulfur using radioactive $^{35}SO_4$, and found that sulfur is taken up from the two to four cell stage onward, but that it is not incorporated into GAG until hatching. During the transition to mesenchyme blastula they found the incorporation of SO_4 into proteoglycan increases 13 fold. Akasaka and Terayama (1984) reported that a sulfated fucan could cause dissociated embryonic cells to reaggregate. Karp and Solursh also determined, by Hale's reaction, that the presumptive PM cells were coated with sulfated GAGs, as were the PM cells after extrusion. Kinoshita and Saiga (1979) focused on the effects of GAG within the nucleus, treating sea urchin embryos with aryl-xylosides, sodium-selenate, and deoxy-D-glucose to block the covalent linkage of SO_4 to the GAGs at various stages. The addition of 2 to 5 mM xylosides, which supplied excess free sugars for completion of GAG chains and thereby blocked the attachment of such chains to the appropriate protein, was found to prevent the translocation of PM cells to the proper location around the archenteron. More severe doses prevented migration of the PM cells Sodium-selenate, which prevents the sulfation of GAGs, allowed erratic movement of the PM within the blas-

tocoel, but development beyond the mesenchyme blastula stage was prevented. Deoxy-D-glucose, which may block polysaccharide chain elongation, but also has an unfortunate number of other effects seriously impared embryonic development prior to mesenchyme extrusion. Kinoshita and Yoshii (1979) further investigated embryos treated as above by adding back exogenous proteoglycan. In this case the embryo advanced to the stage from which the donor proteoglycan was removed, implying that the proteoglycan is stage specific. Akasaka et al. (1980) studied the effects of sulfate free sea water, β-D-xylosides and Tunicamycin on developing sea urchin embryos, with the emphasis on PM migration. They confirmed Kinoshita's and Saiga's results with respect to the PM migration PM cells will not migrate when the ECM develops in a sulfate-free medium, or when the ECM is treated with inhibitors of sulfate incorporation. Katow and Solursh (1981) cultured embryos in sulfate free sea water and verified that either the long slender processes upon which the PM cells migrate would not form, or that the attachments were so weakened the processes disappeared soon after cytoskeletal contraction. Kawabe et al. (1981) studied gastrulae and blastulae through correlative microscopy techniques and reported that the blastocoel was filled with a thick fibrillar matrix which appeared to be continuous with the basal lamina, and stained alcian blue positive in the light microscope. These results suggested that the entire blastocoel is filled with a sulfur-rich proteoglycan

network upon which the PM cells may migrate. Katow and Solursh (1979) showed that this fibrous material contained elongated chains of 30 nm particles, which were absent in sulfate deprived embryos. Furthermore fibronectin, which has been shown to be associated with heparin sulfate and chondroitin sulfate (Culp et al., 1979, Perkins et al., 1979, Yamada et al., 1980, Kleinman et al., 1981, Sekiguchi et al., 1983) has been identified in sea urchin embryos by Spiegel et al. (1980, 1983), and Iwata and Nakano (1984). Dermatan sulfate and heparin sulfate have been extracted and identified from embryos of the stages under investigation herein (Akasaka and Terayama, 1980, Katow and Solursh, 1981). The molecular configurations of the proteoglycans within the blastocoel are unknown, as are their functions, but it is apparent that sulfur is an important element for the development of the embryo.

X-ray Microanalysis

Scanning electron microscopy (SEM) x-ray microanalysis takes advantage of the transfer of energy from the electron beam to the atoms within the biological sample. This interaction produces two primary energy conversions. First, the primary electron may decelerate as it interacts with the nuclear field of an atom within the sample, producing a photon (bremstraahlung) with any energy up to the primary electron's energy. Second, the primary electron may excite the atom with which it interacts ejecting an inner shell

electron. In this case, a cascade of photons with energies precisely equal to the energy bands separating resting shells of that particular element are emitted as the remaining electrons occupy the vacated levels. These are the characteristic x rays An analysis of the energies of these x rays will disclose the elemental composition of the biological sample of interest.

Biological tissue may be prepared for frozen hydrated analysis by two methods: bulk and thin section (Roomans, 1980). Thin sections offer the advantage of a greatly reduced interaction volume and resulting higher spatial resolution so that subcellular analysis may be attempted. It is however not clear that the sections remain hydrated under the heating influence of the electron beam, even under the much improved conditions of modern equipment (Gupta and Hall, 1981 and Saubermann, et al., 1981). A more insidious problem resulting from the heating of thin sections is mass loss which results in the disappearance from the sample of up to 50% of the original concentration of the element under analysis (Glaeser and Taylor, 1977,and Hall and Gupta, 1973). Bulk analysis, the examination of tissue thick enough for the interaction volume to fall fully within the sample, suffers from reduction of analytical spatial resolution to cellular size. However, the tissue bulk provides a superior heat sink and the effects of radiation, mass loss and heating are significantly reduced (Echlin et al., 1981, Fuchs et al., 1977). Bulk tissue preparation also provides

low contamination in a reduced time (Robards and Crosby, 1979). The morphological data of frozen fractured bulk samples are more recognizable than the low contrast sections of cryoultramicrotomy. Furthermore, bulk samples retain positional relationships crucial to some analyses. For these reasons, this study will rely upon frozen-hydrated bulk tissue analysis.

The generation of and collection of x-rays are initial steps in the process of x-ray analysis. The resultant signals are amplified and sorted into appropriate energy channels of a multichannel analyser. Electronic operations introduce statistical variation in the number of charge carriers, and introduce thermal noise (Goldstein et al., 1981), which broaden the energy bands. Overlapping peaks of elements with adjacent energies must be separated. Incomplete charge collection results in non-Gaussian "tails" on the low energy side of each peak. The original spectrum also contains deviations in the form of absorption edges arising at the beryllium window to the detector, coating layer on the detector, and silicon dead layer. After the raw spectrum is computer corrected, quantification retains three inherent problems of x-ray generation. First, electrons will scatter and decelerate differently in specimens with different average atomic weight or with different homogeneities (ie. particles vs. colloidal suspensions). Second, x rays are absorbed within the specimen according to atomic weight, accelerating voltage, take off angle, and specimen-beam

interaction angle. Third, fluorescence resulting from secondary radiation requires higher characteristic energies than are found in this experiment. Either the samples and standards must be well matched or correction factors must be added. A number of methods convert the x-ray intensity to per cent weight weight, most of which fall under the general heading of ZAF (atomic weight, absorption, and fluorescence) techniques and are either the result of mathematical modeling or empirical methodology. A more useful biological technique is the "peak to background ratio (P/B)" method proposed by Statham and Pawley (1978). This method is based on the observation that although the bremsstrahlung and characteristic x rays of a particular energy are generated by different physical phenomena, and subject to different generation probabilities, for a given energy they are subject to the same detection process. The bremsstrahlung background can therefore be used as an internal normalization factor. Provided the standard and sample are in close approximation with respect to density, average atomic weight, detection geometery, and operating conditions (to minimize fluorescence and backscatter factors) the conversion to percent wet weight requires a single experimental conversion factor for each element (for an exhaustive review of all of these methods see Goldstein, et al., 1981). The most significant experimental error arises from secondary x-ray emissions whose origins are not the area under examination. The particular methods employed to correct for

extraneous emission will be discussed at length in the body of this thesis.

The following study is an attempt to correlate differentiation events of the sea urchin Strongelocentrotus purpuratus with compositional variations as reflected in changes in relative concentration detected by characteristic x-ray emission from fully frozen-hydrated tissue. Changes in concentration occur in a number of diffusible and nondiffusible molecules, both intracellularly and extracellularly. Because fixation techniques for autoradiography allow movement and loss of diffusible ions, and because these techniques require thin sectioning of the biological material, the results are subject to artifacts which may be interpreted as in vivo concentration. Bulk analyses cannot examine cell types which are not readily separated from the rest of the embryo and include intracellular and extracellular molecules. This experiment is designed to compare relative concentrations of elements within microvolumes the size of a cell. This method allows comparason of volumes in close proximity without the need for dissection or bulk analysis. This technique also reduces ion movement during processing by examining the specimens in the fully frozen hydrated, unetched and uncoated state.

Materials and Methods

Preparation of Biological Tissue

Eggs from gravid Strongelocentrotus purpuratus sea urchins were released by 0.5 M KCl introduction into millipore-filtered sea water (MPFSW) and fertilized with sperm released into a dry dish by an identical proceedure. Fertilization and normal development was verified by light microscopic examination. The zygotes were washed two or three times with MPFSW to remove debris, and cultured at 15° C in MPFSW under constant aeration. Samples were collected when embryos reached the appropriate stages as judged by light microscopy, and held at 0° C to avoid further maturation during preparation for freezing. The embryos were allowed to settle to the bottom of Falcon plastic centrifuge tubes, and the MPFSW was removed by pipette. The remaining MPFSW was drawn off with filter paper until no more than 25 µl remained. Further dehydration of the embryos risked translocation of diffusible elements and deformation damage to the embryos. A 25 µl mixture of 50% C (spectrographic grade graphite from Johnson Matthey Chemical Ltd.), 20% hydroxyethyl starch (HES, dialyzed against distilled water and freeze dried) and 30% MPFSW was rapidly added to the embryos, mixed and the solution frozen within 15 seconds.

Freezing Techniques

The suspended embryos were transferred onto a carbon

specimen stub with four cylindrical depressions. Beads of embryos in matrix, not exceeding 2 mm in diameter, were placed on the stub so that they were anchored in the depressions. The inverted stub was then pressed into solid nitrogen to try to obtain the most rapid freeze possible. The samples thus frozen were stored in a large Dewar under liquid nitrogen (LN_2) until examination in the SEM.

Examination Proceedures

Final processing of the sample occurred in a low temperature biological preparation unit (AMRay Biochamber) attached to an AMRay 1000 SEM. A full description of the capabilities of this chamber can be found in the paper by Pawley and Norton (1977). The samples were exposed to temperatures greater than -176° C only during transfer from the LN_2 to the preparation chamber cold tank (no longer than 35 seconds). This transfer occurred within a precooled transfer device, initially at LN_2 temperature. The beads were fractured under high vacuum to expose uncontaminated, randomly oriented embryo fractions. These fracture faces were neither coated nor etched, to assure a fully hydrated sample for examination. The sample was transferred into the SEM specimen chamber by use of the preparation chamber shuttle and rod under continuous high vacuum ($<10^{-5}$ torr), and secured on a Joule-Thompson cold stage, where the temperature was maintained at -190° C throughout examination.

Embryos were selected for examination according to the following morphological and physical criteria. The topography of the fracture plane was evaluated at 500X by stereo pair photography at a 20^{o} parallax. Any beads exhibiting variations in height greater than 5 µm were eliminated from further analysis. To maintain constant beam-specimen interaction and takeoff angles, only embryos located on surfaces normal to the beam at a 0^{o} stage tilt angle were analysed. Only embryos with clearly identifiable poles were analysed. Embryos without cellular tissue exposed above intercellular ice were eliminated. Since ice crystal size and damage increased with distance from the edge of the matrix bead, embryos were selected for small crystal environment.

X-ray analysis was carried out at a magnification of 2000X, and 20^{o} stage tilt angle, with a reduced raster of 5 µm on a side. Locations of sampling areas were mapped on secondary images. The emitted x rays were collected by a Si(Li) detector and processed by a Kevex 5100C energy dispersive system (EDS). Data was collected for 100 seconds live time. Electron beam acceleration voltage was held at 15 KV to produce an interaction volume no larger than 6 µm in depth. Beam current was held in the lower 1.0 namp range, to avoid charging. X-ray maps were produced at 10 KV accelerating voltage from frozen dried samples. Samples were freeze dried overnight under high vacuum on the slowly warming cold tank of the preparation chamber.

Preparation of Calibration Standards

Standards for the conversion of P/B to concentration were prepared according to the method of Whitecross et al. (1982) and Echlin et al. (1983). Slurries of $MgSO_4$, C graphite, and water distilled to a resistance greater than 18 MOhm produced standards of 0.058%, 0.115%, 0.235%, 0.35%, and 0.70% S, and 0.022%, 0.043%, 0.088%, 0.132% and 0.36% Mg. The C content was approximately 50% for all of the standards. It was found that the C provided sufficient nucleation sites that cryoprotectant was not necessary to prevent large ice crystalization. The spectrographic grade C graphite was purchased from Johnson Matthey Chemical Ltd. Analytical reagent grade $MgSO_4$ anhydrous powder was purchased from Mallinckrodt Chemical Works. The KH_2PO_4 standards were processed in a similar manner except that HES was supplied to prevent ice crystal formation prior to the discovery that this step was unnecessary. Final wet weights of these standards were 0.51%, 0.25%, and 0.127% K, and 0.40%, 0.20%, and 0.10% P. The KH_2PO_4 was also purchased from Mallinckrodt Chemical Works, and maintained the same analytical grade quality.

To assure homogeneity, the slurries were mechanically mixed immediately prior to freezing. Beads were formed on carbon stubs identical to the ones containing sea urchin samples, and the same freezing and processing proceedures were followed. Fractured faces met the same criteria of

smoothness and perpendicular orientation to the beam. The stage was tilted to 20^{o}, and the accelerating voltage was held at 15 KV. Data were collected from 20 locations on each bead of known concentration and the averages were used to calculate the correction factor for conversion of the unknown P/B ratios to concentration. The standard deviation for each concentration was less than 7% of the mean P/B ratio, verifying a homogeneous mixture.

Results

Morphology of Frozen Hydrated and Frozen Dried Tissue

Appropriately fractured C/HES matrix beads exhibited numerous randomly oriented embryos fractured at various depths within the blastocoels. Figure 2 shows a portion of such a bead, fully frozen hydrated (a) and freeze dried (b). Arrow #1 points to an embryo which was analysed for elemental content. By comparing the hydrated and dried images, it is possible to verify structures in the frozen hydrated embryos. Size differences reflect depth of the fracture plane. A small diameter in the frozen hydrated embryo results from a fracture plane falling either short of or past the center of the embryo. In the first case, a small ring of cells surround the blastocoel matrix. An example of this fracture plane is seen at the tip of arrow #2. Fracture planes falling below the center of the embryo will not contain sufficient matrix material to cover the far interior of the blastocoel. These embryos exhibit cells forming a closed bowl. (arrow #3). Immediately to the left of the numeral "2," an embryo appears to be acceptibly oriented, but the frozen dried image shows only cells at the vegetal pole can be identified by type. The cells at the opposite side may be animal II, or even vegetal I cells. Rings composed of cells of almost uniform size, forming a circumference the diameter of a normal embryo are the result of fracture planes which intercept the center of the blastocoel

without intercepting either of the poles. None of these cells can be reliably identified by type (embryo #4) Two artifacts of the frozen hydrated/dried examination system are seen in this figure. First, shrinkage occurs during drying and results in twisting and relocation of the embryos with respect to the stage coordinates, although size differences were resolved by increasing the magnification. The magnitude of this effect can be appreciated by observing the side of the bead in the upper right corner of the photographs. The top of the bead dries more rapidly than the base and therefore suffers greater shri..kage. The translation in Y may be the result of docking inaccuracies of the shuttle upon the stage. Second, by the following evidence, the pattern of the dried bead matrix is presumed to be determined by ice crystals formed during the freezing process. Read et al. (1983) noted that the percent of water present in the sample determined the size of the spaces between artifactual remnants. Echlin (1978) pointed out ice crystals and resulting artifact in etched cells which closely resemble the pattern seen in the C/HES matrix. Lewis and Pawley (1979) referred to this artifact by "eutectic margins" and suggested that it may be the remains of biological material. Carr et al., (1983) concluded varying degrees of "ice damage" were relfected in the sizes of spaces between the artifactual remnant. Finally, Echlin has noted that the ice crystal size in hydrated standards is similar to that of biological material (unpublished

results). These crystals are considerably larger than those produced in thin sections because the bulk of tissue being frozen produces a relatively slow rate of freezing. The large ice crystals of bulk samples do not interfere with analysis, provided they do not penetrate cell membranes and sampling volumes are large enough to average over compressed salts and the intervening ice. Cryoprotectant such as HES may be used to minimize crystal size (Pihakaski and Seveus, 1980, Echlin et al., 1982) although penetrating cryoprotectants must be avoided (Kuijpers and Roomans, 1983, Carr et al., 1985a). The HES chosen for this experiment was shown to be osmotically inactive in two ways. First, the MPFSW was analysed in a Fisk osmometer and shown to be 900 mOs. A mixture of C/HES/sea water chosen to equal the highest concentration found in the samples, 50% C and 20% HES, was measured and shown not to alter the osmolarity. Second, a sample of blastulae were allowed to culture for one hour in the 50/20% mixture at 15°C. They were then examined by light microscopy. The ciliary action and swimming activity were unaltered.

A pattern similar to the C/HES matrix is present within the interior of the blastocoels, but this artifact represents the native material of the blastocoel matrix. The matrix material may act as a natural, high molecular weight cryoprotectant, preventing ice crystal damage to the cells. The matrix appeared to remain intact in the frozen dried state (figure 3), closely resembling critical point

dried material (for example see Katow and Solursh, 1979). It must not be assumed that this was a reflection of the in vivo morphology, as critical point and freeze drying are likely to produce similar artifacts. The freezing process however did not damage the matrix more than other fixation techniques. The matrix in figure 3 is continuous with the basal lamina (arrow) at a number of separate locations, and appears either as thick fibers or thin sheets of material, often presenting a number of enclosed beads or knobs. Although these sheets seem to be centrally located, this is probably a result of the matrix pulling away from the epithelial sheet as it dried. No gross changes in the matrix were noted as the embryos progressed from blastula to gastrula (with the exception of a thickened matrix at the tip of the archenteron, noted later).

Figure 4 presents a higher magnification of embryo #1 at an orientation for more advantageous secondary electron collection. The animal and vegetal poles are evident in this micrograph. Cell preservation resulting from the freezing and drying processes is acceptable. As the PM cells round up and detach from their neighbors, the surrounding vegetal II cells flatten out with their long axes normal to the radial direction to fill the spaces. The absence of obvious protrusions on the surface of the PM cells during ingression agrees with images recorded from more traditionally prepared material (Gibbins et al., 1969, Katow and Solursh 1981). Vegetal cells which have not

rounded up or flattened out tend toward club shapes. Other cell types are trapezoidal with the larger base distal. The triangular shape of the cells and the loss of basal fibrous material toward the lower left of the micrograph is assumed to be a drying artifact. Basal fibrous attachments are not apparent in the vegetal region, but intercellular fibers appear which are not found between cells in other regions of the blastula (see figure 5). All other cells appear to be attached only at radial extremeties, as described previously (for example see Gufstafson and Wolpert, 1967, etc.). The relatively loose association between cells produces fractures between cells rather than within them (figure 5). Higher magnification than figure 5 is not possible without coating the specimen, but at this magnification the integrity of the cell and hyalin membrane appears to be preserved.

Frozen dried specimens exhibited morphology typical of sea urchin embryos which were critical point dried (for example Akasaka et al., 1980, Katow and Solursh, 1979) and embryos which were processed by combinations of dehydration, embedding, sectioning, rehydrating and critical point drying (for example Kawabe et al., 1981, McCarthy and Spiegel, 1983a). Because the freeze drying process probably results in more artifactual changes than the freezing proceedure, it is assumed that the hydrated specimens are more representative of the in vivo morphology than previously published micrographs of sea urchin embryos. Blastocoel fluid can be

seen to fill the spaces between epithelial cells in the hydrated form (figure 6). The cells are covered with 1 μm spherical beads (encircled in figure 6) which largely disappear in the dried cells (figures 4 and 7). The overall cell shapes are not significantly different from those in the dehydrated specimens. Cells in the animal and vegetal poles are elongated, PM are round (see figures 7, 13, and 49), and cells near the equator of the embryo are thinner radially. The cells of the vegetal pole become gradually more closely associated as the archenteron invaginates. A reflection of this can be seen in the hydrated image of the mesenchyme blastula of figure 6. In this figure it is difficult to distinguish intercellular spaces in the vegetal region.

The depth of the blastocoel and the tendency of the PM cells to migrate relatively closely to the blastocoel wall made it difficult to locate mesenchyme blastulae with visible PM cells and two poles. It was necessary to accept blastulae for analysis which displayed only one identifiable pole. In these cases, no assumptions were made concerning PM location or epithelial cell type for cells not in intimate contact with the identified pole. For example in figure 7a, 3 PM cells are visible at the surface of the fracture plane (arrows). The cells in the immediate vicinity are elongated, and comprise almost a third of the epithelial ring. This indicates that the PM cells are at the vegetal pole. The cells at the opposite end of the mesenchyme blastula, however, are not elongated. The small diameter of the

embryo indicates that they are likely Veg I cells. Figure 7b of the same mesenchyme blastula frozen dried confirms the presence of 3 PM cells at the surface, and an additional 4 which could not be seen in the hydrated image. The mesenchyme blastula suffered elongation in the drying process, but it is clear that the oral plate was not intersected. The inset diagram indicates a likely fracture plane. Because only the vegetal pole was intersected, no assumptions were made as to cell type or embryonic locale to the right of the line in figure 7b. The PM cells were never seen in intimate contact with the oral plate in the frozen hydrated samples, and in fact were seldom located in the animal half of the blastocoel.

Figure 7 also demonstrates the trend in mesenchyme blastulae vegetal cells noted in figure 6. The cells are closely bound to one another and it is difficult to identify intercellular space. As invagination progresses, increased proximity continues; cell shapes become irregular until it becomes difficult to discriminate between one cell and its neighbors. Notice the clear delineation between cells around the periphery except for the region directly at the center of the vegetal pole. Figure 8 is the image of a hydrated early gastrula where the fracture has fallen outside the archenteron. The blastocoel side of the cells are exposed to the electron beam. Two groups of PM cells are designated on either side of the archenteron. Figure 9 shows a slightly younger, frozen dried embryo from the interior of

the archenteron (the sea water side is exposed to the electron beam). The top of the archenteron, the blastocoel side, presents a thickened mass of matrix extending toward the animal pole. PM are located on either side of the invagination. The gastrula has pulled away from the C/HES matrix in drying, and exposed the exterior of the embryo. The vegetal side of the specimen is covered with the rippled unbroken remnants of the hyalin layer (compare this to the interior images of figure 10 where individual cells are clearly distinguishable). The cells continue to become closer until fractures occur through them. Figure 11 is a stereo image of the archenteron of a late gastrula (fusion between the oral plate and archenteron has begun). This hydrated sample was etched to reveal the intercellular detail exposed by the fracture. Ice can be seen within the interior of the forming gut. The exterior surface (ES) of several cells is exposed along with the interiors of others. Structures suggestive of cytoskeletal elements (CS), a mitochondrion (M), and endoplasmic reticulum (ER) are designated in the micrograph. These cells look much like the interiors of mamalian gut cells recorded by Carr et al. (1983).

A few of the late gastrulae fractured fortuitously at the tip of the archenteron. Figure 12 demonstrates such a fracture (again deeply etched). The archenteron extended from above the plane of the photograph toward the oral plate, which lay below the plane of the photograph. The cells at the tip of the archenteron have barely been removed

by the fracture. What remains is the partially hydrated form of the matrix marked "M" in figures 9 and 10. The thickened matrix has prevented the formation of ice crystals as large as those in the surrounding blastocoel. Large rounded beads and indentions which may have held beads are present. Although these beads are approximately 1 μm in diameter, much larger than the 30 nm beads observed by Katow and Solursh (1979) and the 26 nm beads identified by Kawabe (1981) as sulfated GAG, it is possible that these structures are the same granules. Fixation and dehydration may account for the size discrepency. It also may be significant that these beads are the same size as those seen on the cells in figure 6. The continuous peripheral sheath appeared to be open at the distal end (the structure was badly damaged in drying). Two secondary mesenchyme cells can be seen embedded within the sheath.

Artifacts of the Frozen Hydrated/Dried System

Two specimens experienced visible beam damage to the PM cells during the 100 seconds of data collection. Figure 13 displays 3 photographs taken before data collection, after data collection and after drying for the first of these cases. The three PM cells figure 13b have large pits where the beam was located during analysis. These cells were examined after the associated vegetal cells also visible in the micrograph. There was never apparent damage to the epithelial cells. The incident beam maintained constant

accelerating voltage (and therefore maximum incident energy) and the current was verified to be stable during the analysis of the entire embryo. The temperature of the shuttle upon which the sample was examined remained constant at less than -190^{o} C. A thermal conductivity change between the sample and shuttle would not explain the lack of damage to the vegetal cells. The corresponding micrograph of the embryo frozen dried shows damage to the tissue. Such cells were eliminated from quantitative analysis because of the rather obvious possibility of elemental loss.

Several embryos had a lacy sheet overlying a portion of the epithelial ring (figure 14). These structures persisted in the dried specimens and did not appear to be debris. The sheets did not collect charge as if they were insulated from the bulk. The structures were never seen at random within the blastocoels or in the C/HES matrix outside of the embryos, but always on the epithelial ring, oriented along the circumfrence as in figure 14. They showed no regular orientation with respect to the direction of fracture progression. Finally, the material seems to be solid; cells underlying the dried structure cannot be seen. It is possible that a plane of ice spread into the embryo during freezing, prefracturing the sample, but in such a case one would expect the pattern of ice crystals to be continuous with the exterior matrix. A similar artifact has been identified by Carr (personal communication) in frozen hydrated gut samples.

Charging Phenomena and Frozen Hydrated Tissue

The techniques employed in this study were designed to avoid coating frozen hydrated samples. In most cases the C/HES matrix was sufficient to conduct charge away from the sample during examination. Where it was not sufficient, a number of effects were observed.

The most common charging effect was expressed in a brightness intensification of the secondary image (figure 15). This phenomenon occurred most often in areas where ice was prevelent, such as the blastocoel, possibly because of large crystal formation and scarcity of conducting material. Although brightness could be compensated for by adjusting the level of the monitor quantitative data was not collected from these areas (see the following discussion).

A second charging effect evident in the secondary electron image was reduced intensity. This effect is visible over the fractured surface of the bead in figure 16. The linear appearance of the lighter areas was typical and followed chatter. The embryo (arrow) appears raised out of the surface because it is surrounded by a dark area. This variation in secondary electron coefficient (δ = number of secondary electrons/number of primary electrons) often produces a false topographical sense. High magnification of these dark areas resemble attempts to image disadvantageous topography with respect to the secondary detector and beam. Images are out of focus and lack detail. They differ

however in that extreme contrast variation is present due to edge effects.

The third type of charging observed in secondary electron images was a transient burst of secondary electrons. This type of charging manifested in photographs as bright lines recorded at the time of discharge (see figure 10). The duration of discharge can be calculated from the number of bright lines and the scan rate of the CRT. Charging is not unique to hydrated specimens, and may occur less often in hydrated specimens (Goldstein et al., 1981), it is significant that all three of these phenomena occur in frozen hydrated material.

In addition to charging effects in the secondary electron images, two charging phenomena appeared during the collection of quantitative x-ray data. The first of these produced Al peaks, an element not found in biological samples but present in the specimen chamber of the microscope. A significant increase in the P/B ratio for Al implied that the other elemental P/B ratios may also have been affected by material not located within the microvolume selected for analysis (see discussion). The level of significance was determined by averaging 20 P/B ratios for Al which were collected from metalurgical standards containing no detectable Al and shown to be conducting sufficiently so as not to display any of the visual charging effects. The level of confidence was arbitrarily set at 95% and the test assumed

to be one sided (the P/B ratio was altered only by an increase in cases of stray x-ray emission). Applying the following criteria for critical rejection value (Remington and Schork, 1970):

$$z = (x - \mu_o) \ (\sigma/n^{1/2})$$

led to a rejection of data when Al P/B ratios were greater than 0.0180; it was assumed that Al P/B ratios exceeding 0.0180 signified an alteration in the sampling volume. The second effect visible in the x-ray spectrum was a change in the shape of the bremstraahlung background. The slowing of electrons in biological samples causes emission of x rays with energies up to the initial energy of the incident beam. This background emission has a typical shape, skewed toward the low energy end of the spectrum. A representative background of the type expected under the present experimental conditions is shown in figure 17. The curve starts at 0.1 KeV due to the presence of a Be window on the detector. The curve rises rapidly to a maximum at around 2 KeV, and slopes off gradually to 15 KeV (the curve is visible only to 10 KeV because of the limited display). An increased slope in the high end of the x-ray background represents a reduction in the number of high energy electrons entering the specimen. This effect could be quantitatively monitored by the number of counts registered between 6 and 10 KeV. If the number of counts in this range was less than 300, the computer could not satisfy criteria for analysis. When the number of counts within this 6 to 10 KeV range was less than 5% of the

total number of counts (including the characteristic peaks) the data point was considered to be electrically charged and rejected. This percentage represented a safe margin before a change in slope shape could be seen on the monitor.

It is significant that the charging effects were distinct and separate. Two manifestations seldom occurred at a single sampling location, and never more than two. X-ray analysis was performed on a number of visually charging areas to test for simultaneous effects. No regular correlation was found. In fact, in cases where the spectrometer showed a truncated background, a high Al P/B ratio was never found. Any one of the charging effects was sufficient to eliminate a data point from consideration.

Effects of Long Term Storage in Liquid Nitrogen

In spite of considerable care to assure that stored tissue remained well submerged in liquid nitrogen, a number of effects were apparent in stored material. Although the exact period for safe storage has not been determined by this experiment, tissue stored longer than three months showed marked effects. Because some of these effects reflected a possible change in tissue density which would affect the interaction volume (see following discussion) for emission of x rays, these samples were not used for quantitative analysis. Figures 18 through 21 are secondary electron images of material stored more than three months.

The first phenomenon encountered in material stored longer than three months was a change in fracturing characteristics. Attempts to fracture the C/HES beads were largely unsucessful. Although three or more attempts were possible for each stub, and each stub held four beads, any one of which could produce an acceptable fracture, most samples had to be discarded without secondary electron imaging. Beads seemed more resistant to fracture; some lifted completely out of their anchoring depressions in the stub and were lost in the preparation chamber. Others, like the one in figure 18, sustained considerable chatter damage (C) as the knife cut into the sample. The beads also experienced sporadic pits (P) and ridges (R) or plateaus with sharp vertical sides. Edges of the beads chipped away at large angles from the fracture plane, resembling compression pits (CP). When fresh material was struck with the knife, the resistance occurred as a sharp impact with a clean release as the fracture progressed and the top of the bead lifted off. When long stored matrial was fractured, a repeated series of small resistances occurred, and the top was often torn from the bead, remaining attached to the knife blade. More debris tended to accumulate on the knife blade and on the samples. Smearing of the matrix indicated an increased melting due to the heat of fracture (see figure 19a). Fractures which were examined by secondary electron imaging exhibited a number of other abnormalities.

Long term stored material commonly suffered reduced secondary electron emission. This is visible in figure 19a at the arrow (C) and at the tip of the archenteron. Charging was followed by spotty dehydration of the matrix and increasing charge buildup. Figure 19b was taken just a few minutes after the previous micrograph. It is difficult to differentiate between dark areas due to charging and due to dehydration. The area circled and labled "1" is dehydrated and exhibits a previously hidden PM cell. The area circled and labeled "2" is presumed to be a charging artifact because of the smooth ice surface surrounding the darkened area. The ice near "1" has a speckled appearance (similar to area "3"). The dehydration process of long term stored material was notably different from conductive etching (compare figure 19b to figure 11). The ice remaining in radiantly etched samples is of uniform depth. The ice surrounding the PM cell in area "1" has completely sublimed while other areas are fully hydrated. Smearing which is extremely suceptible to dehydration effects is still present. This sample was never exposed to a reduced raster, or magnification greater than 760 times actual size (the magnification of figure 19). The frozen dried image (figure 19c) verifies that these effects damage the tissue as well as the surrounding ice. Separation of the cells from the hyalin membrane was common in these samples and the space was filled with fluid in the hydrated images. Cell loss (arrow 1) and severe shrinkage (arrow 2) occurred. The blastocoel matrix

material suffered numerous perforations (arrow 3) which were not seen in well preserved material (compare to figure 3).

Dehydration is not the result of etching by the electron beam or local heating of the specimen. Figure 20 shows a low magnification image of another bead on the same carbon stub as the previous specimen. This image was taken immediately following figure 19. The second bead was exposed to the beam only long enough to focus the image and expose the photographic film; its appearance did not change noticably from when the beam first contacted the bead. The Joule-Thompson stage was verified to be at less than -190^{o} C during the examination of all samples. Although it is possible that thermal contact between the stub and stage was poor, it is unlikely that this occurred with each of the long term stored samples, and none of the fresh samples.

The final unique phenomenon in long term stored material is illustrated in figure 21. Many embryos cracked open during overnight drying. This embryo in the hydrated state showed only minor effects from long term storage. The frozen dried specimen exhibited cell loss (CL) as well as the aforementioned crack. These cracks appeared preferentially through embryos which had been examined with the electron probe, as if the sample structure had been strained in the examination. The arrow points to perforations in the blastocoel matrix.

X-ray Mapping

When the signal to the CRT is generated by the x-ray detector rather than the Everhart-Thornley detector, it becomes possible to record images produced by x rays of a selected energy (Heinrich, 1963). In the x-ray imaging mode, an area containing a particular element will generate x rays at the K_α energy for this element producing a bright area superimposed upon the local background at the same energy. This imaging mode is accordingly a qualitative pictoral reflection of relative amounts of a particular element at specific locations, producing a map of elemental location. Approximately 4000 counts were accumulated in the energy band defined for the element of interest (approximately one standard deviation to either side of the K_α x-ray energy of the element of interest). This produced images of acceptable clarity for most elements. Elements which did not produce clear images at the 4000 pixel density (10 minutes for the lowest count rates) did not improve noticably if the time was tripled.

Figure 22 shows an example of two maps produced by this technique. The center micrograph is the secondary electron image of the sampled mesenchyme blastula at the same magnification and orientation as the x-ray maps to either side. The first image of figure 22 is a map produced by x rays emitted at the K_α energy of Cl atoms. The outline of the embryo is obvious and the blastocoel is easily detected

except in the area where six PM cells were located near the vegetal pole. The density of exposed pixels within the epithelial ring is representative of the noise level plus the relatively low cellular [Cl]. The final frame of figure 22 exhibits K sequestered within the cells of the epithelium. A bright ring is depicted at the location of the embryo, although it is less well defined than the dark ring of the Cl image. There are two reasons for this lack of definition. First, the K contains a larger Bremstraahlung contribution than the Cl. Second, the blastocoel contains considerable K, obscuring the inner limit of the epithelial ring and the PM cells enclosed within. A shadow surrounds the embryo as if the sea water immediately adjecent to the cells had been depleted of K.

The maps of Cl and K demonstrate elemental location within and surrounding the embryos. The maps showed no gradients within the blastocoel although there may be a less well defined gradient across the basal lamina than across the hyalin membrane. Figure 23 shows the corresponding maps for Na and S. Again the epithelial ring is evident, both elements are excluded from the epithelial cells. Because all of the images from this mesenchyme blastula display a slightly higher intensity in the upper left portion of the blastocoel, this cannot be construed as a gradient of any particular element and is probably due to the shifting of the blastocoel matrix during drying. The S x-ray image is difficult to see. Considerable S exists on, between and

within cells, and is plentiful within the blastocoel; there are no areas of particularly high relative S concentration. Also a high percent of the counts within the energy band defined for S are due to Bremstraahlung radiation. Attempts to establish an image at higher magnification failed as well. Figure 24 shows the secondary image and correspondong S map for 4 PM cells. No variation in relative S concentration between the PM cells and the surrounding matrix is identifiable. An increased count would not improve the image because of the high noise component within the energy band.

A number of gastrulae were investigated as well as the blastulae and mesenchyme blastulae to explore changes within the archenteron or blastocoel matrix due to secondary mesenchyme cell migration. Figure 25 displays the Na, Cl, and S images of an early gastrula. All three elements were excluded to similar extents in the archenteron as in the earlier epithelial cells. There was no noticable increase in S within or surrounding the invagination. Also, there was no noticable increase in the S content of the matrix between the archenteron and the (absent) oral plate. The Na and Cl images are presented as verification of the maintainance of elemental location.

Elemental Analysis

The data collected was divided into six cell types and four raster locations:

1. An1	1. Cellular
2. An2	2. Sea Water (H_2O)
3. Veg1	3. Blastocoel (BC)
4. Veg2	4 ECM
5. PM	
6. Archenteron (Arch)	

Because the raster size and interaction volume resulted in sampling volumes of cellular dimensions (250 μm^3), the data labeled ECM, BC and H_2O are not representative of the concentrations within the ECM, basal lamina and blastocoel, and hyalin membrane respectively, but rather the result of sampling volumes overlapping these zones. Often the increases or decreases in concentration (compared with the cell volume) may be misleading due to local changes in concentration on the plasma side of the membrane. P/B ratios from these areas however may be used to verify the accuracy of the interaction volume location since significant differences in concentration should be detected when the sampling volume overlaps extracellular spaces. Figures 26, 27, and 28 present the results of such comparasons. The minimum number of embryos sampled for each bar was 3 and the minimum number of points per area type per embryo was also 3 (a minimum of 6 degrees of freedom). Error bars represent one standard error of the mean (sem). These errors are large because of variation between individual embryos. The student's t-test was applied to affirm significant difference between points:

$$t = \frac{\overline{X}_1 - \overline{X}_2}{[(S_1^2)/n_1 + (S_2^2)/n_2]^{1/2}}$$

with

$$d_f = \frac{[(S_1^2/n_1) + (S_2^2/n_2)]^2}{[(S_1^2/n_1)/(n_1+1)] + [(S_2^2/n_2)/(n_2+1)]} - 2$$

(Remington and Schork, 1970). The level of confidence was set at 80%. Because of the elimination of data points according to the previously listed criteria, some of the area types and cell types did not provide the acceptible minimum number of points. These are represented as blanks in the bar graphs. Figure 26 shows the K P/B ratio variation according to beam location in mesenchyme blastulae. Because K is sequestered within the cells of the epithelium (see figure 22), the highest P/B ratios should result from cellular volumes (C). With the exception of the An2 cells (where the H_2O and ECM P/B ratios not significantly higher) and the Veg2 cells the cell volumes produced the highest P/B ratios. Because the K pumps are located in the cell membrane, the concentration of K may be higher close to the membrane. The overlapping extracellular volumes will yield falsely large K levels which appear close to the cellular levels. The sea water/C/HES matrix may exhibit large variation within or between cell types due to the presence of large ice crystals which have removed elements from one or more microvolumes. This can be verified by showing that all elements sampled from that area follow the same pattern. The blastocoel (BC) side of the Veg1 cells is significantly lower in K concentration, but the blastocoel side of the

Veg2 cells is not. This is likely because the Veg2 BC volume overlaps both the Veg2 and PM cells, but the Veg1 BC volume overlaps only one cell membrane. Figure 27 presents a similar comparison of S values. Variations in S are more dramatic than those in K because of the cellular variation both in sequestration and pericellular secretion. While the cellular concentration of S is equal to the highest values in three cell types, it is significantly lower in the Veg2 cells. The S content of the Veg2 BC volumes equals the other 3 intracellular volumes. The sea water side of the epithelial ring registers low S concentration although variation is large again. There is no significant difference (less than 70% confidence) between cellular and ECM volumes whereas the differences between the vegetal BC and cellular volumes are significant at the 99% level. Figure 28 shows the same arrangement of data taken from the early gastrulae (EG). The An1 and An2 cell volume S P/B ratios are significantly different (97.5% confidence) and the Veg1 cells are significantly higher than the An2 cells (99.5%). The differences amoung the Veg1 cell volumes are not significant (75% confidence); the variation between BC and cellular volumes in the Veg2 cells is significant at the 80% confidence level, while the difference between the ECM and C has 90% confidence level.

The next series of bar graphs shows elemental variation corresponding to different developmental stages organizing the data according to cell type (content vs. stage).

Significant changes in K P/B ratios during development were discovered in the Veg2 cells (figure 29). The increase from blastula to mesenchyme blastula stage was significant at the 80% confidence level and the increase from mesenchyme blastula to early gastrula was significant at the 95% confidence level. Other increases were not significant (below the 80% level), but the decrease in the An1 early gastrula volume was significantly different from both the mesenchyme blastula and An2 early gastrula volumes (at the 90% confidence level). The blastula P/B ratios were low with the exception of the presumptive PM cells. The K P/B ratios throughout the 3 stages and 5 cell types remained consistantly close to a value of 0.22.

The cellular S data (figure 30) present very different relationships. The S content of An1 cells in blastulae is low and is significantly different from the An1 cells at later stages as well as the other cell types of the blastula stage (at least a 95% level of confidence). The An2 and Veg1 cells, which do not undergo extreme morphological differentiation, show no significant differences with stage. The Veg2 cells display two shifts in S content. The content drops as the cells pass through the mesenchyme blastula stage and rises again to a level higher than the first ratio at the gastrula stage. The decrease in S from blastula to mesenchyme blastula in the Veg2 cells is statistically significant (95% confidence level) as is the subsequent increase (at the 97.5% confidence level). The increase in

the gastrulae over the blastulae is also significant (80% confidence). The presumptive PM cells of the blastulae presented a high S concentration with impressively little variation. There was only one sucessful sampling of a PM cell volume from the mesenchyme blastula. This point does not meet the requirements of a minimum 6 degrees of freedom, but because the P/B ratio recorded was low (0.03), the PM S content may be less than that of the presumptive PM. The S content of the PM surrounding the archenteron is the second lowest intracellular S level detected (second to the An1 cells). Although the data for intracellular P appears to follow the same trends, the differences in most cell types are not statistically significant (figure 31). The An2 and Veg1 cells show significant increases (90% confidence) and the P content of the blastula An1 cells, like the S content, is low.

An examination of the changes in Ca with development (figure 32) displays 4 significant variations from a P/B ratio value of 0.017. The large content of the An1 cytosol (the increase above 0.017 is significant at the 95% confidence level) is verified by the adjacent BC (mean P/B = 0.043) and ECM (mean P/B = 0.030) ratios. The Veg1 cells of the mesenchyme blastula and the archenteron of the early gastrula contain significantly less Ca than other cells (97.5% confidence). The PM cells of the early gastrula will soon begin to lay down the calcium carbonate skeleton of the pluteus, and would be expected to reflect a high

concentration of Ca in preparation for that event. This large concentration of Ca within the PM filopodia has been recorded at a later stage, after the skeleton had begun to form. The content of the early gastrula PM cells is however significantly lower than the presumptive PM cells' content and the average P/B ratio for this element (both at 90% confidence).

If the S content of the sampling volumes which included blastocoel, basal lamina and basal portion of the cell (BC) are correlated with embryonic age, relationships different from those of the cytosol contents are discovered. These are therefore presumed to vary because of the basal lamina and blastocoel matrix. Changes in P/B ratio from one stage to another cannot be considered valid unless the corresponding cell volume P/B ratios were constant or opposite in direction during this transition. If the extracellular change is significantly different from the adjacent cellular pattern, the change is assumed to have occured in the small fraction of the sampling volume occupied by the blastocoel material. Figure 33 contains error bars which are considerably larger than those of previous graphs because of the variation in local extracellular S. If the sampling volume contained a large amount of blastocoel matrix, the S content was higher than those volumes which contained little or no matrix. Also, due to the charging phenomena (see following discussion), no data were available for 7 of the points on the bar graph (locations are consequently blank). The most

significant change in S concentration within the blastocoel during development is the increase the PM cells exhibited during migration and formation of the mesenchyme ring (85% confidence level). This increase is opposite the trend of intracellular volumes (figure 30). The blastocoel volume of the An1 cells is considerably higher than the cellular content (figure 30). There are also significant differences amoung the An2, Veg1 and Veg2 basal volumes of the early gastrulae (80-85%) and no significant differences between the An1 blastula and An2 gastrula volumes. The PM cells of the mesenchyme blastula stage exhibit a higher extracellular S content than the blastocoel side of the archenteron, so that unless the PM matrix is shed prior to the gastrula stage, this relationship remains between the stable mesenchyme ring and the base of the archenteron. Because of the polarity of the epithelial cells, it is possible that the ECM content differs from the basal exudate.

The final bar graph of this series (figure 34) explores the S content of adjacent cells and intervening ECM as the embryo matures. The large sampling volume chosen to eliminate fluctuations due to ice crystals overlaps the cell volume in all cases. The difference occuring in the An1 cells' ECM during oral plate formation is not significant. However, a significant increase was found in the cellular transition from blastula to mesenchyme blastula (figure 30), and the cellular P/S ratio is nearly half of that found in the blastula ECM sampling volume (see figure 30). This

implies an relatively high S ECM concentration during the blastula oral plate formation. There is no significant difference between the ECM and cellular sampling volumes for the mesenchyme blastula stage. The increase in ECM S content of the oral plate zone in the early gastrula is significant (99% confidence level), and occurs while no increase was found in the cellular P/B ratio. Although there is a small but significant increase found during the transition from blastula to mesenchyme blastula in the Veg1 cells ECM, this trend follows that of the cell volume and may be attributed to the cytosol. The increase in Veg2 cell ECM is larger but also follows the cellular increase and can not be separated from that phenomenon. The PM cells do not have an ECM which is distinct from the area overlapping the blastocoel. The ECM for the presumptive PM cells displays extreme variability.

Figure 35 presents the cellular P/B ratios for both Mg and Mn. Comparasons cannot be made between the right and left halves of the graph, as two different conversion factors (f) need to be derived to arrive at the concentrations for these two elements. Although the P/B ratios are similar, the concentrations may be different. The Mg content exhibited by the Veg1 cells is significantly lower than both the An1 (at the 97.5% confidence level) and Veg2 (at the 90% confidence level) cells. The decrease in Mg as An2 cells pass from the mesenchyme blastula stage to early gastrula (80% confidence) and the increase in the Veg1 cells (90%

confidence) during the same time are both significant, and the cellular content is thereby equalized in the gastrulae. Only the PM cells of the gastrulae exhibit a small but significant increase in Mn (80% confidence level). There are similar significant changes in An2 cells during development from mesenchyme blastula to early gastrula. The mesenchyme blastula PM readings are below the detection level of the aparatus, although the required minimum 6 data points were received and other P/B ratios collected.

The final series of bar graphs compares P/B ratios for cell volumes and extracellular spaces as the sampling circumscribes the embryonic epithelial shell (content vs. location). Figure 36 shows a dramatic increase in the S content along the blastocoel wall as the interior of the mesenchyme blastula is examined, with the highest content occuring at the vegetal pole. No data was available for the An1 cells and only 1 datum point was available for the An2 cells (P/B ratio = 0.04). The steady increase in S is not repeated in either the ECM samplings, or the cellular volumes. In fact, the ECM between Veg2 cells appears to contain less S than that found elsewhere within the mesenchyme blastula (85% confidence level). The cytosol P/B ratios do not vary significantly from each other or from their respective ECM measurements (the level of confidence for the Veg2 decrease is only 70%).

The following figure (37) exhibits the same correla-

tions for data received from early gastrulae. All of the P/B ratios increase from the mesenchyme blastulae P/B ratios (figure 36), which agrees with earlier studies (Kinoshita and Saiga, 1979, Kinoshita annd Yoshi, 1979, Sugiyama, 1972). The S gradient seen in the mesnechyme blastula blastocoel is no longer present. The low P/B ratio recorded from the Veg1 cells is significant at the 80% confidence level, and the other apparent variations are insignificant fluctuations. A comparison of figures 36 and 37 suggests an increase in animal pole blastocoel S, while the vegetal pole remains nearly constant. The increase in the Veg1 and Veg2 blastocoel P/B ratios is about the same, whereas the increase in the An2 P/B ratio is large. The volume containing the ECM presented fairly consistant P/B ratios regardless of embryonic location. The measurement from the archenteron is not significantly lower than other ECM P/B ratios. The measurement from An1 ECM is larger than other ECM (at 95% confidence), and larger than An1 cellular P/B ratios (at the 97.5% confidence level). This increase preceeds archenteron fusion. The cellular samplings show small but significant increases in the Veg1 and Veg2 cytosol S. The Veg2 increase occurs during a period of extracellular stability. This may imply a small decrease in the extracellular S. The PM cytosol is comparatively low, yielding S P/B ratios reminiscent of mesenchyme blastulae cellular ratios (see figure 36). The cellular volumes now mimic the blastocoel trends seen in the mesenchyme blastulae, as

if the cells are accumulating the S previously shed into the blastocoel. The final graph compares P content as the sampling circumscribes the the embryo (figure 38). The apparent increase in the P content of the blastocoel volume of the PM cells is significant (80% confidence level), but may be due to the intracellular variation. Data from the mesenchyme blastulae did not provide sufficient points for an intracellular analysis of the PM cells. The increase in ECM of the An2 cells is significant (95% confidence) and occurs in the absence of a similar intracellular increase. The increase in the intracellular volume of the An1 cells is also statistically valid (90% confidence). Other P/B ratios are stable and clulster around a P/B ratio of 0.05.

Discussion

Morphology of Frozen Hydrated and Frozen Dried Tissue

A number of techniques have been employed in the preparation and examination of frozen hydrated biological samples, the particular technique selected depending upon the type of analysis performed. This experiment was designed to examine the elemental composition of fully hydrated Strongelocentrotus purpuratus embryos, and to compare that composition to the morphogenetic behavior during development. For this reason, Marshall's (1979) techniques for freezing bulk samples on solid nitrogen, fracturing the samples and examining them without etching were employed. When the beads are properly fractured, the surface is flat with small deviations in height where the fracture plane has been diverted to run along easily fractured material such as intercellular spaces. Figure 39 presents two stereo pairs, taken at a 20^{o} paralax. If the knife scrapes across the surface of the bead the only variations in height are caused by irregularities in the edge of the blade. This is illustrated in figure 39b. A small area of fractured surface can be seen sloping off the normal surface. On this face, embryos are obvious. No embryos can be seen on the normal plane, although the usual number could be identified in the dissecting microscope of the preparation chamber. Because this is a difficult technique to master, many investigators have chosen to rely upon simpler techniques for more rapid

results. When elemental concentration is not of concern, the tissue may be radiantly etched to expose structures lying on or below the shaved surface by removing the surface fluids. This technique has been applied by Echlin (for example see Echlin et al., 1979) and Carr (for example see Carr et al., 1983) among others (Lewis and Pawley, 1979, Hook et al., 1980, Bastacky et al., 1983), and is illustrated in figures 11, 12 and 42 of this thesis. An alternative etching method heats the sample by conduction (Gardner et al., 1979, Bullock et al., 1980, Read et al., 1983). Because this method heats water throughout the sample, the recrystalization and density changes are more severe. Although cells retain a hydrated morphology both of these techniques alter the size and shape of the interaction volume (Marshall, 1981). The resultant change in size and shape would not result in a significant change in P/B values from lightly etched standards (Echlin and Taylor, 1985) because of the homogeneity of carbon and suspended salt beads. The large raster size utilized during examination of biological samples to average over ice crystals and compressed salts is approximately equal to cellular dimentions. An enlargement of the interaction volume could result in expansion beyond the cell membrane. Reliable location of the interaction volume is essential for reproducible x-ray data. Furthermore, the depth of the etch cannot be regulated with acceptable accuracy. The extent of water removal is estimated by the height of the remaining artifact

after the etch has been completed. Regulating the duration of heating only approximately matches the depth of etch from sample to sample. To avoid the potential for unsystematic error in the sampling volume, this experiment used only well fractured samples which did not require ice removal.

Samples were not coated with electron conducting material (recommended by Nei, 1974, Koch, 1975 and Echlin and Burgess, 1977). Although most coating metals cannot be used on biological samples from which compositional information is sought, alternative materials have been used sucessfully to conduct excess charge. Echlin et al., (1979) employed the evaporative coating module of the preparation chamber which was used in this experiment to apply carbon film on the surface of frozen hydrated Lemna minor roots. They found this proceedure sufficient to prevent charging under most examination proceedures. Unfortunately, the evaporation temperature of C is 3000° C. Heating the C to this temperature results in radiant heating of the sample which is reflected in the P/B ratios, although the surface may not appear etched (Echlin, unpublished results). Echlin has since abandoned C in favor of Cr (Echlin and Taylor, 1985) to avoid etching. Marshall and Carde (1983) coat their samples with Be. This element evaporated at low temperature but is highly toxic and must be used with extreme caution. The present experiment avoided radiant heat from coating processes by placing the specimen in conducting material prior to freezing. By surrounding the embryos with a C

matrix, charge could be dissipated through the bead even at the relatively high currents required for quantitative analysis. Two notable exceptions occurred. First, the interiors of the embryos tended to collect charge and second, material stored longer than three months experienced charge buildup. Because of problems incurred within the blastocoels of the sea urchin embryos, this technique of embedding a sample within a conducting material is not recommended for large samples of multicellular construction.

The temperature of the specimen shuttle was continuously monitored except during transfer from the LN_2 to the preparation chamber. The stub was housed within a precooled transfer device initially at LN_2 temperature, and the surface to be examined was not exposed until after the bead had been fractured. It is unlikely that dehydration of the embryos examined occurred prior to interaction with the electron probe. During electron mediated examination, the stage temperature was monitored and verified to remain below -185° C. Dehydration effects were not visible under the electron beam (with the exception of the damaged tissue noted earlier). There was no loss of structures such as the 1 µm beads in figure 6, demonstrated to be suceptible to loss during dehydration, or exposure of previously hidden structures (such as the PM cell in figure 19) in samples classified as acceptable for quantitative analysis.

Dehydration also occurs by energy transfer from the

electron beam. The tissue may appear hydrated while suffering a loss in density which results in poor definition of the sampling volume. As tissue dehydrates, the absorption factor decreases and the interaction volume increases. Although this loss might be detected through careful stereology, a more straight forward quantitative method was chosen for this experiment. The increase in x-ray yield was calculated by collecting data from 5 blastulae for extended times. The normal examination time for each datum point, 100 seconds, was extended to 200 seconds. The number of x rays detected per second (count rate) was recorded at 25 second intervals. The mean values of recorded counts are plotted in figure 40, and the least squares slope indicated. There is a linear relationship between count rate and collection time up to the 200 second limit (Pearson's R = 0.81106), indicating a 20% increase in count rate during that period. If calculated using only the data up to 100 seconds, the slope is not altered, indicating a 10% increase in count rate during experimental data collection. Twenty five points were recorded from fully frozen hydrated embryos and from their frozen dried form. The yield from the dried samples was 91% greater than the hydrated samples. These results imply an insignificant dehydration under the beam's influence during normal data collection. The P/B ratio is also sensitive to dehydration of the sample. Water molecules are responsible for much of the bremstraahlung radiation in hydrated samples. As water is removed, the

background of the x-ray spectrum is greatly reduced (Gullasch and Kauffmann, 1974, Saubermann and Echlin, 1975, Fuchs and Lindermann, 1975, Dorge et al., 1975, Saubermann et al., 1977). At the same time, the characteristic peak is increased because of reduced characteristic x-ray absorption. The result is a rapidly increasing P/B ratio (Gupta et al., 1976, Echlin, 1978, Gupta and Hall, 1981). Figure 41 illustrates the changes in P/B ratio for the elements Cl and K due to an initial and a repeated 100 seconds of data collection. Cl and K were chosen as representative elements because their energies are located on the smaller slope of the Bremstraahlung curve and they are also close enough to the maximum of the curve that the effects of background reduction are large. The inserted diagram of figure 41 illustrates their locations on the background. Although it appears from the diagram that Cl should experience greater variation as the background is reduced, the histogram does not reflect this. Cl is volatile under the electron beam (Echlin, et al, 1983) and may be driven off as the specimen dehydrates. The P/B ratios from homogeneous standards imply a 250% increase for Cl, and a 218% increase for K in dried material (Echlin, unpublished results), and larger increases have been reported by Lai and Hayes (1980). The P/B increase during the second collection, although significant, does not imply considerable dehydration when compared to dried material.

Beads of approximately 1 μm diameter can be seen on the surfaces of the cells (see figure 6) and within the matrix of the blastocoel (see figures 12 and 42) of hydrated material. It is possible that these beads are lipid vacuoles within the cells; they closely resemble those recorded by Carr et al. (1983) within goblet cells. The embryo depends upon lipids for nutrition and such granules are plentiful within the sea urchin egg. The 30 nm beads are present in dehydrated matrix when the embryos have been fixed prior to dehydration (Kawabe et al., 1981, Katow and Solursh, 1979). Lipids are particularly suceptible to dehydration (Barnard, 1980) and would exhibit behavior similar to the disappearance noted in the dried samples. Lipid beads, however, would not be expected within the blastocoel matrix. Cellular blebs examined in the frozen hydrated and freeze dried states do not appear suceptible to dehydration (Finch, 1985). If the beads location results from the extension of matrix over the cell surface, their appearance both on the cell and within the matrix is understandable. Furthermore, if the beads are the same beads described by Katow and Solursh (1979) and Kawabe (1981) they are formed of sulfated GAGs. This hypothesis could be tested by depriving the embryos of SO_4 (sulfate free seawater, for example) and examining the frozen hydrated specimens. The size discrepancy between the 30 nm beads identified by Katow and Solursh and the 1 μm beads presented in figure 12 may be caused by the difference between hydrated and dehydrated forms of the ECM.

Hascall and Hascall (1981) predict an increase in size of hydrated GAG's due to charge repulsion which would produce aggregates as large as a small organelle. This estimate agrees with the size of hydrated 1 µm beads identified in these samples. Beads were present throughout all cell types, although they tended to cluster on the PM cells. Since the beads within the matrix were not visible unless the surface of the sample was deeply etched, and since this experiment was designed to examine fully hydrated material, an exhaustive study of these structures, their locations and relative densities was not performed.

The morphological and physical changes observed in the early gastrulae suggest intercellular developmental change. Only the cells of the forming gut exhibit evidence of increased adhesion during the early gastrula stage; the other epithelial cells continue to fracture between cells and continue to present easily identifiable cell boundaries (figure 9). Blastocoel fluid is not excluded from between the cells except in the archenteron wall. If the invagination process were assumed to be the result of changes occurring within cells surrounding the orifice of the archenteron, the cells of the archenteron would be expected to be pressed together, but to continue fracturing between cells. Since the fracture progresses through and between the archenteron cells, the frozen adhesion between cells approximates the forces which maintain frozen cellular integrity. This supports theories of gastrulation which rely upon

autonomous processes within the Veg2 cells of the archenteron. Gufstafson and Wolpert (1967) proposed that shape changes in cells surrounding the archenteron pore could be responsible for the invagination, provided they were accompanied by decreased and increased adhesion between cells at various times. The changes in morphology of the archenteron experienced in the present experiment are not accompanied by changes in the rim cells. The osmotic theory of gastrulation proposed by Dan (1960) is not supported by the frozen hydrated images because it requires that all epithelial cells behave similarly. Recently, Ettensohn (1984) performed a variation of the experiment reported by Moore and Burt (1939). He removed the Veg2 cells as early as 16 hours after fertilization, and prevented reformation of the blastocoel by holding the edges apart with tungsten needles. Gastrulation proceeded as usual within the normal time framework, implying an autonomous process within the Veg2 cells. In agreement with Ettensohn's observations, no gross changes in cell shape were observed in frozen hydrated samples of this experiment; only the edges of the cells changed form whereas the overall shape remained rectangular. The apparent increased adhesion observed in fracturing the archenteron may be related to the electron dense bands presented by Ettensohn (1984). These bands are located only in the vegetal cells of the archenteron and are reminiscent of zonulae adherens. Although the present experiment was not designed to investigate the invagination process the

present evidence suppports the autonomous theories of invagination.

Analysis of Frozen Hydrated and Dried Tissue Artifacts

The experimental proceedure described under Materials and Methods is illustrated in figure 43. The top micrograph, 43a, shows the size and locations of 8 data points (experimental numbers 303;18-25) taken from this embryo. The lower micrograph, 43b, illustrates the transfer of data locations to the frozen dried image. This transfer is accomplished by overlaying the negatives of the two photographs and printing a double exposure image as a working print. Benchmarks from the frozen image are located in the double exposure, and the raster is drawn on the working print. Benchmarks resulting from the dried image are then located, and the raster outline is redrawn a third time onto the dried image. The magnifications are matched before the dried image is photographed by fitting the realtime secondary image to a transparency outline of the frozen hydrated sample. The template for raster size matches the actual raster plus 1 μm for maximum lateral extension of the interaction volume. This extension, for Na (which has the lowest K_α energy and therefore the largest interaction volume), was calculated from the formula provided by Echlin et al. (1982)

$$R_L = 0.0231 \left[\frac{E_o^{1.5} - E_c^{1.5}}{\rho}\right]$$

$$R_D = 0.64 \left[\frac{E_o^{1.68} - E_c^{1.68}}{\rho}\right]$$

where R_L = lateral range, R_D = depth, E_o = initial beam electron energy, E_c = characteristic x-ray energy for the element of interest, and ρ = the density of the sample. The map presented in figure 43b determines that points 18 and 19 are well within the cytosol, but point 22 includes the ECM between the cells containing points 21 and 24. The raster labeled 23 contains the hyalin membrane and sea water. The reliability of this approach was tested by comparing the P/B ratios obtained from points labeled "cytosol" with those containing extracellular locations. Figures 26 through 28 verify statistically significant differences between these locations. Although developmental inferences are difficult because the sampling volumes overlap up to three different cell volumes, the differences due to extracellular chemistry verify the location technique.

The techniques employed in this experiment produce artifacts resulting from hydrated sample preparation and examination as well as frozen dried sample preparation and examination. Some of these artifacts have been discussed at length earlier (for example see Gardner et al., 1979, Lewis and Pawley, 1979, Hayes, 1980, Pawley et al., 1980, Bullock et al., 1980, Hook et al., 1980, Bastacky et al., 1983, Beckett et al., 1982, and Read et al., 1983), and will not be repeated here. Other artifacts particularly germane to the analysis of samples within aqueous environments were

addressed in the Results section of this thesis. One additional artifact, believed to be the result of incomplete dehydration, is presented in figure 44. Although the C/HES matrix appears dried in both samples, the cells appear hydrated. These two mesenchyme blastulae are typical of embryos contained in two separate samples which were frozen and examined at different times. The cell boundaries are vague throughout the epithelium. There is either cell loss (at the arrow) or the ECM covering certain cells- is excessively thick. A horizontal sheath of blastocoel matrix was present within all of the blastocoels which contained at least half of their original volumes. The dark charging is also typical. Because cells divide asynchronously, it is unlikely that the poor definition of cell limits is due to mitosis. Samples which display these characteristics may be returned to the drier for further dehydration or heated through conductive or radiative techniques until the images appear more typical of dried samples.

A second artifact signifying severe damage to the PM cells during microprobe examination deserves further discussion (see figures 13 and 45). This damage was not observed in other cell types. Beam intensity and accelerating voltage were verified to remain constant during the damaging episodes. It is possible that the cells were unable to dissipate heat as effeciently as the cells in contact with the C/HES matrix surrounding the epithelial shell. Dubochet (1981) reported a dependence of visible beam damage upon

thermal and electrical conductivity. The PM cells exist in an environment quite different from that of the other cells. The blastocoel fluid does not appear to contain high ionic concentration, but rather to contain a highly ionic matrix. The high resistance ice which contains a low resistance web does not conduct heat (or charge) as readily as the C/HES/sea water surrounding the epithelial shell. The resistance of ice is approximately 5 nOhm/m whereas the resistance of saltwater is reduced to the μOhm/m range (Hobbs, 1974). Although this study originally intended to concentrate upon the PM cells and their migratory behavior, data from only one PM cytosol in one mesenchyme blastula remained valid after the criteria for acceptibility were applied. A future solution may be to reduce the beam current and accelerating voltage. This reduces the x-ray yield and requires a more efficient detector system. A model for such a detector exists in the experimental work being conducted on annular HgI detectors which produce low resolution spectra, but operate at ambient temperatures (Iwanczyk, 1984). A low voltage, low current microscope equipped with an annular detector and computer enhancement program should produce acceptable x-ray analyses of uncoated, frozen hydrated specimens. Without such a system, this experiment demonstrates an inherent difficulty in attempting to investigate structures which cannot be coated or surrounded with conducting material. This includes cells enclosed within structures, such as the PM cells of sea

urchin embryos, and multi layered structures.

The artifacts unique to samples stored longer than three months might be explained by a slight shrinkage of the C/HES bead away from the carbon stub. The bead would then sit upon the stub, secured by a protrusion into the depression, but no longer anchored to the sides of the depression. In this case, fracturing would no longer produce a smooth plane, but rather catch and chatter as the bead wobbled within the confines of the depression. Knife chatter, compression pits, secondary contact points (ridges) and sporadic pitting commonly occur when samples lack proper stability. Frequent dislocation of the bead from the stub would also be expected. A number of other artifacts could be caused by reduced contact between bead and stub. The sample would accumulate charge, producing aberrant electrical field effects. The heat sink would no longer include the stub, shuttle and stage. Furthermore, the Joule-Thompson refrigerator would no longer cool the samples effectively, resulting in sublimation of ice within the vacuum of the microscope specimen chamber. Separation of the bead from the stub would not explain two remaining artifacts indicative of the material stored longer than three months: separation of the epithelium from the hyalin membrane and damage to the blastocoel matrix. Similar artifacts have been noted in stored material which was not embeded within a matrix. Carr et al., (1985b) froze and stored mouse gut in LN_2, and later clamped the frozen stored

material within a specimen vice for fracturing, coating and examination. They also also noted changes in P/B data which caused them to conclude that fresh material is advisable for morphological and x-ray analysis. The introduction of ice between epithelium and hyalin membrane and perforation of the matrix material could result from ice crystal growth within the stored material. Steinbrecht (1985) has recently reported experiments performed with biological samples in amorphous ice which explored the effects of heating on crystal formation and growth. He discovered a time and temperature dependence which implies that even at very low temperatures (100K) ice crystal growth can be considerable over long periods of time. This crystal growth depends upon environment for size and shape. The blastocoel matrix suffers numerous small perforations, suggesting the growth of many ice crystals originating from small, frequent nucleation points. The ice between the hyalin membrane and epithelium is smooth and sheet-like, apparently following the hyalin membrane. Although the cause of the morphological deformation remains speculative, any specimens stored in LN_2 require careful comparason with recently frozen material.

Charging Phenomena

The occurence of charging noted previously have been documented and the physical basis is understood (Wells, 1960, Everhart, 1968, VanVeld and Shaffner, 1971, Pawley,

1972, Everhart and Hayes, 1972, Marshall, 1975, Shaffner and Hearle, 1976,). That these effects seldom transpire simultaneously in frozen hydrated samples undergoing x-ray microanalysis has not been discussed. Figure 46 illustrates the electric field set up within and immeiately above the sample during the 5 types of charging identified earlier. The sampling volume beneath the raster is represented as two metal plates, one on the surface and one at some depth within the specimen. The electron beam supplying electrons to the system is analogous to a conducting lead. Because the interaction volume extends some distance into the specimen, the primary electrons tend to accumulate below the surface. This is represented by the negative metal plate. In a conducting material, these electrons are drained to ground (i_g). The electrons passing through the sample eject secondary electrons, which escape from the sample when they are generated close to the surface. This results in an electron depletion region, which is represented as the positive metal plate. The escaping secondaries are represented in the figure as a conducting wire exiting the system (i_s). Two electrical fields are represented: the external field (E_x) and the specimen field (E_s). In a conductor, figure 46a, the E_x equals 0 (ignoring the field set up by the Everhart-Thornley detector). In order that no charge accumulate within the sample, the current entering the sample (i_B) must equal the two currents leaving the sample ($i_s + i_g$). If they do not, the sample becomes a semiconductor, and charg-

ing occurs. These cases are of current interest. Figure 46b, demonstrates the fields set up which contribute to the most common type of charging, an increased emission causing bright areas in the image (Everhart and Hayes, 1972). Here the lead to ground is impaired because of incomplete pathways (i_g is reduced to some small value, ϵ). The actual charge accumulation is small. A small external field, E_x, is generated between the escaping electrons and the surface. The trajectory of the secondary electrons can be affected if the E_x is accompanied by changes in topography or texture (Pawley, 1972). A strong, local E_x can occur such that secondary electrons are directed back into the sample, instead of the detector. This case is depicted in figure 46c, where the deflection current (i_d) nearly equals the i_B, and both i_g and i_s are small. Figure 16 illustrates the resulting secondary image where the fields are set up by the changes between the C/HES matrix and embryo. The transient discharge of secondary electrons is caused not by a stronger external field but a narrower one (McKay, 1948, Pawley, 1972), allowing for electron tunneling. Field emission produces the resultant sporadic discharge of secondary electrons. The last two schematics of figure 46 address the charging conditions detected during x-ray data collection. In figure 46e, the E_x may not be significantly altered, but the charge separation within the sample results in a large E_s which acts upon the primary beam electrons as they enter the sample (Brombach, 1975, Fuchs et al., 1978). Decelera-

tion is rapid; the interaction volume becomes pancake shaped (Echlin, et al., 1982). A reduction in x ray production and an increase in backscattered primary electrons occur. The number of backscattered primary electrons is proportional to the stopping power of the sample (for review see Niedrig, 1978). These backscattered electrons cause stray x-ray emission from parts of the specimen chamber containing Al as well as parts of the sample not observed in the secondary image. When i_g is small enough and the work function of surface (determines i_s) is high enough the sample resembles an insulator and the resultant E_x may become strong enough to affect the beam of primary electrons (Weitzenkamp, 1969, Van Veld and Shaffner, 1971). In this case (figure 46f), the E_x will reduce the energy of electrons entering the sample, or deflect the beam along equipotentials so that x rays arise from areas of the sample not chosen for examination. Because the secondary current is not negatively affected by the reduction in V_o, the secondary image may appear completely normal unless the beam is deflected. Because backscatter decreases with decreasing V_o, a high Al P/B ratio would not be expected to coincide with spectra exhibiting a truncated bremsstrahlung. Figure 46 demonstrates that each of these phenomena is explained by different physical states. Although it is not peculiar to observe more than one, or for a particular image to exhibit different effects at different times, simultaneous charging effects are not anticipated. Furthermore, the recurence of identical

phenomena at identical locations (beam damage) could be explained by the permanent alteration of the conducting qualities of the biological material. Monitoring the P/B ratio for Al is not sufficient for detecting sampling volume irregularities. Finally, the importance for developing an adequate grounding mechanism for samples which are to be microprobe analysed cannot be overemphasized.

Elemental Analysis

The x-ray mapping proceedure proved to be unsatisfactory for two reasons. First, the data were collected from frozen dried samples. Maps could not be created from hydrated material; the P/B ratio of any element within a 10 µm section was too low to provide discernable images. This resulted in interaction volumes within the blastocoel at least as deep as the blastocoel. The distance an electron will travel within a material depends upon the probability of interactions which depends upon charge and density. Although it is difficult to estimate the density of the dried blastocoel, assuming the blastcoel is 90% water, the interaction volume for Na is 131.7 µm deep at 15 KeV initial energy, according to the formula of Echlin et al. (1982). To compensate, the accelerating voltage was reduced to 10 KV. X-ray maps are actually three dimensional projections of the blastocoel onto its surface. Gradients may be masked because the poles contain less volume and subsequently a smaller content. An image within a noisy background must

contain 5 times as many exposed pixels before the eye can detect it (Goldstein et el., 1981). A low concentration precludes this criterion unless the element occurs in small pockets of high concentration. The signal for Na, Cl, and K is sufficiently high that there is no problem in discriminating the location of the element but gradients may be obscured. S and P have high background and are therefore more difficult to discern.

The P/B ratios presented in figures 26 through 38 exhibit large standard errors of the mean. This variation may be due to differences between individuals, sampling locations or experimental runs. Since up to 3 embryos constituted a continuous experimental run (lasting approximately 20 hours), and the variations amoung these individuals were as large as those from separate runs, it is unlikely that the errors arose from variations between sampling runs. Furthermore, these 3 embryos were often located in a single C/HES/sea water bead, fixing the physical parameters for a particular run. It is unlikely that differences in topography influenced the errors for two reasons. First, the criteria for a flat surface normal to the beam at 0° stage tilt were rigidly applied. Second, Statham and Pawley (1978) showed the P/B ratio to be relatively independent of local topography. The P/B ratios for a particular element within each embryo are more consistent. Data of this phenomenon are presented in table 2. Two elements, P and S, have been selected as representative. Two cellular volumes, Anl and

An2, and one extracellular point, the ECM, were selected as random examples. Under the experimental numbering system, 200 signifies blastulae, 300 signifies mesechyme blastulae, and 400 signifies gastrulae. Individuals were numbered 201, 202, etc. Averages in table 1 contain all points (minimum of 3) from all of the embryos at each developmental stage (one embryo for each entry in the lower half of the table). Although the standard deviations (SD) throughout the table appear similar, it is clear that the variation within an embryo is smaller when expressed as a percent of the mean. The considerable variation within individuals is not unusual. Errors as large as 12% resulting from fractured surfaces have been predicted by Boekstein (1980, 1985). Other authors have predicted slightly smaller errors (Hess 1980, Marshall, 1981, Statham and Pawley, 1978). Large variation between individuals has been noted by Echlin et al. (1982), and Taylor and Echlin (1985) in botanical material, Carr et al. (1985b) and Fuchs and Fuchs (1980) in mamalian tissue. The universality of this phenomenon is impressive and speaks directly against the practice of chemical analyses which require averaging over millions of individuals to arrive at cellular characteristics.

The result of correlation matrices comparing chemical similarities between cells are presented in table 2. Only points within the cytosol were compared (extracellular points were influenced by variations in the amount of biological material contained in the sampling volumes). A

perfect correlation is equivalent to 1.000; any correlation over 0.300 is noted (large fluctuations in the data result in low correlations). The most striking correlations occur between the gastrula PM cells and the An1 cells, appear in three elements (P, S and K) and nearly equal 1.000 in all three cases. This correlation suggests that the migration into the animal hemisphere may alter the PM cells into An1-like cells. Gastrulae An2 and Veg1 cells (the equatorial region of the embryo) correlate in the same three elements to a lesser degree (all approximately equal to 0.5). The calcium content of the PM cells is comparable only to the An2 cells. Because the Ca flux within the mesenchyme ring is unique, the specific content of those cells at any given time does not reflect intracellular function, but rather transient concentration during Ca transport to the skeleton. At the mesenchyme blastulae stage, the cells in the vegetal half of the embryo show correlations although not as high as in the gastrulae. The An1 cells are similar to both the Veg2 cells (correlations approximately 0.60) and the Veg1 cells. In fact, only the An2 cells of the mesenchyme blastulae exhibit little similarity to the other cells of the epithelium. The blastulae exhibit the greatest degree of variation. The An1 and Veg1 cells have similar Ca and P content, possibly a prelude to shape changes as the oral plate forms and ingression begins. The only noteworthy correlation occurs between the An1 and presumptive PM cells' K content. Mn exhibited no close correlations. Mg content

is similar in the Veg2 and PM cells of both the blastulae and mesenchyme blastulae. Table 2 demonstrates that the animal and vegetal poles are not necessarily chemically distinct, nor are any consistent similarities detected throughout the three stages investigated.

For complete analysis, it is necessary to compare the correlations in table 2 to figures 26 through 38 (some information is not reported in these figures because of criteria for a minimum of 3 points per embryo and 3 embryos per type). In the early gastrulae, P, S and K are all lower in the An1 and PM cells than in the other cells of this stage. This is not a sign of systematic error; the S content of the Veg2 cells is significantly higher. The An2 and Veg1 cells of the early gastrulae are not so consistent. The P content is higher than in the remaining cells, but the S and K contents are in the midrange. In the mesenchyme blastulae, the An2 cells, yielded apparently lower P/B ratios for P, S and K. The differences however are not significant (less than 70% confidence for each). In the blastulae, Ca is higher in the An1 and Veg1 cells, but P is lower. The An1 and presumptive PM cells are high in K. The An2 and Veg2 cells are high in P.

Divalent cations, Ca^{+2}, Mg^{+2} and Mn^{+2}, have been implicated in a number of proliferative and differentiation events. Balk et al. (1879) reported that Ca or Mg ions must rise above a critical level to initiate fibroblast

replication, and it is apparently this activity which lacks control in neoplastic cells. Levenson and Housman (1980) reported that Ca^{+2} is necessary for erythroid differentiation as a triggering mechanism; Hennings et al. (1980) reported the effect of Ca^{+2} on the terminal differentiation of mouse epidermal cells, and Bridges et al. (1981) reported similar effects in erythroleukemia cells. Others have also reported that Ca^{+2} is involved in cell proliferation (Sawyer and Cohen, 1981, Winkler et al., 1980). Metcalf et al. (1980) reported a large Ca^{+2} influx associated with Con A introduction. Embryonic induction effects were reported by Takata et al. (1981). With the exception of Balk et al. (1979), the above work found Mn and Mg not to be suitable substitutes for Ca in the processes under investigation. In fact, Ca^{+2} and Mg^{+2} often appear antagonistic. They are nonetheless all involved in the construction and maintainance of the cytoskeleton which has implications in differentiation and proliferation (for example see Roberts and Hyams, 1979, Weeds, 1981, Inoue, 1981). Grinnell (1978) reported that high concentrations of Mn enhanced adhesion (even in serum free cultures). High concentrations of these ions may signify a particular cell has a potential for differentiation, division and intracellular rearangements, although this experiment does not differentiate between free and bound states. Processes which depend upon transmembrane influx of ions appear only during the transient increase, and cannot be separated from cells with

long term high content (although the deviations will most likely be large).

Another ionic mechanism associated with cell differentiation and proliferation is the Na/K flux across the plasma membrane. Rozengurt et al. (1981) reported that increased Na^+ entry into quiescent mouse (Swiss 3T3) cells stimulated DNA synthesis, and Mendoza et al. (1980b) showed that vasopressin, a powerful mitogen, stimulated the Na^+/K^+ pump. This evidence suggests that a Na^+ influx triggers the Na^+/K^+ pump and results in proliferative activity. Furthermore, one might expect a subsequent increase in K as the influx is removed. Mendoza et al. (1980a) indeed found an increased ^{86}Rb uptake stimulated by serum and verified increased intracellular K^+. The verification of increased intracellular K is important to the experiment reported herein because, although many authors have reported a Na^+ influx associated with proliferative effects (Koch and Leffert, 1979, Moolenaar et al., 1981, Rozengurt et al., 1981) the detection of Na is difficult in hydrated material. Because high K is also implicated in cellular adhesion (Rappaport 1971) interpretation of the P/B changes must be made cautiously.

The P content of the cell may be associated with the energy potential, which is separate from the cytoskeletal activities requiring the previous elements. The majority of P is contained in cyclic nucleotides, nucleotide phosphates,

high energy glycolysis products (PEP, etc.), creatine phosphate, and so on. Thus a cell presenting a low P P/B ratio might be less active metabolically than a cell with a higher content. This simplistic view is complicated by the fact that cyclic nucleotides have been implicated in differentiation and proliferation (Brooker et al., 1979) and protein phosphorylation (Pawson et al., 1980, Kurth et al., 1981).

The investigation of S within the cell and ECM has enjoyed recent popularity among developmental biologists. Extracellular S, in the form of SO_4 moieties attached to glycans within the blastocoel matrix and ECM, has been implicated in translocation of the PM cells (Gibbins et al., 1969, Karp and Solursh, 1974, Katow and Solursh, 1981), cellular adhesion (Sugiyama, 1972, Laterra et al., 1983) and ingression (Akasaka et al., 1980, Mizoguchi et al., 1983). Heparin sulfate, chondroitin sulfate and dermitan sulfate appear in the basal lamina and basement membranes of various organisms (Hay, 1981) including the sea urchin embryo (Katow and Solursh, 1981, Solursh and Katow, 1982). Intracellular S may either be in the process of exocytosis (Roff et al., 1983, Akasaka and Terayama, 1980), or may be destined for intracellular functioning (Kinoshita and Saiga, 1979, Kinoshita and Yoshii, 1979, Furukawa and Bhavanandan, 1983). The intracellular P/B ratios will be accordingly compared to the extracellular P/B ratios at both the concurrent stage and the subsequent stage (for blastulae and mesenchyme blastulae) for a qualitative evaluation of the final destination

for intracellular S.

A review of the previously reported clustering with respect to the physiological events reveal interesting trends. At the blastula stage, the similarity of the An1 and Veg1 cells which exhibited high Ca P/B ratios was noted. The An1 cells, which are elongating to form the oral plate, would require elevated Ca for the increased contact and cytoskeletal activity involved in the elongation process. It is surprising that the Veg1 cells contain increased Ca at this time. The conclusion that the An2 and Veg1 cells are actively thinning is unlikely because there is little correlation between those two cell types. It is possible that the Veg1 cells were actively dividing at the time of freezing. The reported large deviations would be expected in a population of dividing cells because of influxes and variations between dividing and quiescent cells. Cell division becomes asynchronous at the fourth division, possibly due to the difference in cell size (Gufstafson and Wolpert, 1967). Low metabolic activity would be expected for nutritional conservation and, in fact, the P content does not vary widely throughout the three stages examined. It is not surprising that the Veg2 and presumptive PM cells contain similar Mg, as they are undergoing similar morphological rearrangement prior to ingression. The S content of the Veg1 and presumptive PM cells is significantly higher than the other cells of the blastula, a result which agrees wi' earlier reports of the presumptive PM cells and associated

highly sulfated ECM (Motomura, 1960, Sugiyama, 1972,). The high content of the Veg1 cells was not expected. Because the local basal lamina and ECM of the mesenchyme blastulae exhibited unchanged levels of S it appears that this S is not extruded from the cell between the blastula and mesenchyme blastula stages. The final destination of the S within the Veg1 cells must be intracellular. The S content of the Veg1 cells drops insignificantly in the mesenchyme blastula data (it remains the highest intracellular level of that stage as well) and returns to the blastula level in the early gstrula, also implying that the S remains within the cells.

The An2 cells of the mesenchyme blastula stage are the only cells within the epithelium which appear to have different elemental content, but their variations are not statistically significant. The data imply a moderate activity for the mesenchyme blastula ectoderm. The low S content of the Veg2 cells is also not significant (75%), but may suggest a lower sulfated GAG secretion during the mesenchyme and early gastrula stages, a conclusion which is supported by the basal lamina and ECM data for these two stages. The basal lamina over the area destined to become the archenteron may be disintegrating during the mesenchyme blastula stage, and is absent over the archenteron (Ettensohn, 1984). The slight increases in these sampling volumes during the early gastrula stage is due to the overlapping of the volume into the cytosol, which experiences an increase in S. The

vegetal pole of the mesenchyme blastula blastocoel has been reported to be heavily sulfated (Akasaka et al., 1980). In view of these results, the majority of the sulfated proteoglycan within the blastocoel matrix is the product of the PM cells. This is further supported by the (single) low S content of a recently extruded PM cell (P/B = 0.021). Apparently, the S within the presumptive PM cell is secreted into the pericellular material during ingression and then transferred to the blastocoel matrix. The S content of the early gastrulae is again at or below average.

At the gastrula stage, the P, S and K content is again consistent, particularly in the equatorial zone. The Anl and PM cells exhibit lower quantities, signifying less exocytotic activity (of S) and less metabolic activity. Ca is apropriately low in these cells, if the above hypothesis is correct. This is an unexpected result for the PM cells, which are known to be elaborating filopodia prior to intertwining and laying down the calcium carbonate skeleton of the pluteus (Inoue and Okazaki, 1977, Harkey and Whitely, 1980). A preliminary hypothesis for this low Ca reading may be that the Ca is sequestered within the filopodia, which were not examined in this experiment because of the resolution limits of the sampling volume. The Veg2 cells and the PM cells showed higher K as well. This result might seem incongruous in the PM cells, which are not dividing at this time, but the P/B ratio is no greater than that of the presumptive PM. It is likely that the K content is

associated with filopodial activity: the invasion of the basal lamina at the late blastula stage and the formation of the syncitial cable at the gastrula stage. This conclusion is supported by McCarthy and Spiegel (1983a), who reported a requirement for horse serum at this precise stage of development in the PM cells. If the serum is not provided, the syncytium will not occur. Serum has been implicated in the activation of the Na^+/K^+ pump (Mendoza et al., 1980, Moolenaar et al., 1981). The high K content of the Veg2 cells however more likely reflects proliferative activity, supporting the claims of Agrell (1953) and Ettensohn (1984). The present data do not support Agrell's conclusion that all of the cells of the epithelium are undergoing division, but demonstrate relatively high K only in the vegetal cells (particularly surrounding the archenteron pore). This would imply a proliferative variation of invagination where additional cells are passed into the archenteron. Ettensohn reported that the cell number of the archenteron nearly doubles (from 66 to 120 in Lytechinus pictus) during invagination.

The correlations displayed in table 2 suggest the hypothesis that cells exhibit chemical contents within a physiological range, and cells at the upper and lower limits of the range will have high correlations. Similarity in content does not necessarily imply similarity in function. Cells which may have similar functions in the blastulae are the An2 and Veg2 cells. The ectoderm of the mesenchyme

blastulae appears to be functioning as a unit. The equatorial cells of the early gastrulae continue to function similarly. Other similarities appear to be coincidental, caused by high or low activities producing different end products.

Other cell functions and morphogenetic trends do not appear in clustering patterns. A significant increase in the amount of K (figure 29) within the Anl cells occurs between the blastula and mesenchyme blastula stages. Because this occurs during elongation of the oral plate the higher K content suggests increased adhesion (Rappaport, 1971) during elongation. Although the Ca content decreased during this same period, the data for the blastula stage exhibited large variability, which may be related to transmembrane flux and the hatching process, rather than cytoskeletal activities. Like the mesenchyme blastula Anl cells, the mesenchyme blastula and early gastrula Veg1 cells, the early gastrula Veg2 cells, and the early gastrula PM and Arch all produced relatively high K P/B ratios (above 0.2). With the exception of the vegetal cells, all of these cells are undergoing obvious shape changes, which implies that K influx is associated with differentiation initiation. However, it is possible that the increase in K within the vegetal cells of the early gastrula is associated with proliferation.

The Anl cells contain significantly less S prior to

elongation of the oral plate. Because S of the ECM and basal lamina is concurrently high, it may be that S is passing through the An1 cells rapidly enough that cellular content remains low. The presumptive PM cells contain high S content; the blastocoel and ECM volumes read low at this stage. The extracellular S surrounding the PM at the mesenchyme blastula stage (labeled "BC" rather than "ECM" because the sampling volume overlaps the blastocoel and not a neighboring cell) increases significantly after ingression and intracellular S decreases simultaneously. This strongly suggests a shedding of the S into the blastocoel. Extrusion of S from the Veg2 cells into the ECM takes place during ingression as the Veg2 cells migrate into the space previously occupied by the mesenchyme. Intracellular S falls between the blastula and mesenchyme blastula stages and rises again by the early gastrula stage. This semi-quantitative analysis agrees with the qualitative description provided by Sugiyama (1972).

In the blastula, the P content of the animal cells suggest a higher metabolic rate than cells of the vegetal pole. The P content of the An1 cells of the mesenchyme blastula stage increased over the blastula content, but in the early gastrula the An1, An2 and Veg1 cells may all experience increased metabolic activity. Bedard and Brandhorst (1982) reported that 20% of the S. purpuratus protein synthetic rates change during development, most of the changes resulting in 10 to 100 fold increases in synthesis. They reported

that most of the new material first appears between hatching and ingression, with another occurance prior to invagination. Figure 31 illustrates a progressive increase in P incorporation into the embryos, perhaps reflecting the synthesis of new proteins. It is interesting that the animal half of the embryo seems to be more metabolically active.

The Ca P/B ratios illustrated in figure 32 are closely clustered, with the exception of high An1 content of the blastula stage, and the low ratios of the early gastrulae PM (due to either rapid efflux or filopodial sequestration) and the archenteron cells. The low Ca of the archenteron strongly implies passive invagination. Considering the data from the Veg2 cells, which implies proliferation, growth and differentiation, it is likely that the archenteron is pushed up into the blastocoel by the Veg2 cells.

Figure 36 shows the P/B ratios obtained in mesenchyme blastulae (analysis of the blastulae was not possible due to the paucity of information from the An2, Veg1 and Veg2 areas) from the blastocoel and basal lamina volume, the cell volume, and the ECM volume. Although the An1 volume data for the blastocoel was not presented, the S tended to be moderate in the 2 embryos from which data was sucessfully obtained. A gradient of increasing S toward the vegetal pole is obvious. On the other hand, the ECM S remains constant. The lower reading from the Veg2 ECM is due to the low intracellular content since the sampling volume overlaps

that area. The cellular S content of the mesenchyme blastulae also does not vary, with the exception of the slightly lower reading from the Veg2 cells (not statistically significant). Possibly because the PM cells actively secrete S into the vegetal pole blastocoel, it may be unnecessary for the Veg2 cells to duplicate this process. Horstadius (1939) found that in embryos deprived of micromeres, the macromeres (ancestors of the vegetal cells) performed functions normally performed by the PM. Horstadius postulated that the embryo attempted to maintain a physiological gradient, a vegetal/animal gradient. According to this theory, if the PM cells were removed from the blastocoel, the Veg2 cells may begin to take up and secrete S to compensate for their loss. Figure 37 shows the change incurred in these profiles by the early gastrula stage. The gradient within the blastocoel has virtually reversed. The information from the An1 area was again sparce and the variation in the data for the An2 area is large (possibly due to variations in the amount of material within the sampling volume) but the trend is apparent. The decrease in blastocoel content within the Veg1 zone may relate to the mechanism by which the migration of the PM cells is controlled. It is possible that the animal pole S needs to be fairly high for the migration of the secondary mesenchyme and secondary gastrulation. The S void would not affect the secondary mesenchyme; those cells are elevated past that zone by the first stage of invagination. The only ECM volume which experienced extraordinary S

content was the Anl cells, possibly due to the impending fusion of the gastrointestinal tract. The cellular S experiences a gradient similar to the mesenchyme blastula basal lamina volume. If the uptake of S lagged behind the change in exocytotic activity, such an effect might occur. The PM cells exhibit loss in S content once they are no longer exposed to the S within the sea water and have released S into the blastocoel. These findings neither confirm nor deny the direct involvement of the $SO_4^{(-2)}$ moiety in in blastocoel location.

Conversion of the P/B Ratios to Cellular Concentrations

According to the theory proposed by Statham and Pawley (1978), P/B ratios may be converted to concentration by the formula

$$C_a = f(P/B)_a$$

where C_a equals a known concentration, $(P/B)_a$ equals a known ratio and f is a proportionality constant which may be calculated from the calibration data. This factor is constant for an element of varying concentration within a matrix of the same average atomic number. Ideally, the calibration standard should be identical to the sample from which the P/B ratios was collected. The internal normalization by the background requires that the standard and sample produce similar bremstraahlung. Wet standards, however, contain

large ice crystals which result in concentration variations. Whitecross et al. (1982) sugessted that colloidal carbon graphite dispersant may solve this problem as well as provide a medium for heat and electrical conduction. Echlin et al. (1983) tested standards using graphite and cryoprotectant and have investigated the effects of etching and carbon coating the standards (unpublished). The present experiment also used carbon graphite slurries, but it was found that the cryoprotectant was unnecessary to prevent large ice crystals. The standard deviations for the mean P/B ratios for each of 10 concentrations was less than 7%, indicating homogeneous mixtures in the frozen state. In order to reproduce the conditions present during examination of the biological samples, the calibration standards were processed in a manner identical to the samples. The C and salt solutions were mechanically mixed immediately prior to freezing, placed on C specimen stubs identical to those holding the biological samples, frozen on solid nitrogen, transferred to the preparation chamber, fractured, transferred to the microscope, maintained at the same temperature, and examined at the same angle. Criteria for smoothness of fracture and normal orientation to the beam were met. Microscope parameters were the same as during biological sample examination. Twenty random points on each calibration standard bead were exposed to the reduced raster ($25\mu m^2$) and the resulting x-ray emission was processed in a manner identical to that used for the biological sample. These 20 points were aver-

aged and plotted on a graph of P/B ratio vs. percent wet weight. The resulting graphs for S, Mg, K, and P are presented in figures 47 through 50. Concentrations for the unknowns may either be calculated mathematically or read directly from the graphs. The Y intercept for each of the least squares slopes is very nearly 0.00, as predicted by the conversion equation.

Boekstein (1980) has estimated a limit of error in P/B ratio due to uneven topography as plus or minus 12%. Table 3 lists percents wet weight ± 12% to allow for this error. This mean, however, does not represent the concentration of a particular element ± 12%, but rather the average ± 12% of the expected concentrations. Additional errors due to cell, individual and sample variations are not represented, nor are the systematic errors from collection and calculation. These errors were presented earlier (see figures 26 - 38) and discussed in table 1. The concentrations in table 3 represent total cellular content of all diffusible ions and bound molecules containing the elements listed. The low P concentration is possibly explained by isolation of P near the plasma membrane. This experiment avoided overlap of the probe with the plasma membrane except in the ECM sampling volumes. The P/B ratios of the ECM sampling volumes are not converted to concentration since their physiological content cannot be defined. It is also possible that stored lipid metabolism produces a lower cellular P content. It would be useful to confirm these results using either nuclear

activation or flame spectrophotometry of whole embryos, although the blastocoel contribution could not be removed from those results.

Conclusion

The present experiment has shown that microprobe analysis is proven an informative and practical technique for the exploration of some issues in developmental biology. X-ray microanalysis eliminates the necessity for micro-dissection or bulk analysis, and provides an analysis of selected cells without disturbing their *in situ* location. Several trends noted previously have been confirmed by this experiment and in turn the proceedure is validated by the repetition of results. Furthermore, several new trends have been disclosed. These trends have suggested a number of experiments which might be performed to investigate the influences of events upon the differentiation processes. The results presented here also prompt similar investigations of other species to explore the universality of these events. Although certain cautions must be exercised in order to preserve the tissue and avoid damage during analysis, the proceedure is fairly rapid and the manual techniques may be mastered within a reasonable amount of time. Coating the material with electrical and heat conducting material is recommended for any multicellular material with more than one cellular layer. The technique of embedding biological material in conducting material is

recommended for unicellular and monolayered specimens. Because of uncertainties in the P/B ratios (12%) and their conversions to concentration, this technique may be more valuable for comparison of relative concentrations than absolute quantitative information, although it provides reasonably accurate information obtained from individual cells *in situ*.

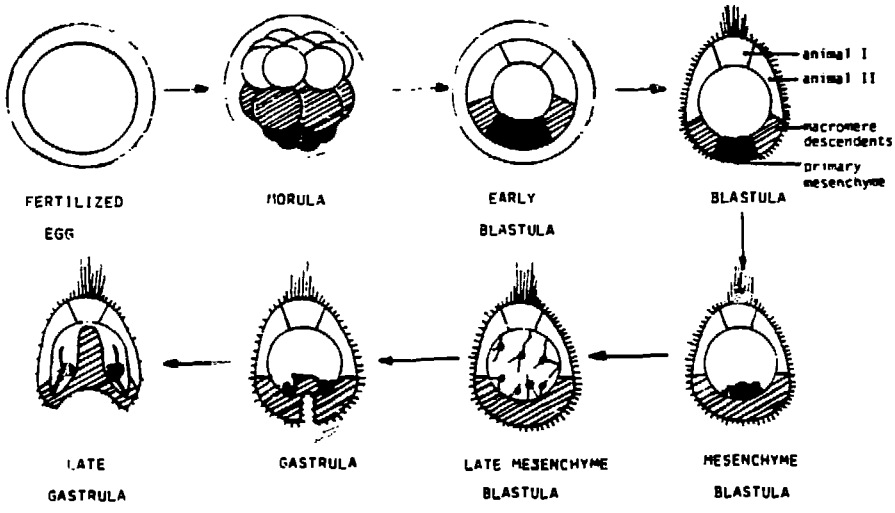

Figure 1. Diagramatic representation of the development of the sea urchin embryo, Strongelocentrotus purpuratus. This study is primarily concerned with the stages blastula through early gastrula.

Figure 2. Frozen hydrated (a) and frozen dried (b) sea urchin embryos embedded in a C/HES and sea water matrix bead. Four embryos are designated in both states. The two photographs were taken at the same stage coordinates.

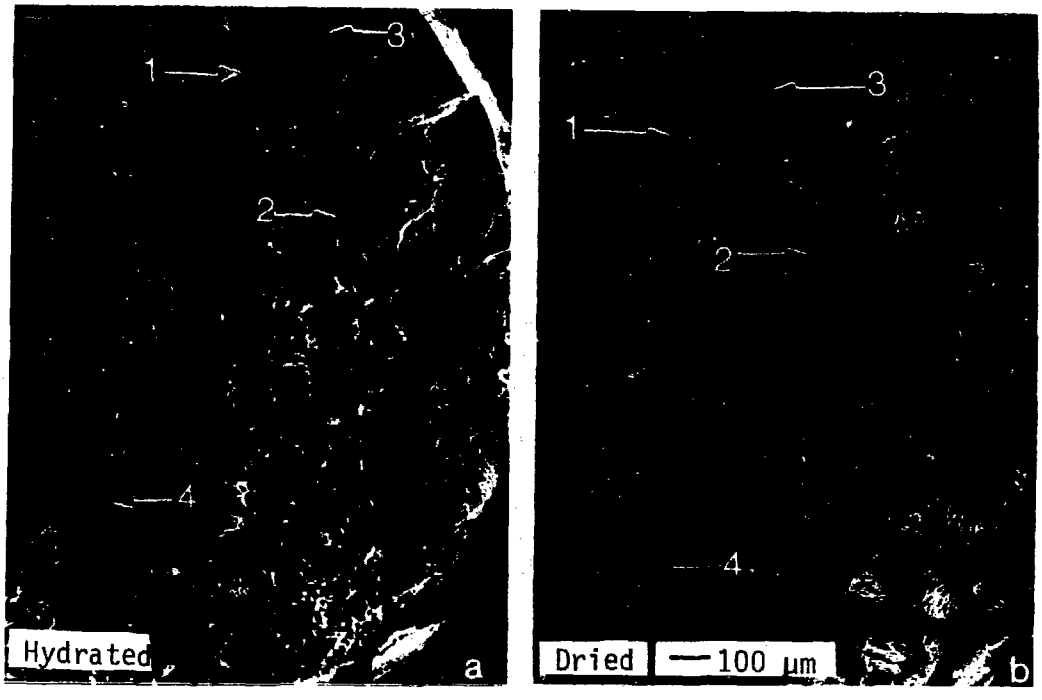

XBB 847-5627A

Figure 3. Preservation of biomaterial demonstrating the SEM freeze drying capabilities in chamber technique. The blastocoel material resembles that resulting from traditional fixation and drying processes. The arrow designates a point of contact between the basal lamina and the blastocoel matrix.

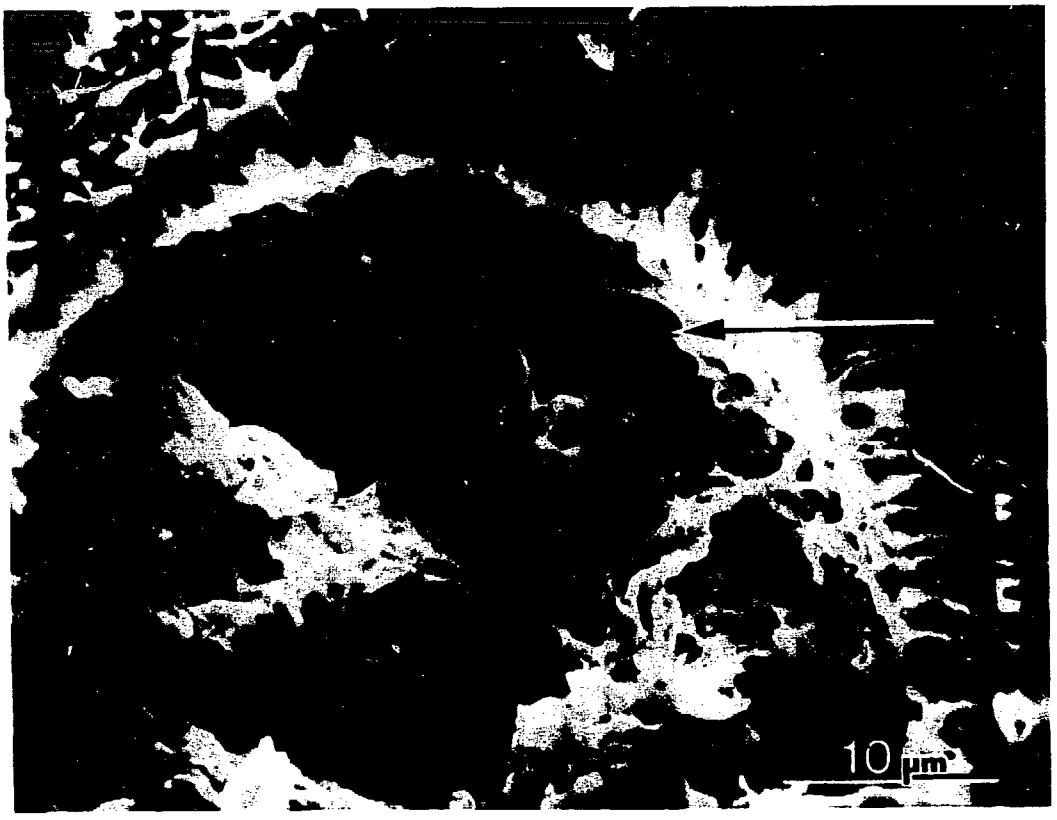

XBB 859-7616

Figure 4. Higher magnification of embryo #1 in figure 1b. The animal (A) and vegetal (V) poles and an invading primary mesenchyme cell are labled. The elongated cells at the animal pole form the oral plate.

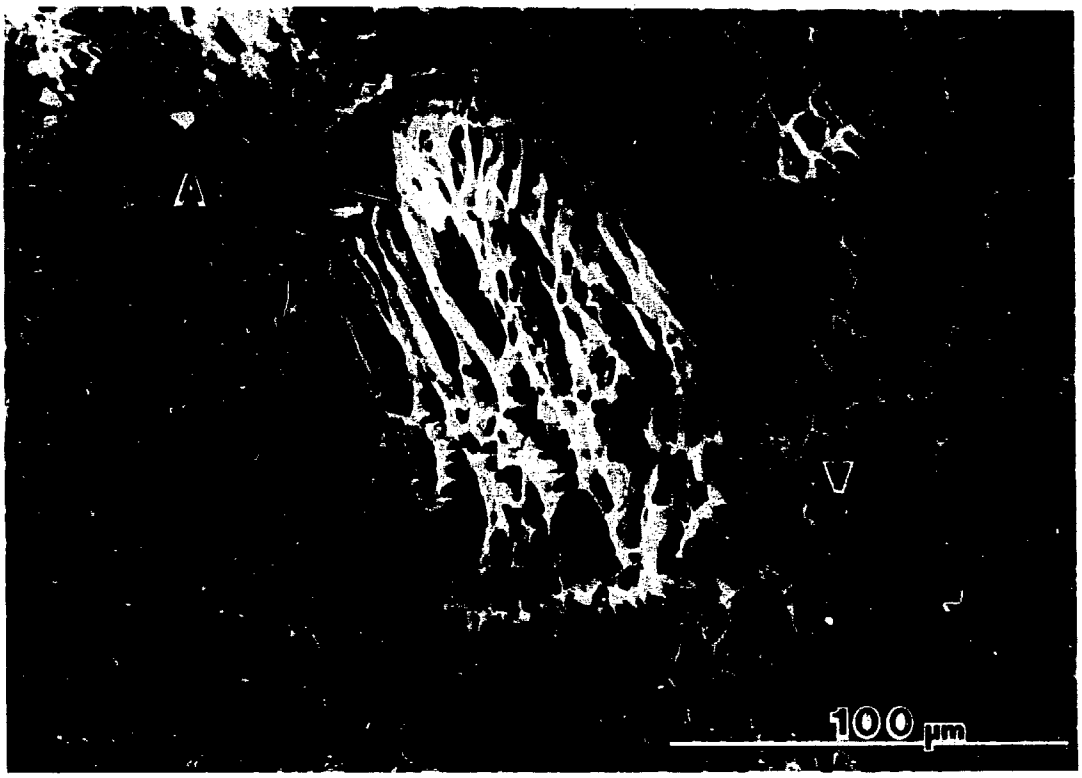

XBB 847-5623A

Figure 5. Higher magnification of figure 4 illustrating the tendency of fracture planes to run between cells, leaving the membrane intact. An intercellular fiber (IF) and a primary mesenchyme cell (PM) are denoted in addition to artifacts resembling the hyalin membrane (hm) and blastocoel matrix (bm).

XBB 847-5620A

Figure 6. Frozen hydrated mesenchyme blastula. Individual cells can be identified. Intercellular fluid (If) and a primary mesenchyme (PM) cell (a nearly perfect, faint circle situated on the ridge above the bright area) are designated. The encircled area exhibits the 1 μm beads seen only in hydrated embryos.

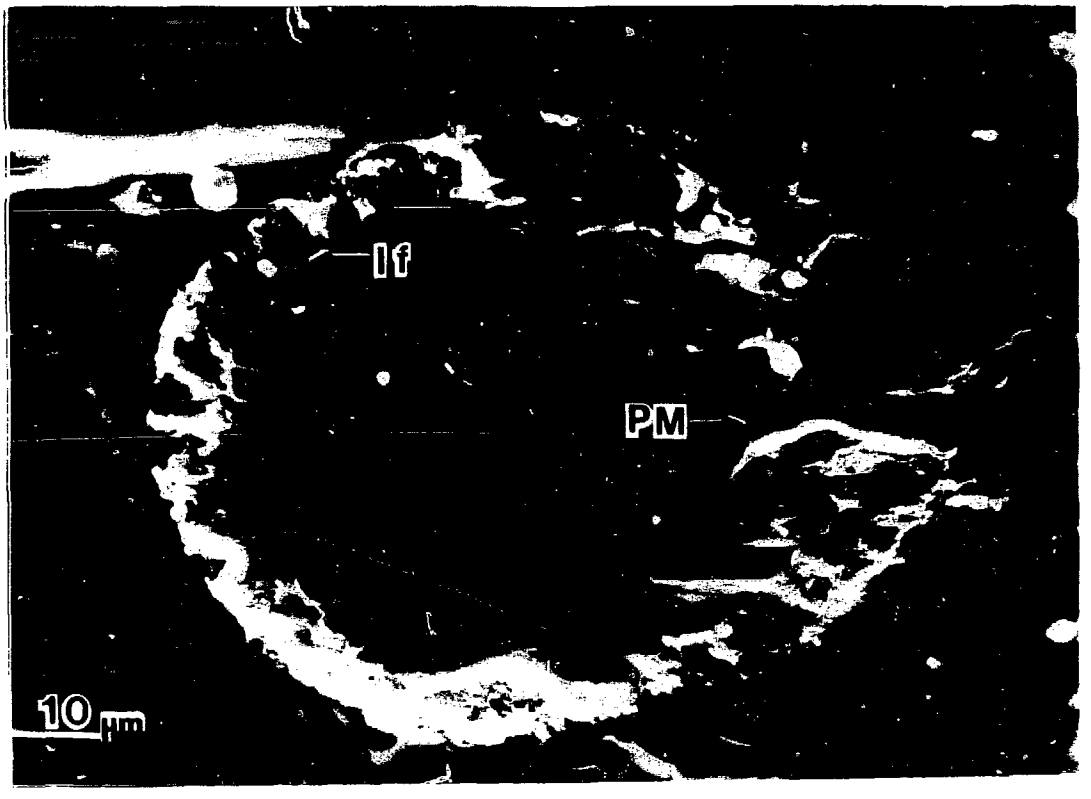

XBB 859-7617

Figure 7. Frozen hydrated (a) and frozen dried (b) images of a mesenchyme blastula. The frozen dried image verifies the animal pole is not on the fracture plane. The inset diagram shows a possible fracture plane. Three PM cells are designated in the hydrated image (arrows), the vegetal pole (V) and unknown arc (?) are labeled in the dried image. No data from the unidentified area (to the right of the line) was included in the quantitative analysis.

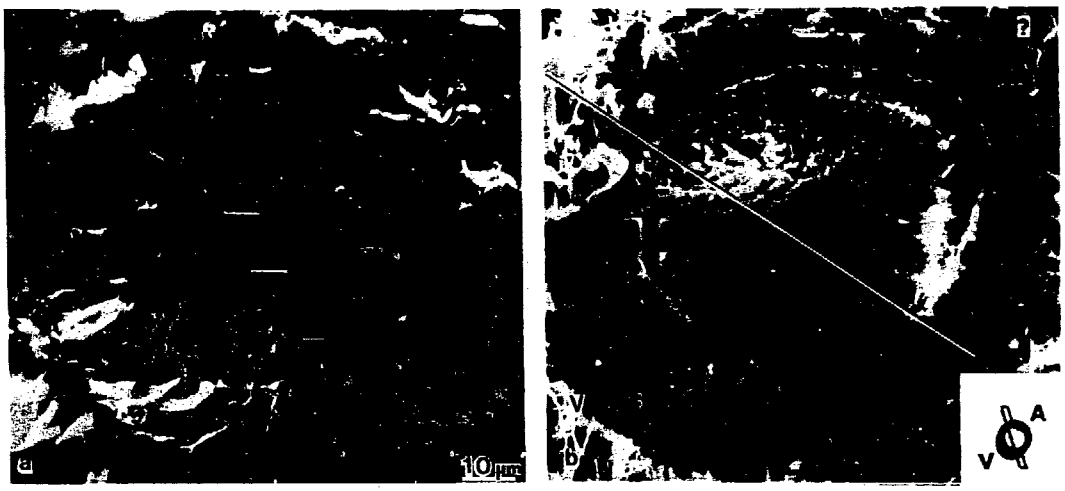

XBB 859-7618

Figure 8. Early gastrula where the fracture has fallen to the outside of the archenteron. The animal pole is not visible. The blastocoel (BC), archenteron (A) and two groups of PM cells (PM) are designated. Confirmation of the fracture plane location and PM presence was made with the aid of the frozen dried image.

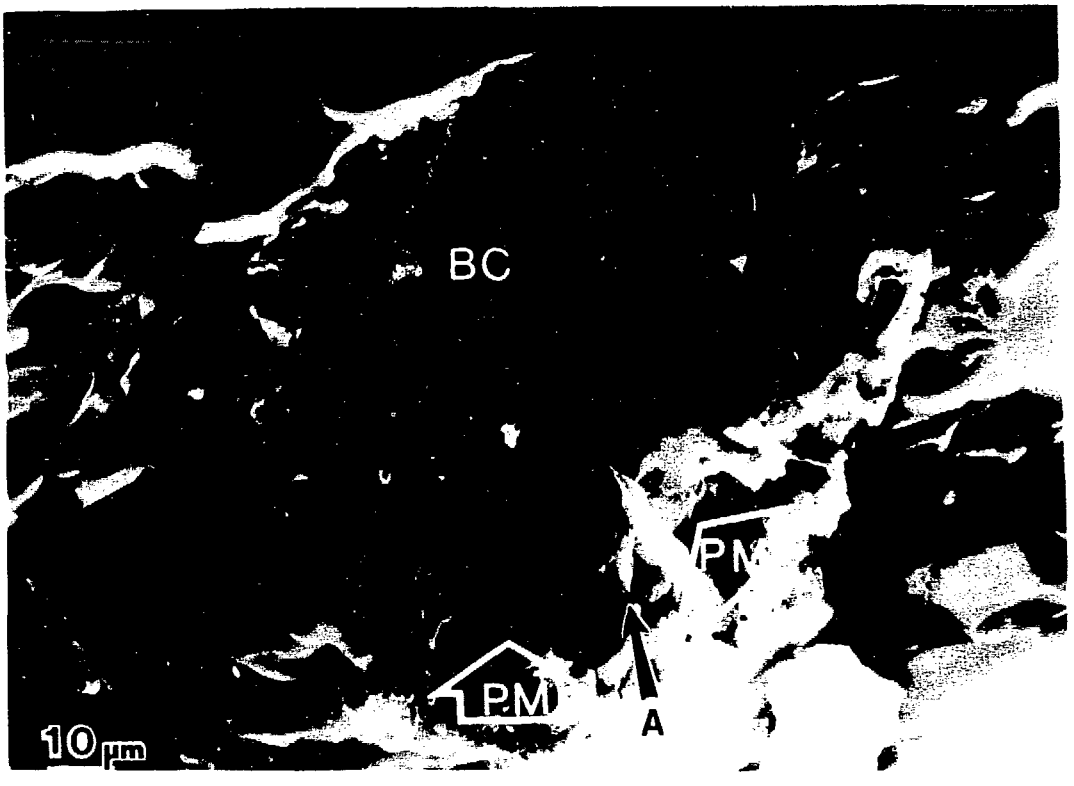

XBB 859-7619

Figure 9. Frozen dried image of an early gastrula where the fracture plane has fallen through the archenteron. Two groups of PM cells (PM), the archenteron (A) and thickened matrix (M) at the tip of the archenteron are denoted in the micrograph. The embryo has pulled away from the exterior C/HES matrix in drying and has exposed the hyalin layer (HL).

XBB 859-7620

Figure 10. Low magnification photograph of two frozen dried, early gastrulae. The oral plate (OP) is visible in the gastrula to the left. The thickened matrix at the tips of the archenterons is designated (M). The archenteron to the left was fractured through the invagination. The archenteron to the right was fractured on the blastocoel side of the invagination. The shrinkage of blastocoel matrix was not common.

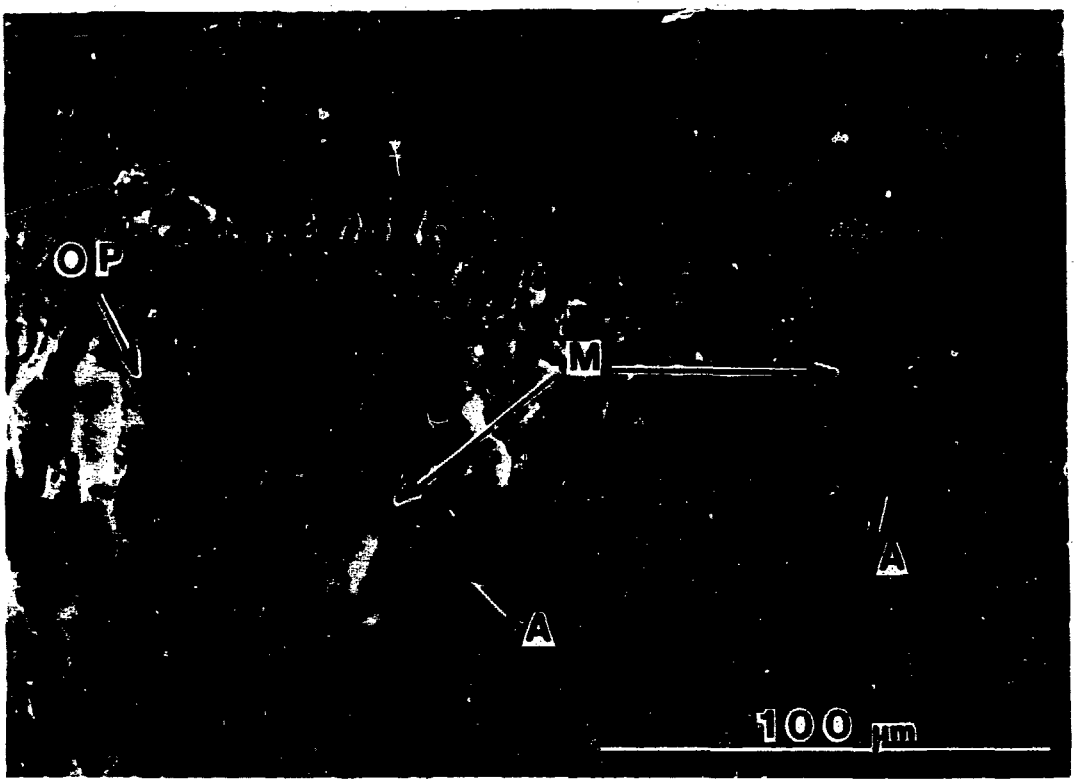

XBB 859-7621

Figure 11. Stereo pair micrographs of a fracture running through the archenteron of a late gastrula. The interior of the archenteron (A) and the blastocoel (BC) are labeled. The sample has been radiantly etched to reveal intracellular details. Possible exterior surface (ES), endoplasmic reticulum (ER), cytoskeletal elements (CS) and a mitochondrion (M) are labeled.

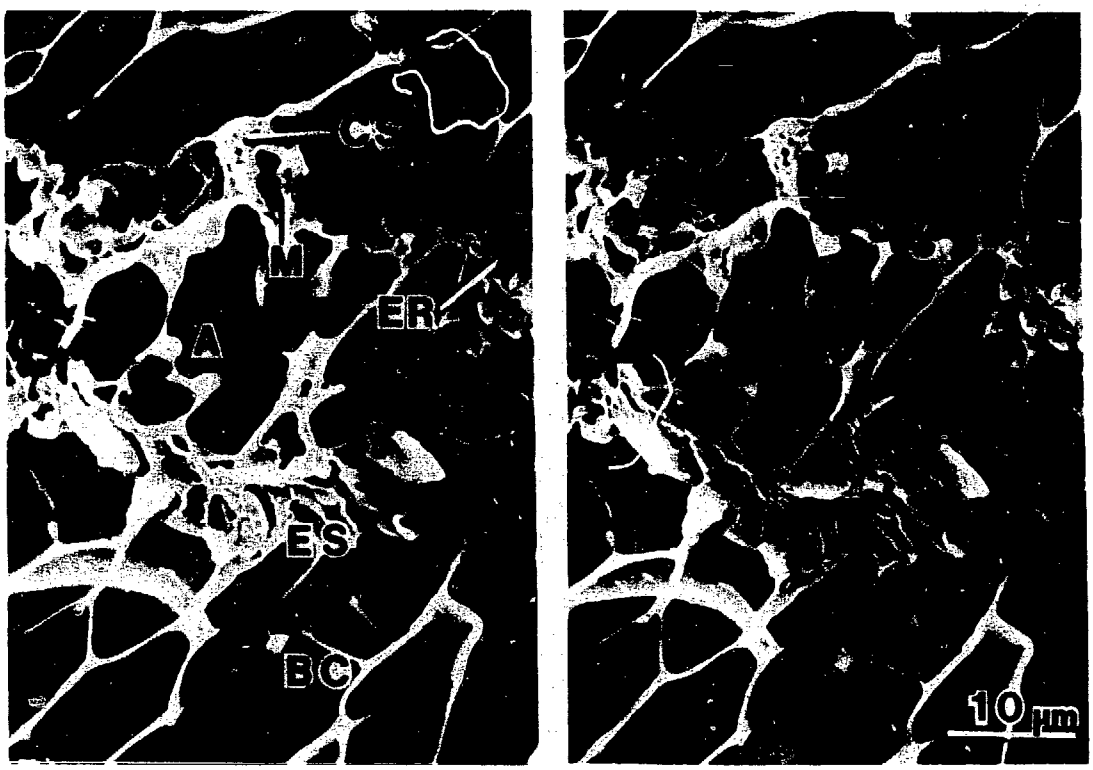

XBB 859-7622

Figure 12. Stereo pair micrographs of the extracellular matrix at the tip of the archenteron. The exteriors of the two secondary mesenchyme (SM) cells are designated. The archenteron was removed fr[illegible]bc beam side of the surface. Further dehydration caused [illegible]round damage to the delicate matrix, but confirmed the location of the archenteron. The matrix is surrounded by a continuous sheath. The 1 um beads of the ECM are evident. The white area is condensed ice contamination.

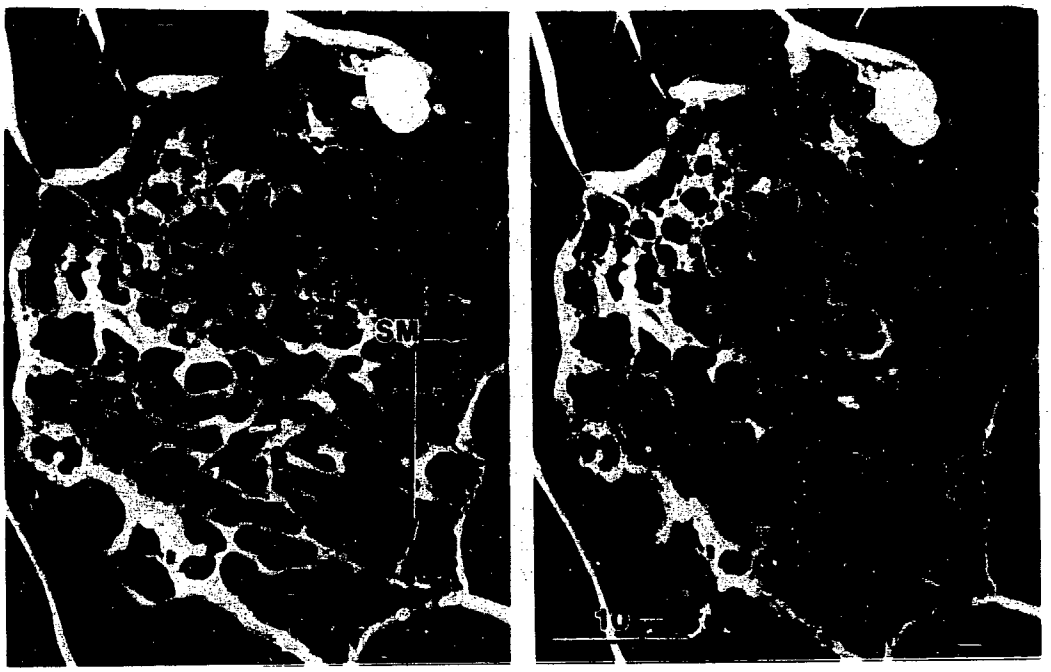

XBB 859-7623

Figure 13. Example of beam damage experienced by PM cells. The first image (a) was taken prior to data collection. The specimen was fully frozen hydrated at that time. An epithelial cell (EP) and 3 PM cells (PM) are designated. The second micrograph (b) was taken after data collection from the epithelium as well as the PM. Only the PM have experienced damage. The final micrograph (c) was taken after freeze drying. The damage is apparent in the PM cells but the epithelium shows no sign of damage.

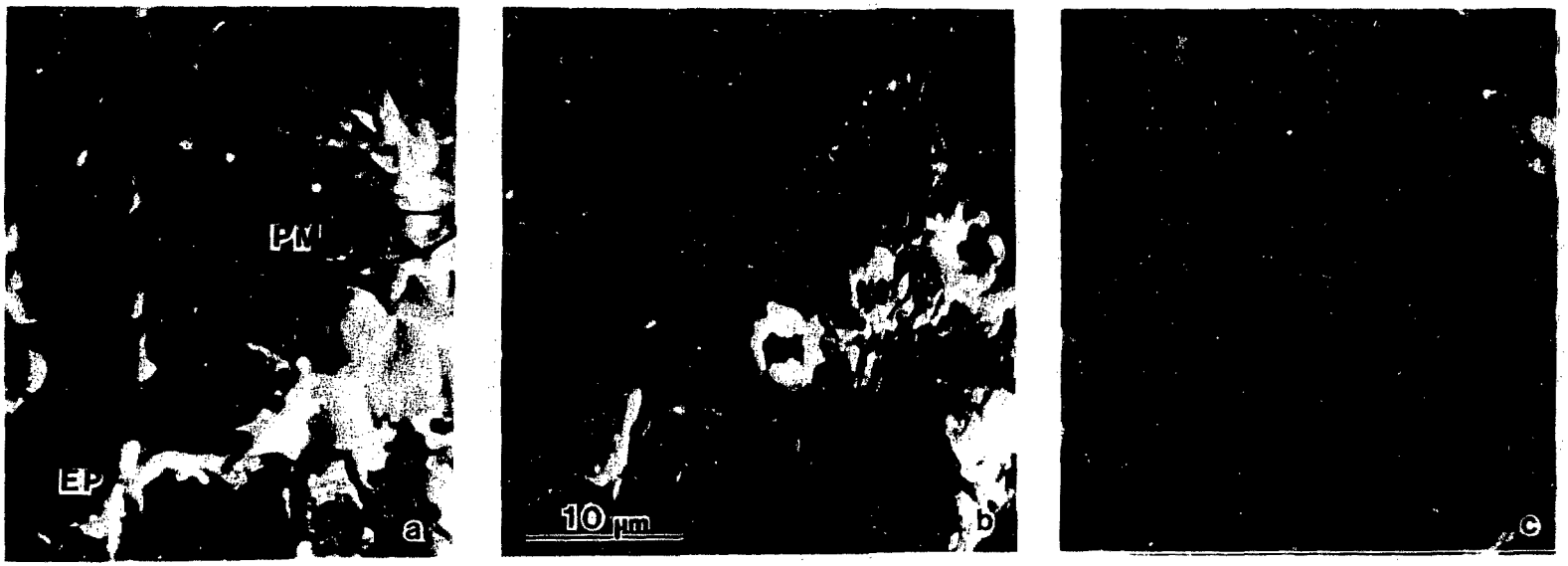

XBB 859-7624

Figure 14. Lacy material overlaying the epithelial ring of a mesenchyme blastula. The crystal pattern does not match that of the blastocoel matrix or C/HES matrix.

XBB 859-7625

Figure 15. Demonstration of charging effects resulting in an increased emission of secondary electrons. The bright areas indicated by the arrow marked "C" are charging. The areas designated "E" are exhibiting edge effects.

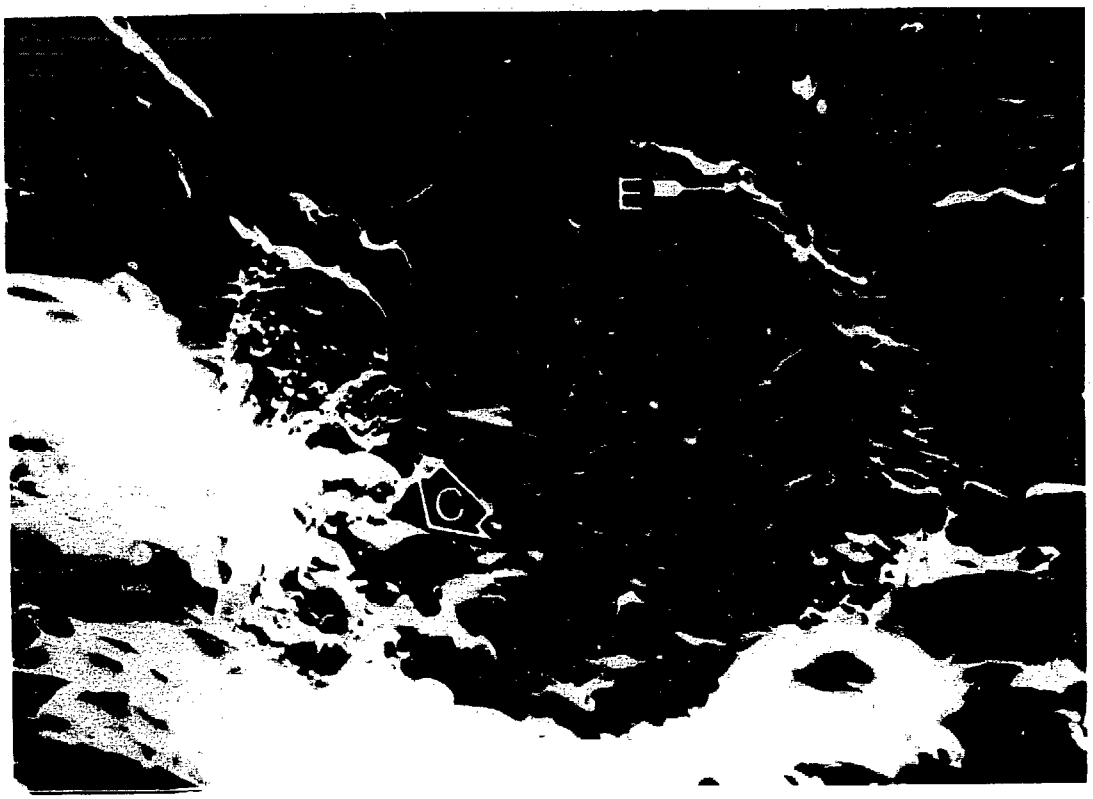

XBB 859-7626

Figure 16. Example of dark charging resulting from aberrant fields which prevent secondary electrons from reaching the detector. The arrow points to an embryo which appears to be standing out from the surface because of the charging pattern.

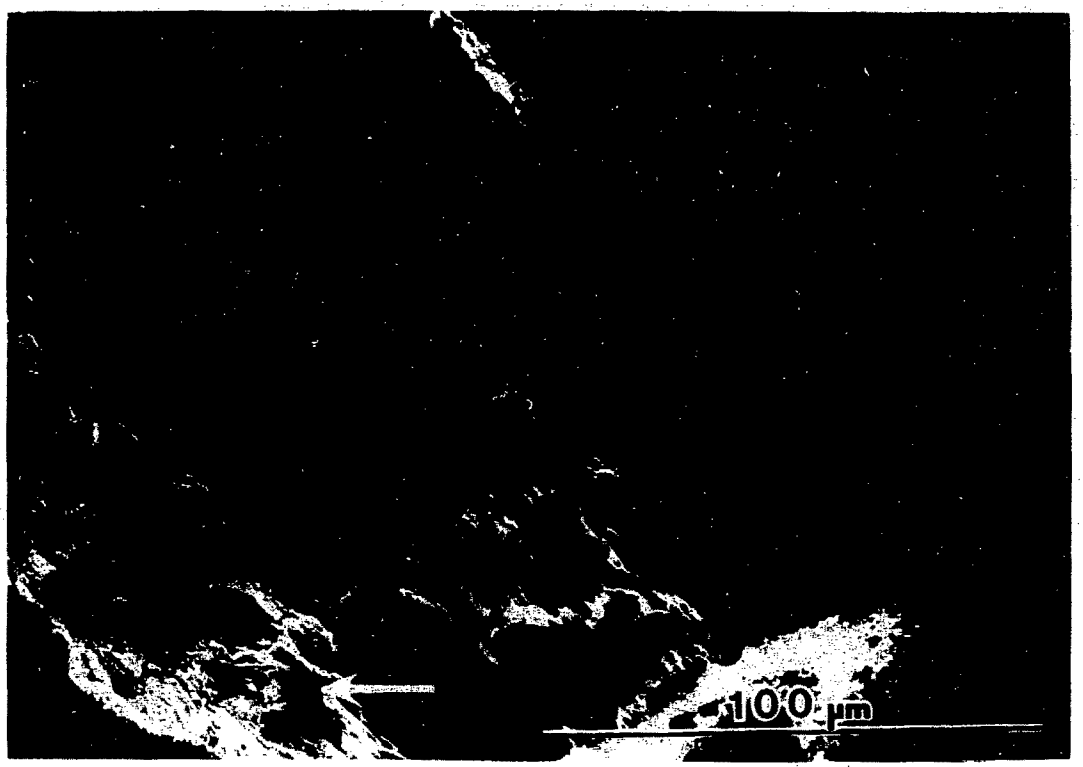

XBB 859-7627

Figure 17. Typical background exhibited on the display monitor of the x-ray spectrometer (after the characteristic peaks had been stripped off for analysis). An increase in the rate of change of the slope above 2 KeV signifies a decrease in the number of higher energy electrons entering the sample.

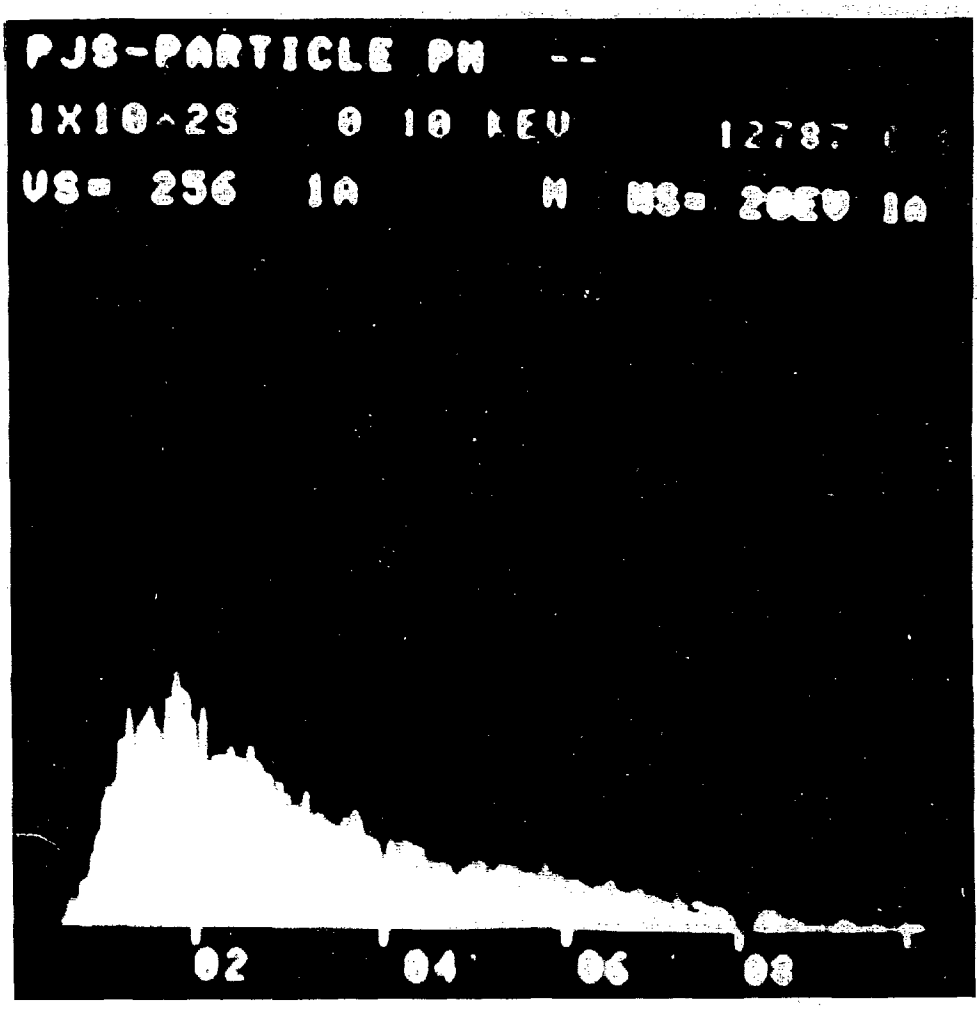

XBB 857-5586

Figure 18. Stereo pair micrographs of the fracture surface of a sample stored longer than three months. Knife chatter (C) is present; 2 pits (P) and 2 compression pits (CP) are designated at the edge of the ridges (R). The lower left has not been fractured and is covered with "snow" accumulated during processing.

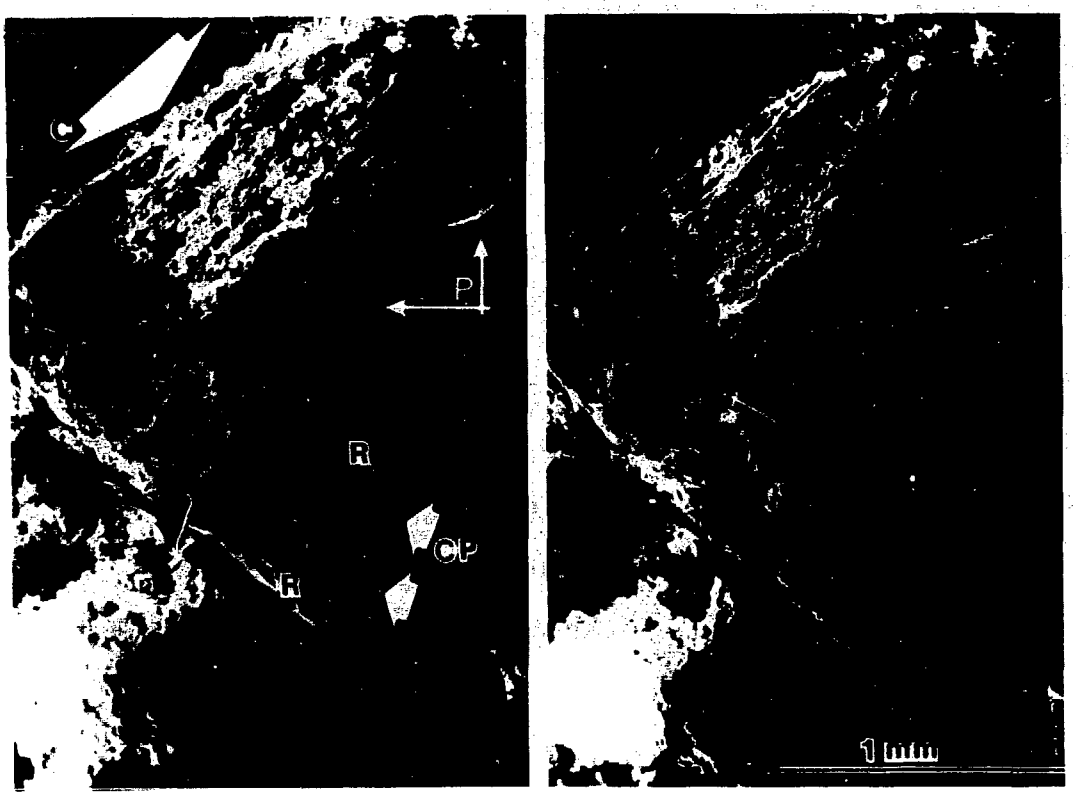

XBB 859-7628

Figure 19. An example of the atypical behavior of long stored samples. The first micrograph (a) displays a fully frozen hydrated embryo imaged immediately after positioning in the specimen chamber of the microscope. The archenteron (A), hyalin layer (HL), a dark charging area (C) and surface ice smearing (Sm) are labeled. The second micrograph (b) was imaged a short time later. The smearing (Sm) is still present. Three areas are denoted for special interest: 1 has been dehydrated, exposing a previously hidden PM cell; 2 is hydrated but charging; 3 displays rough ice. The third micrograph (c) shows the fully dried embryo. The space surrounding the PM cell of area 1 persists. The hyalin layer (HL) is separated from the epithelial ring (Ep). Also demonstrated are cell loss (arrow #1), severe shrinkage (arrow #2) and perforated blastocoel matrix.

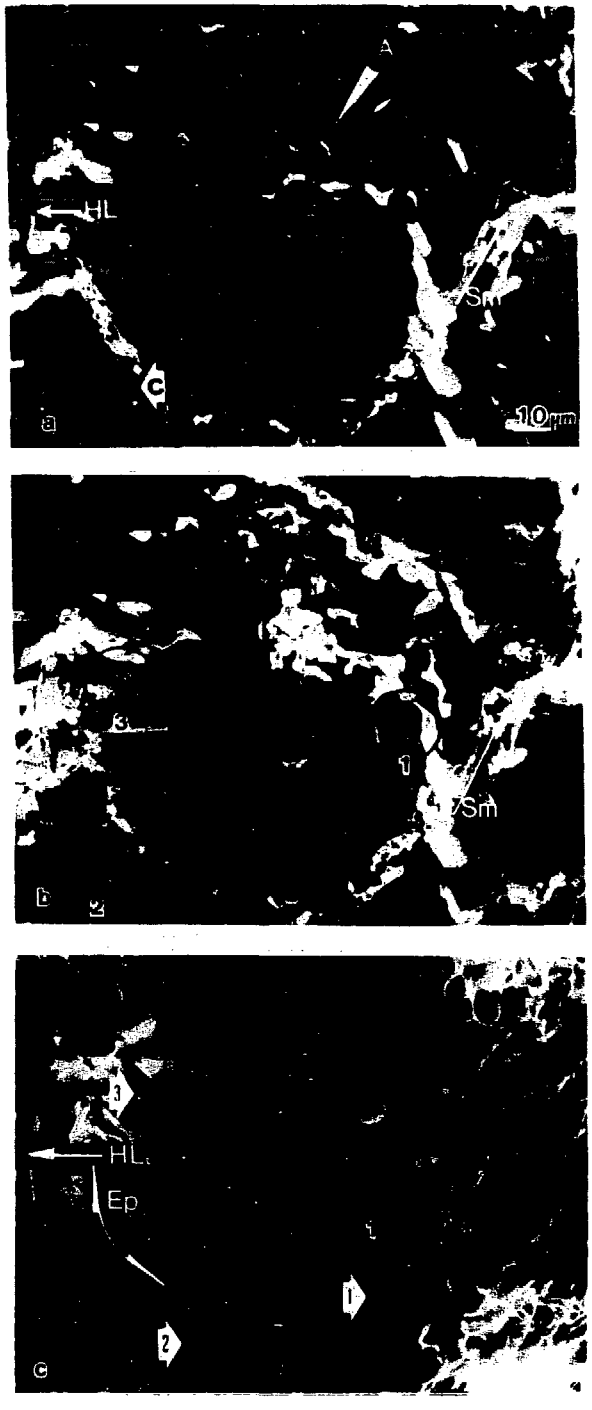

XBB 859-7629

Figure 20. Image of a second bead on the same C stub as the previous figure. Hydrated (H) and dried (D) areas are denoted.

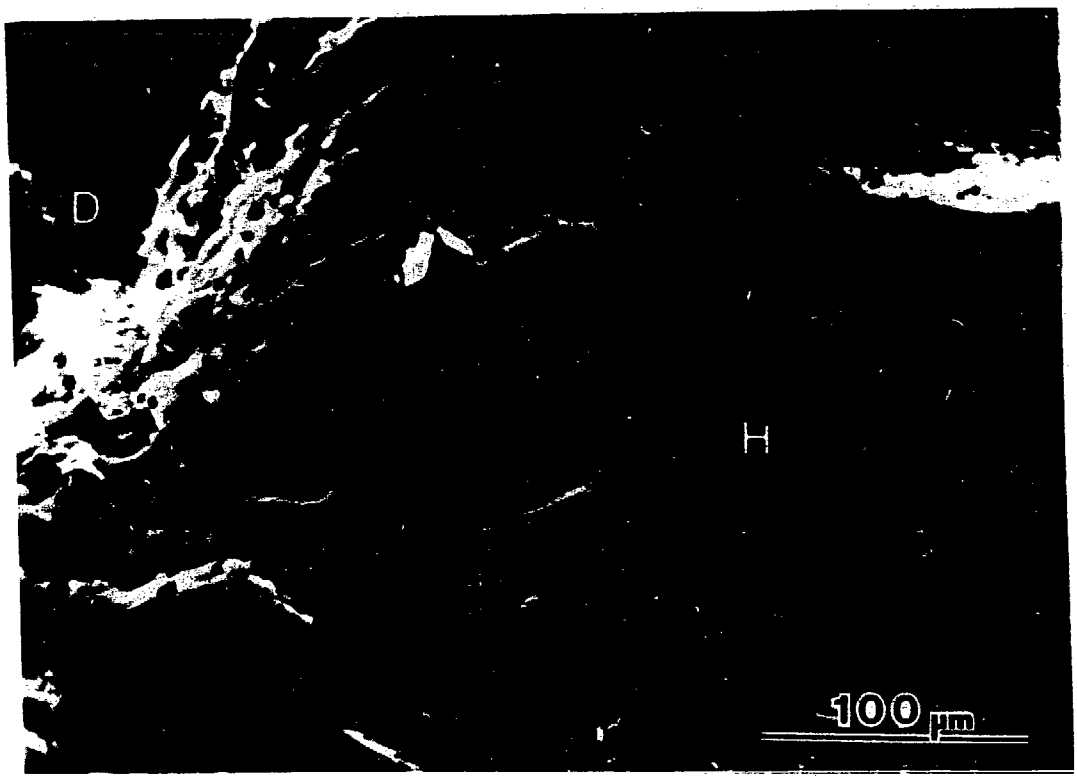

XBB 859-7630

Figure 21. Frozen hydrated (a) and frozen dried (b) images of an embryo stored longer than three months. The archenteron (A) is marked as well as an orientation point (*) and two groups of PM cells (PM). The dried embryo has cracked open in drying. Cell loss (CL) and perforated matrix (at the arrow) are denoted in (b).

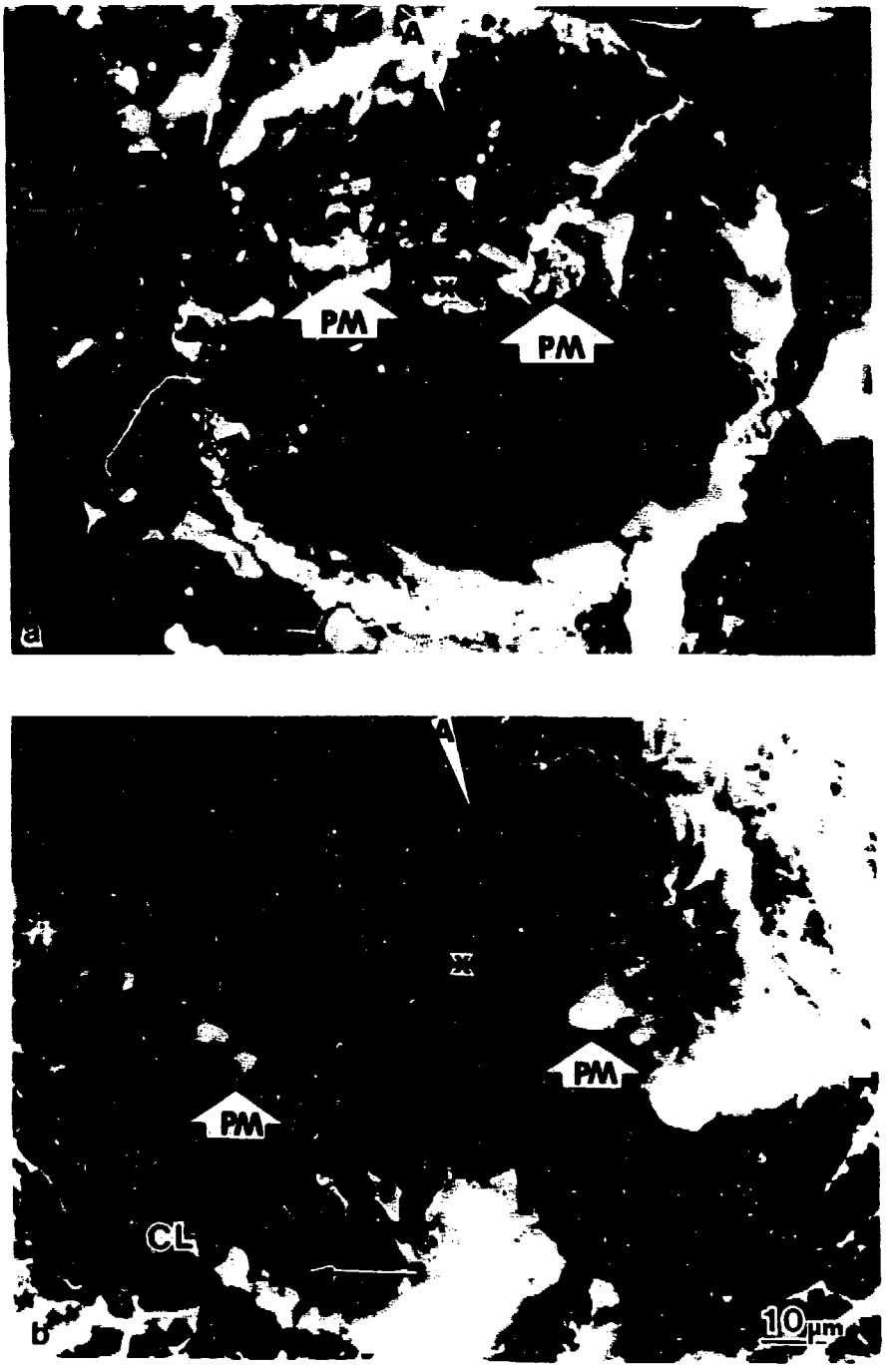

XBB 859-7631

Figure 22. Example of SEM x-ray mapping techniques. The center image is the secondary electron emission image of the mesenchyme blastula. The first image shows that Cl is excluded from the epithelial cells. The third image demonstrates the accumulation of K within the cells.

XBB 840-7875

Figure 23. X-ray maps of Na and S surrounding the same mesenchyme blastula as the last figure. Both Na and S are excluded from the cells but the relative cellular S concentration is higher within the cells. The secondary image is provided again for orientation.

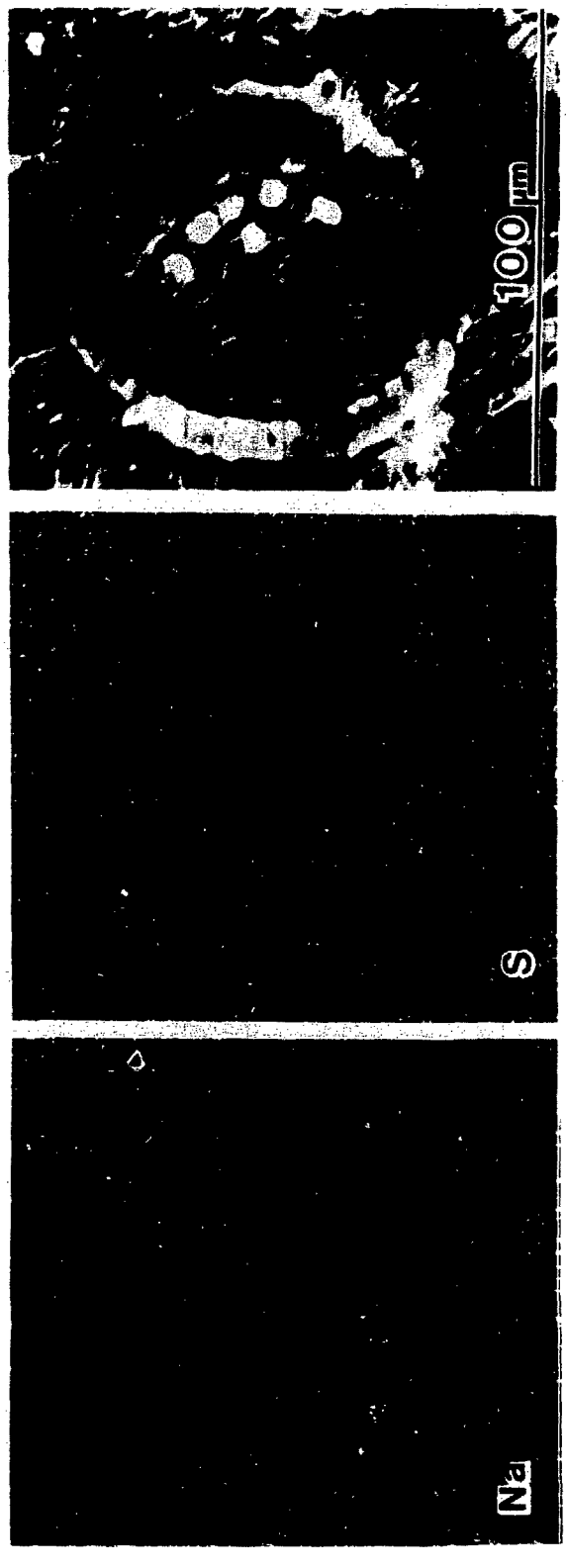

XBB 859-7632

Figure 24. High magnification image and corresponding S x-ray map of 4 PM cells within the blastocoel of a mesenchyme blastula. No pattern of S deposition can be detected above the noise.

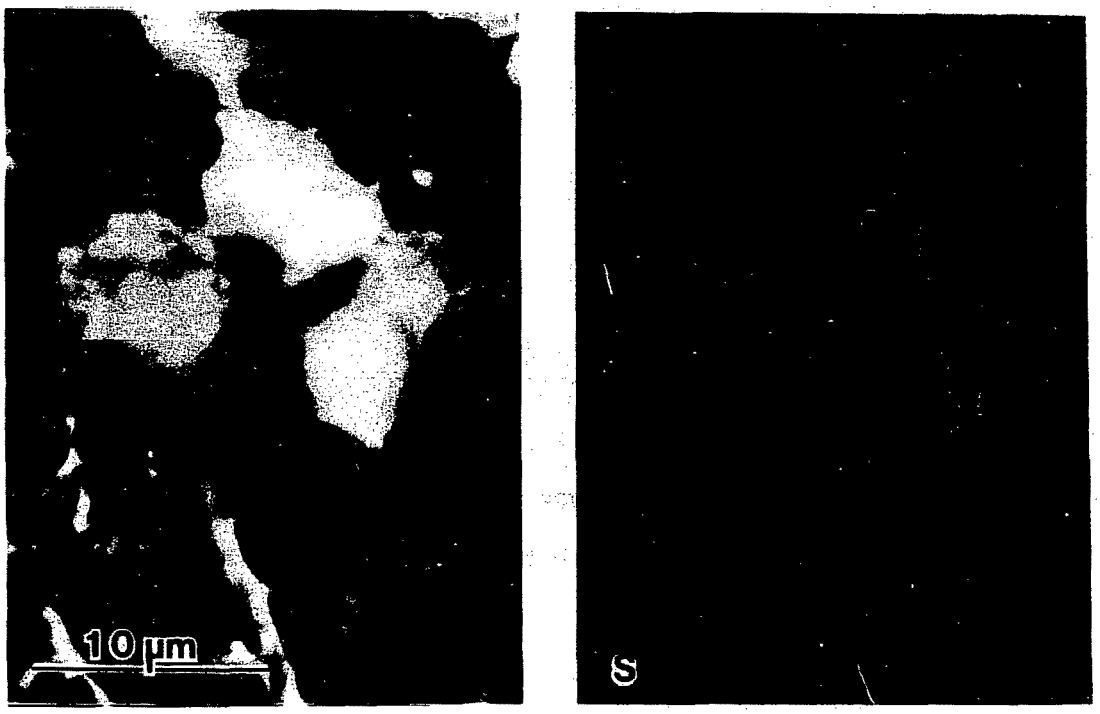

XBB 859-7633

Figure 25. Cl, Na and S x-ray maps from an early gastrula. No difference in concentration can be detected within the archenteron or in the blastocoel matrix at the tip of the archenteron. The increase in S concentration within the blastocoel is recognizable.

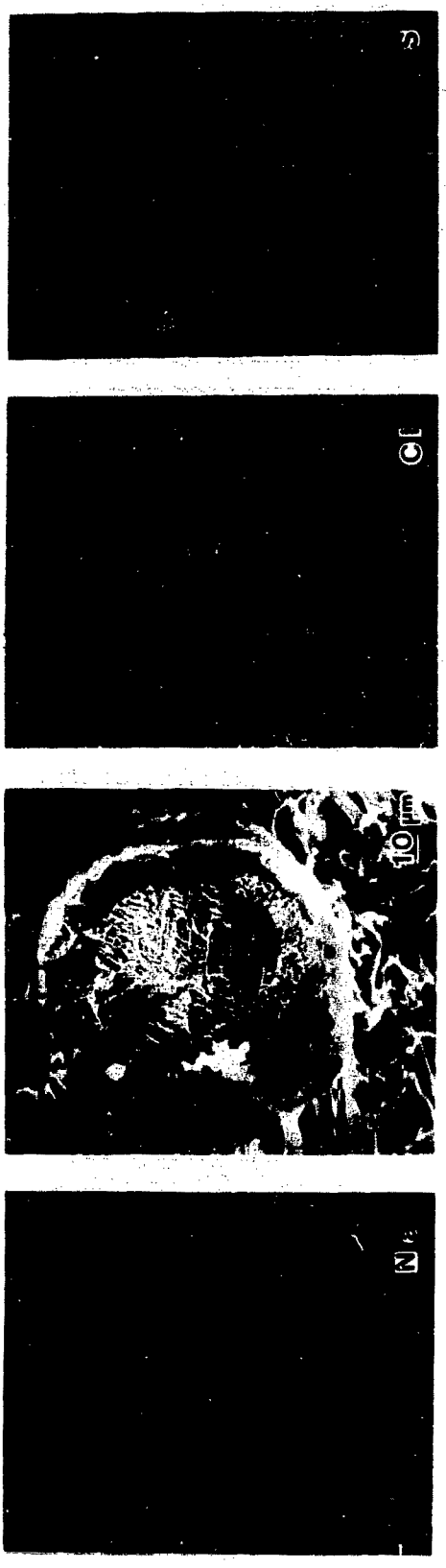

XBB 859-7634

Figure 26. Mesenchyme blastula P/B ratios recorded at 3.3 KeV (the K_a energy for K). The graph compares cellular volumes (C) and volumes which overlap the ECM (ECM), blastocoel (BC) and sea water exterior (H_2O). Variations signify the influence of extracellular chemistry. Error bars = $\pm$ 1 sem.

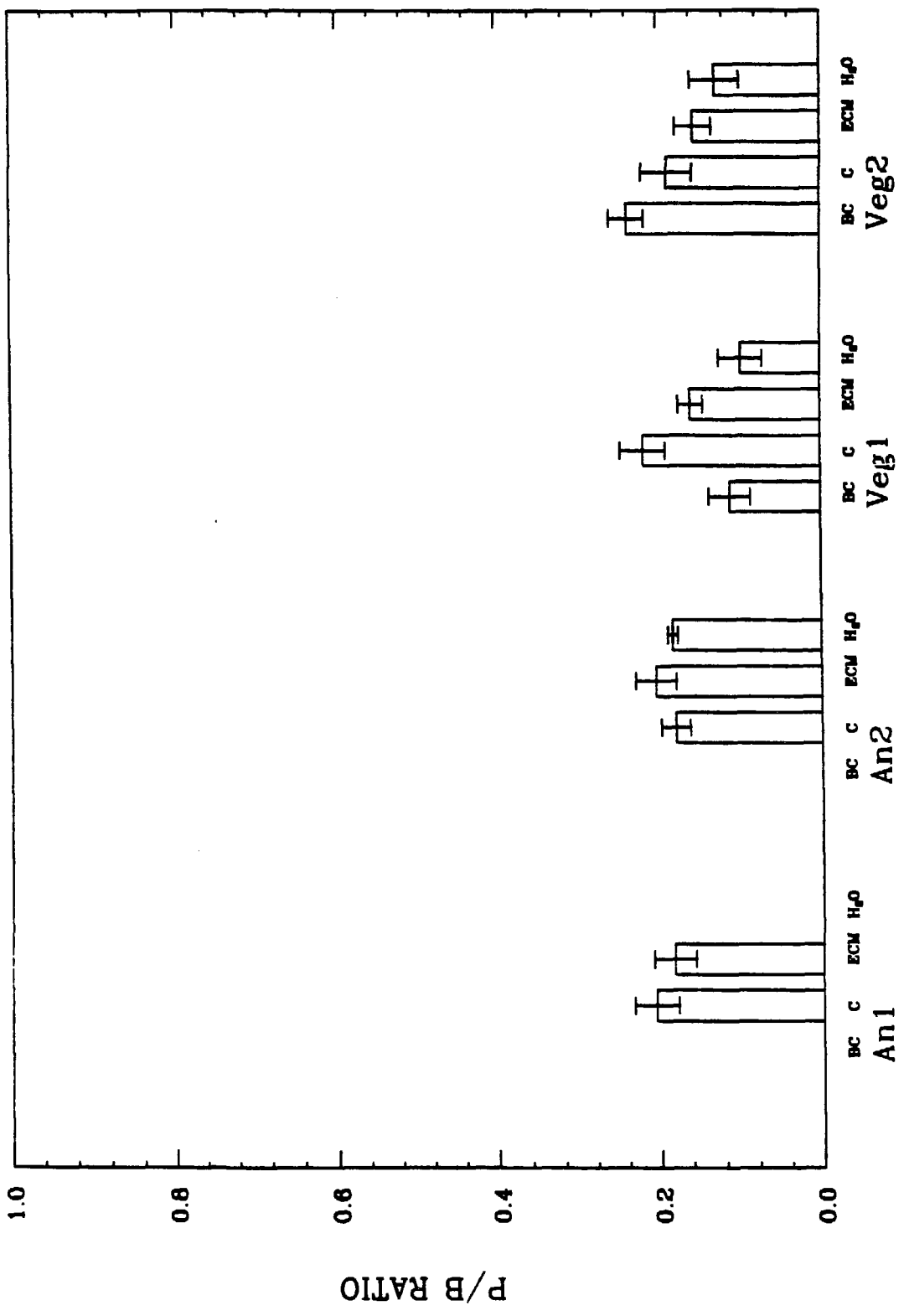
P/B RATIO
1.0
0.8
0.6
0.4
0.2
0.0
BC
C
ECM
H₂O
An1
An2
Veg1
Veg2

Figure 27. Mesenchyme blastula P/B ratios recorded at 2.3 KeV (the K_{α} energy for S). The graph compares cellular volumes (C), and volumes which overlap the ECM (ECM), blastocoel (BC) and sea water exterior (H_2O). Error bars = ± 1 sem.

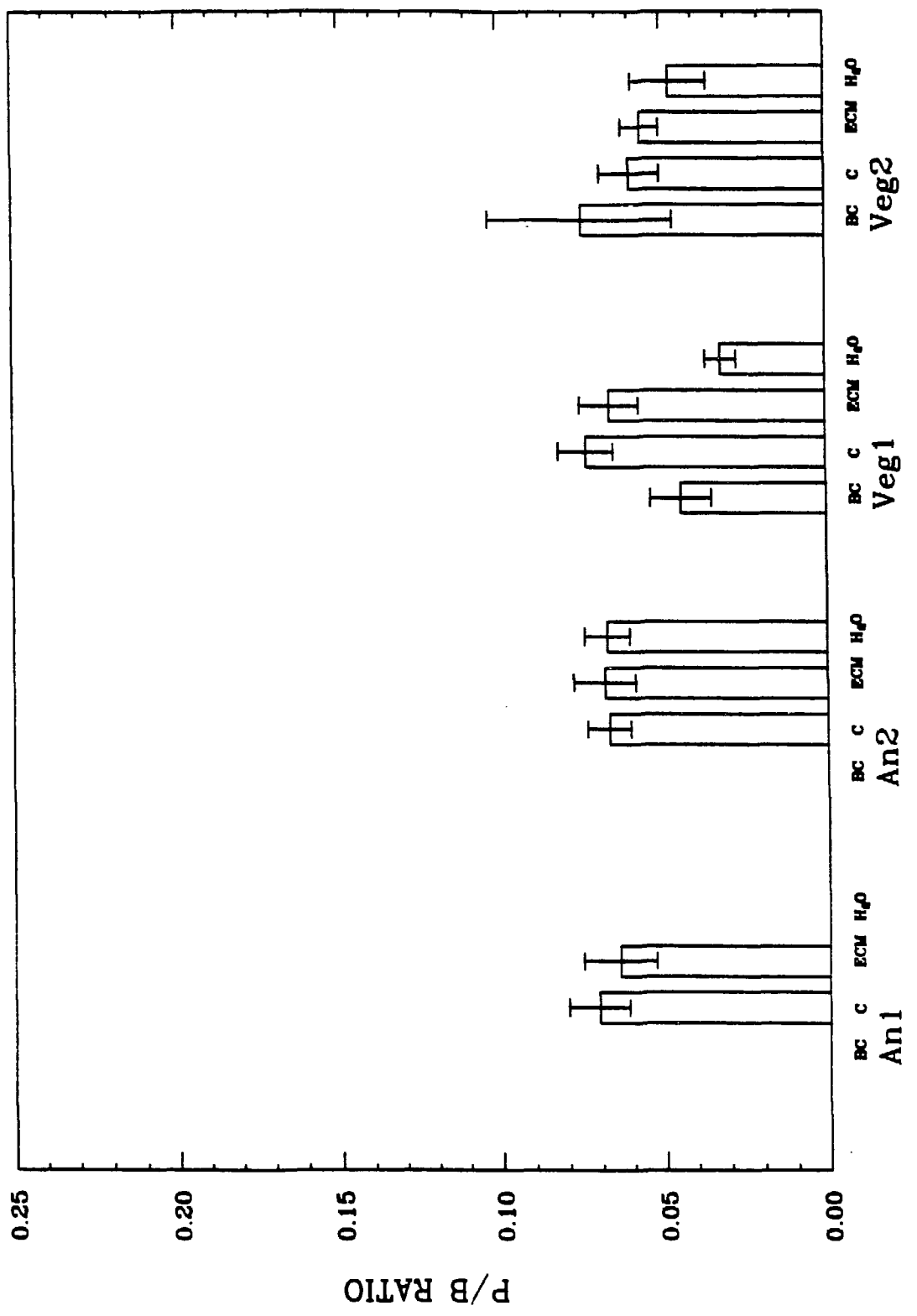
P/B RATIO
0.25
0.20
0.15
0.10
0.05
0.00
BC C ECM H2O
An1
BC C ECM H2O
An2
BC C ECM H2O
Veg1
BC C ECM H2O
Veg2

Figure 28. Early gastrula P/B ratios recorded at 2.3 KeV (the K_a energy for S). This graph compares cellular volumes (C) and volumes which overlap the ECM (ECM), blastocoel (BC) and sea water exterior (H_2O). Error bars = $\pm$ 1 sem.

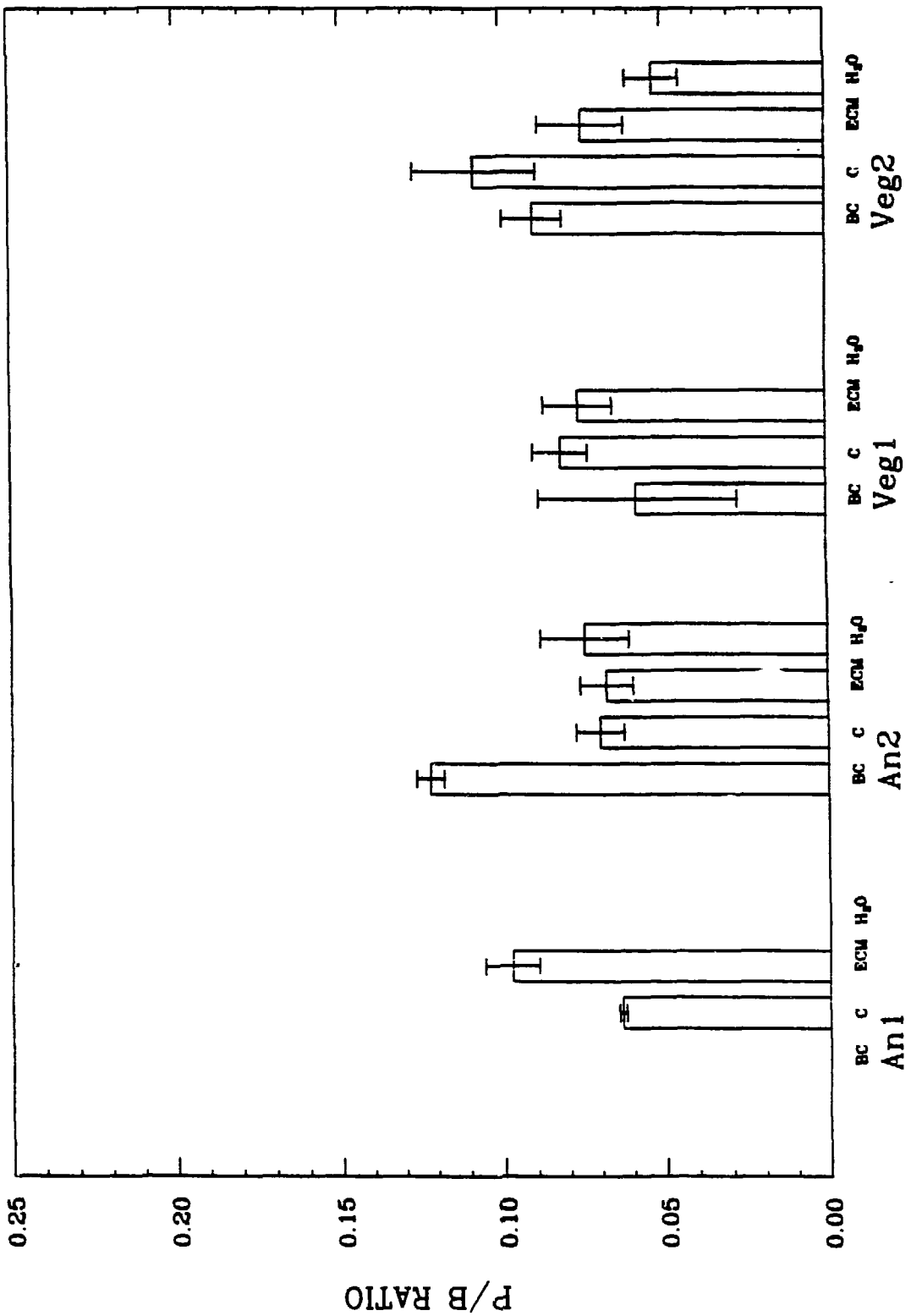
P/B RATIO
0.25
0.20
0.15
0.10
0.05
0.00
BC
C
ECM
H2O
An1
An2
Veg1
Veg2

Figure 29. Cellular P/B ratios as the embryo matures, recorded at 3.3 KeV (K). Three stages, blastula (B), mesenchyme blastula (MB) and early gastrula (EG) are presented according to cell types defined in the introduction. Error bars = ± 1 sem.

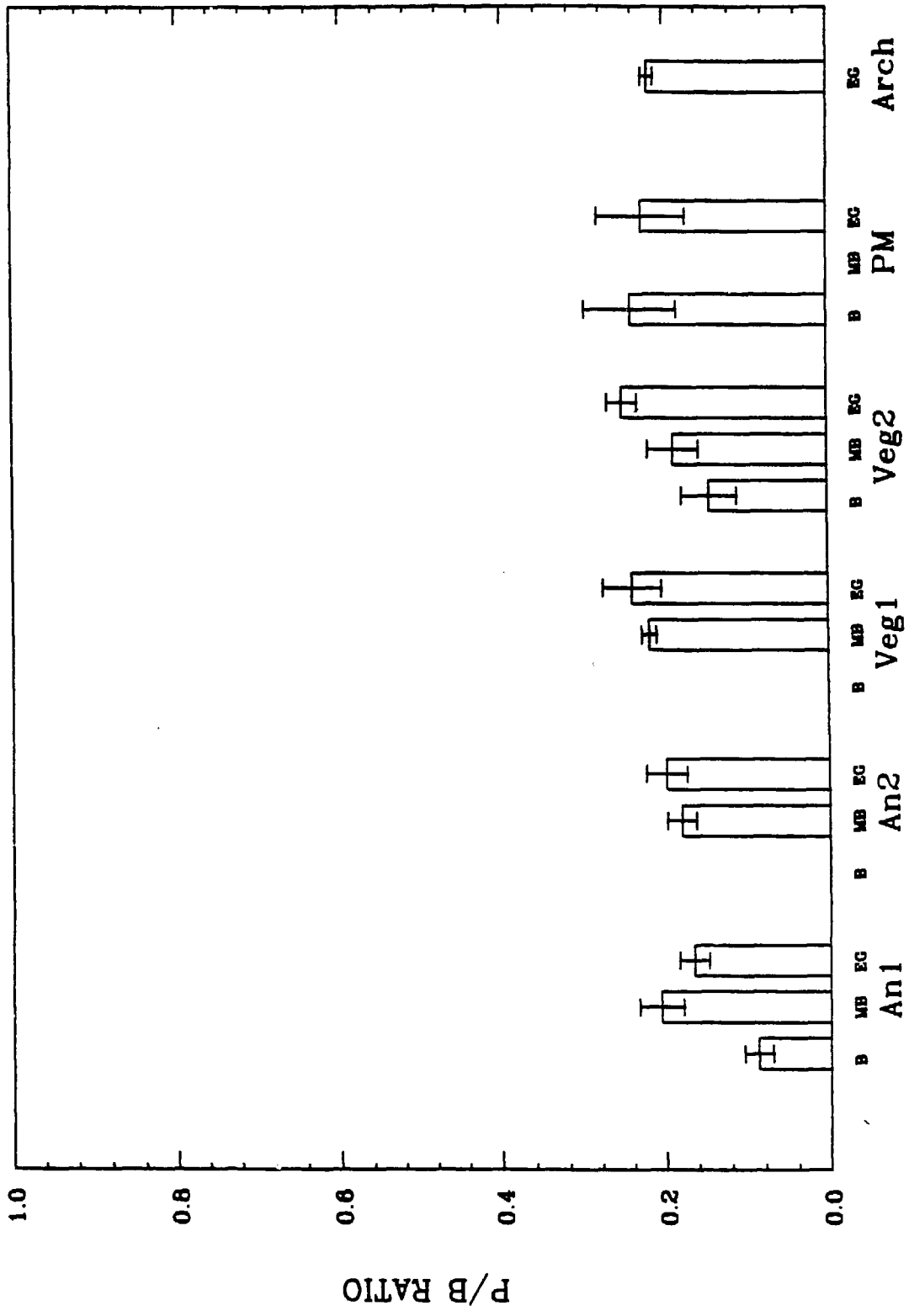
P/B RATIO
1.0
0.8
0.6
0.4
0.2
0.0
B
MB
EG
An1
An2
Veg1
Veg2
PM
Arch

Figure 30. Cellular P/B ratios as the embryo matures, recorded at 2.3 KeV (S). Three stages, blastula (B), mesenchyme blastula (MB) and early gastrula (EG) are presented according to cell types defined in the introduction. Error bars = $\pm$ 1 sem.

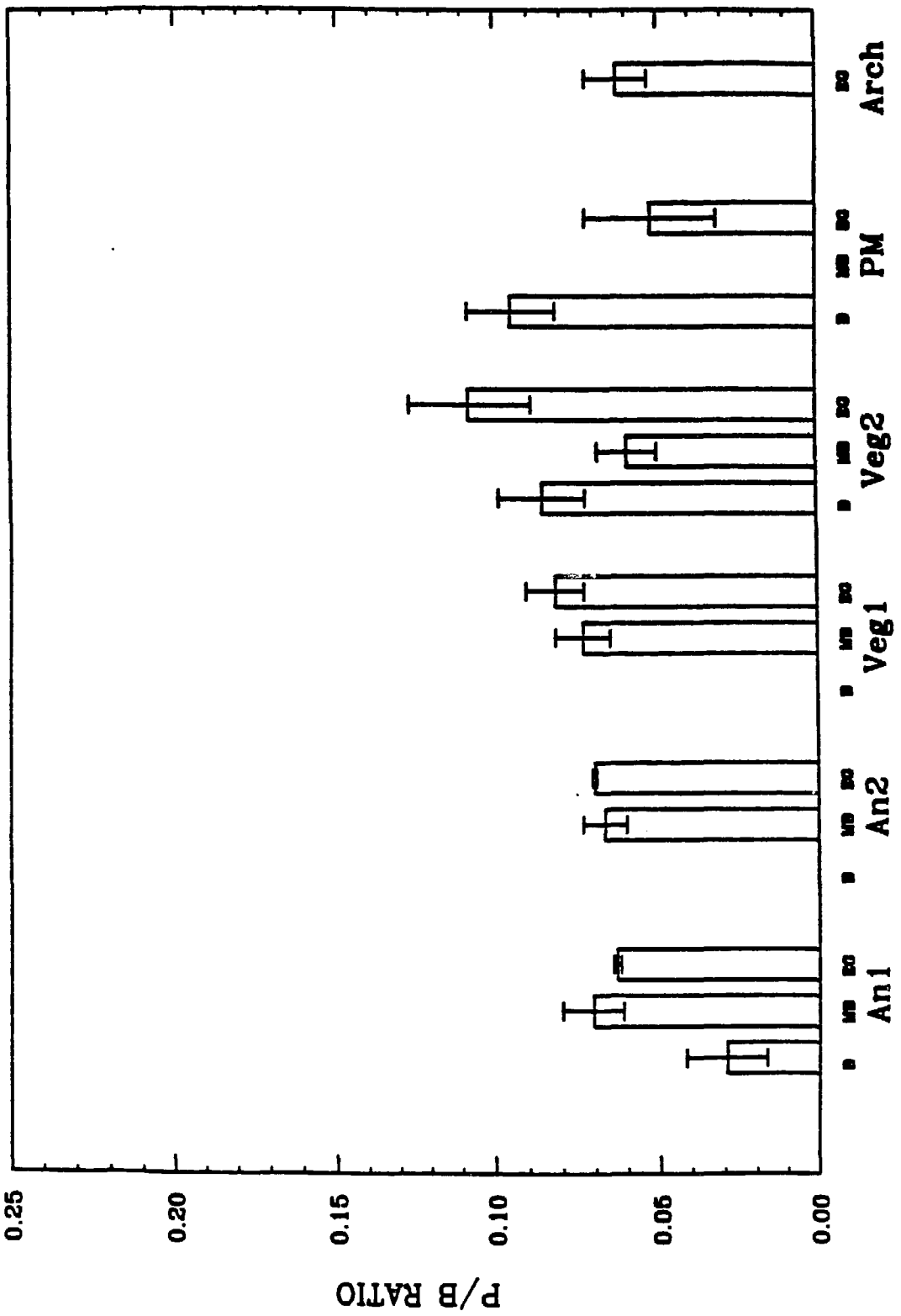
P/B RATIO
0.25
0.20
0.15
0.10
0.05
0.00
An1
An2
Veg1
Veg2
PM
Arch

Figure 31. Cellular P/B ratios as the embryo matures recorded at 2.0 KeV (P). Three stages, blastula (B), mesenchyme blastula (MB) and early gastrula (EG) are presented according to cell types defined in the introduction. Error bars = ± 1 sem.

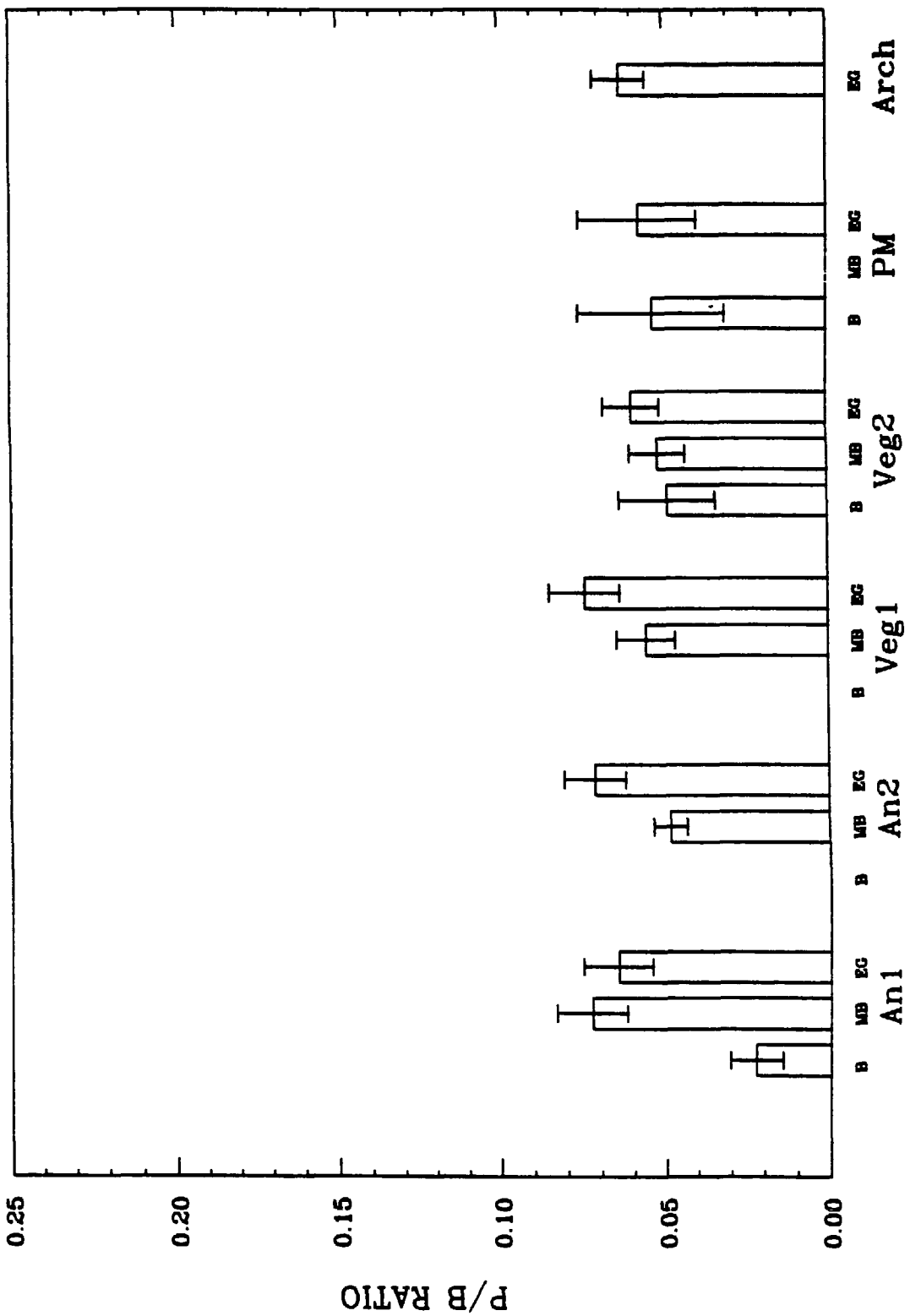
P/B RATIO
0.25
0.20
0.15
0.10
0.05
0.00
B
MB
EG
An1
An2
Veg1
Veg2
PM
Arch

Figure 32. Cellular P/B ratios as the embryo matures, recorded at 3.7 KeV (Ca). Three stages, blastula (B), mesenchyme blastula (MB) and early gastrula (EG) are presented according to cell type defined in the introduction. Error bars = $\pm$ 1 sem.

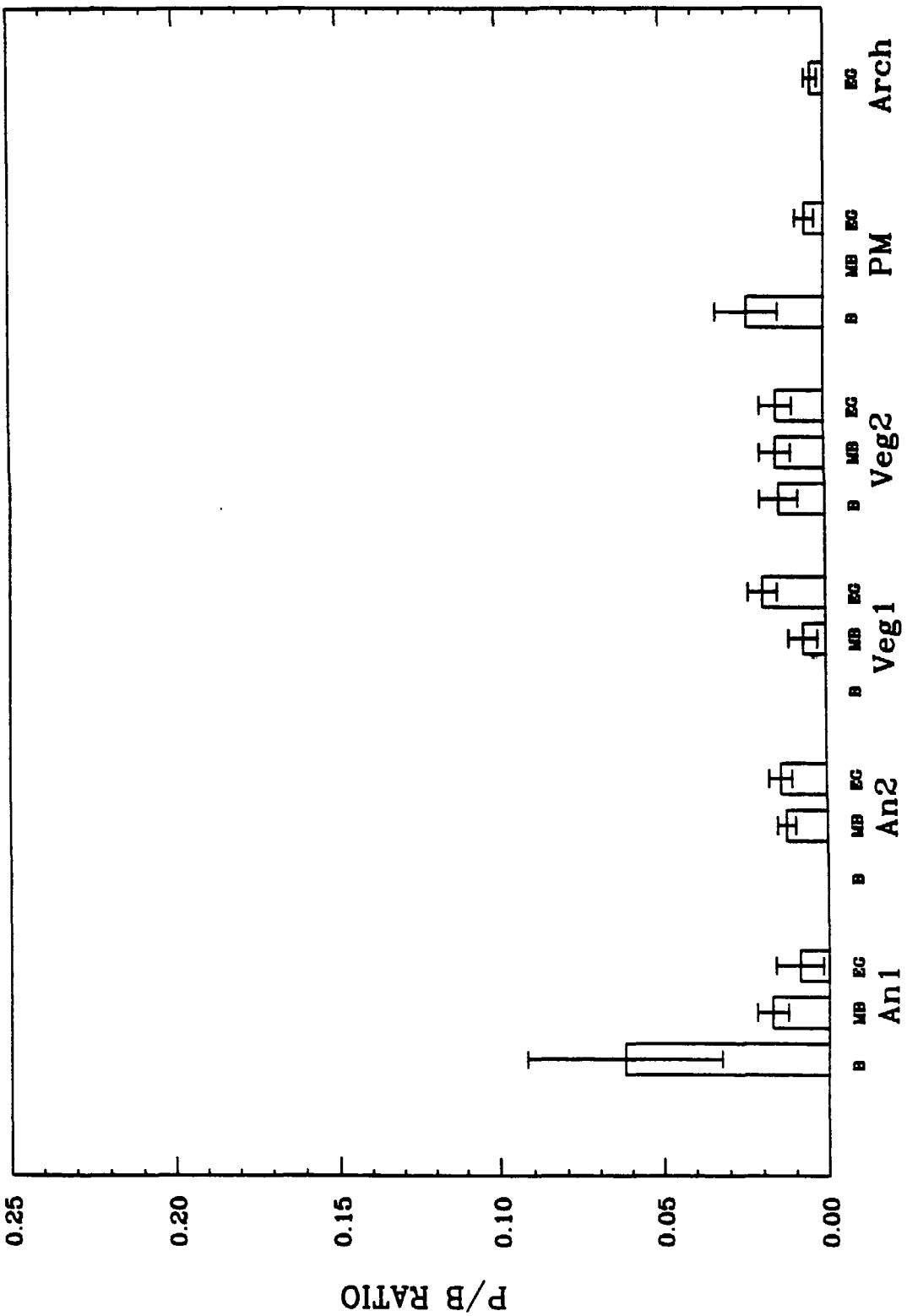
P/B RATIO
0.25
0.20
0.15
0.10
0.05
0.00
B
MB
EG
An1
An2
Veg1
Veg2
PM
Arch

Figure 33. BC P/B ratios as the embryo matures, recorded at 2.3 KeV (S). Three stages, blastula (B), mesenchyme blastula (MB) and early gastrula (EG) are presented according to cell types defined in the introduction. Error bars = $\pm$ 1 sem.

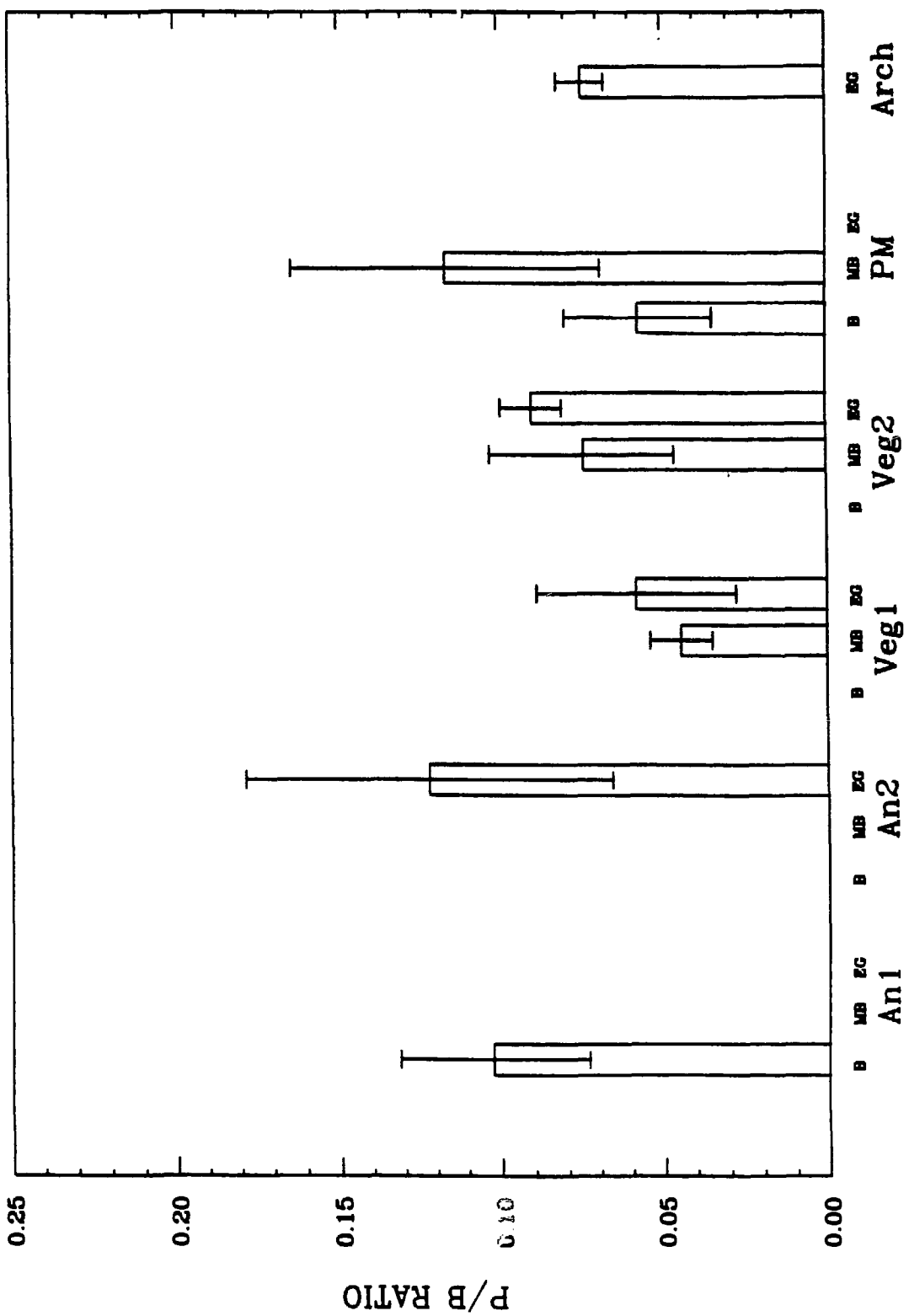
P/B RATIO
0.25
0.20
0.15
0.10
0.05
0.00
B
MB
EG
An1
An2
Veg1
Veg2
PM
Arch

Figure 34. ECM P/B ratios as the embryo matures, recorded at 2.3 KeV (S). Three stages, blastula (B), mesenchyme blastula (MB) and early gastrula (EG) are displayed according to cell types defined in the introduction. Error bars = $\pm$ 1 sem.

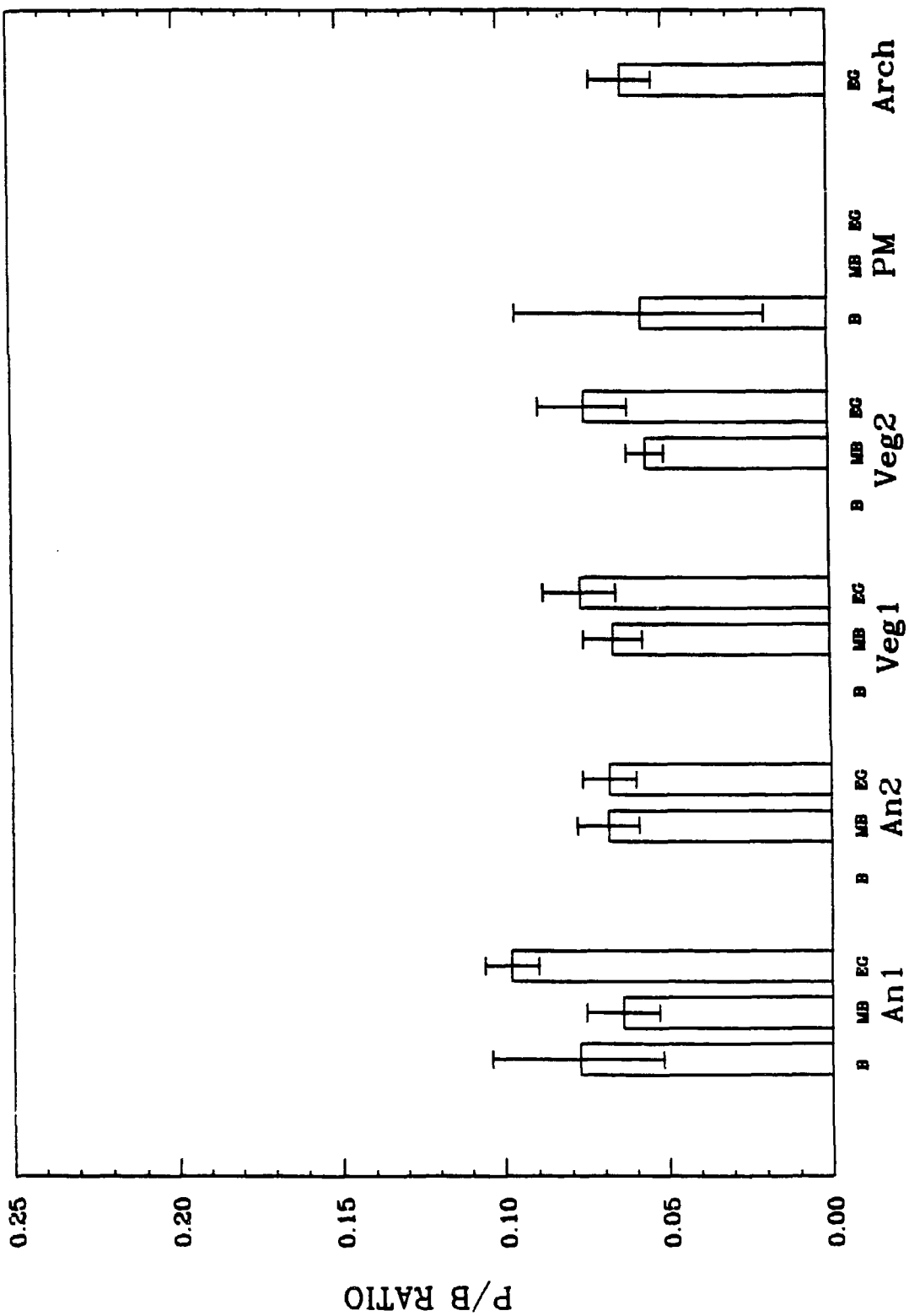
P/B RATIO
0.25
0.20
0.15
0.10
0.05
0.00
B
MB
EG
An1
An2
Veg1
Veg2
PM
Arch

Figure 35. Cellular P/B ratios as sampling circumscribes the embryo, at 1.25 KeV (Mg) and 5.9 KeV (Mn). Mesenchyme blastula (MB) and early gastrula (EG) stages are compared. Error bars = $\pm$ 1 sem.

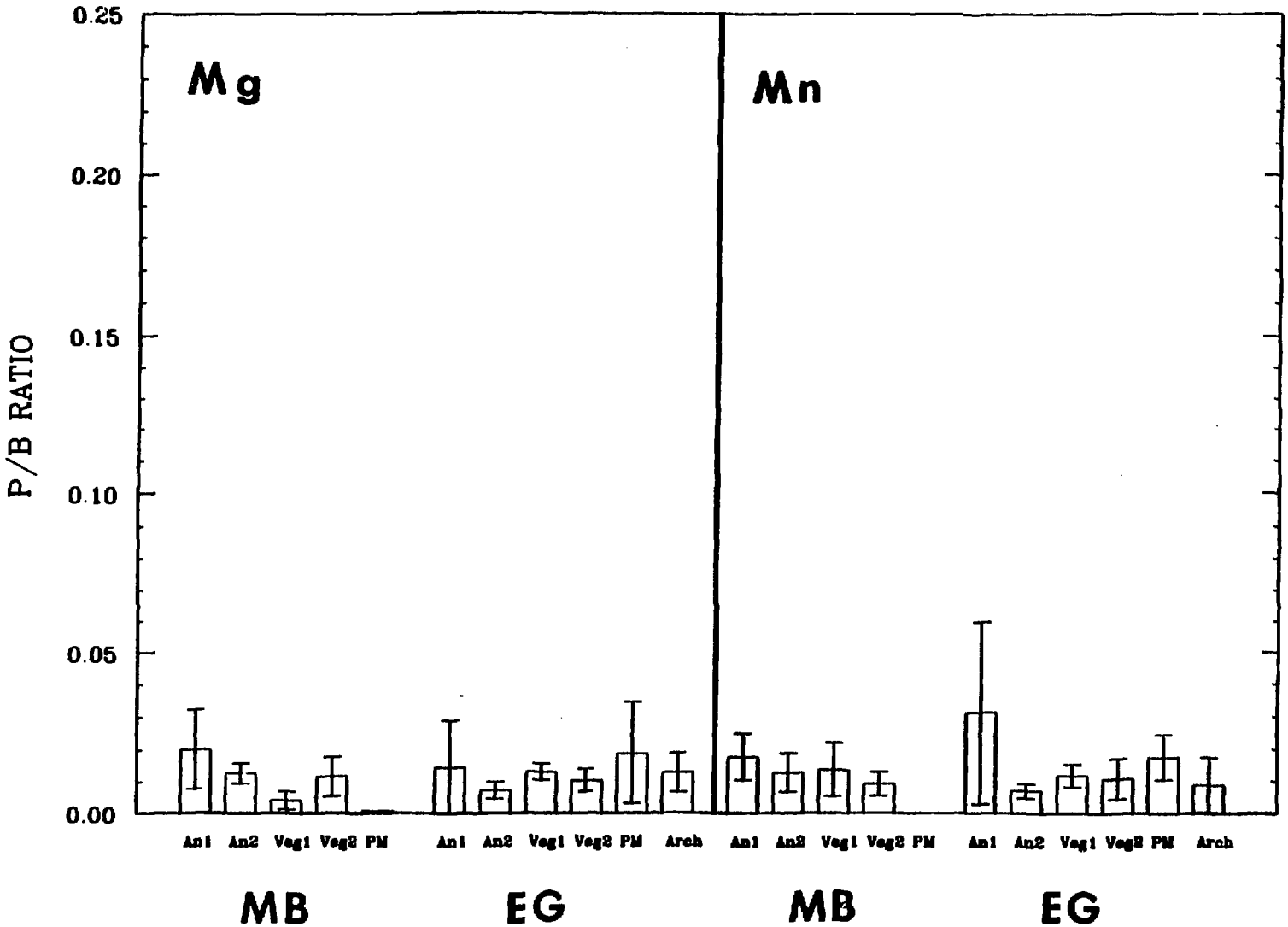
Mg
Mn
P/B RATIO
0.25
0.20
0.15
0.10
0.05
0.00
An1 An2 Veg1 Veg2 PM
An1 An2 Veg1 Veg2 PM Arch
An1 An2 Veg1 Veg2 PM
An1 An2 Veg1 Veg2 PM Arch
MB
EG
MB
EG

Figure 36. Mesenchyme blastula P/B ratios at 2.3 KeV (S) as sampling circumscribes the embryo. Sampling volumes overlap the basal portion of the cell, basal lamina and blastocoel (BC), the cytosol of two adjacent cells and intermediate ECM (ECM) and the cytosol of a single cell (C). Error bars = $\pm$ 1 sem.

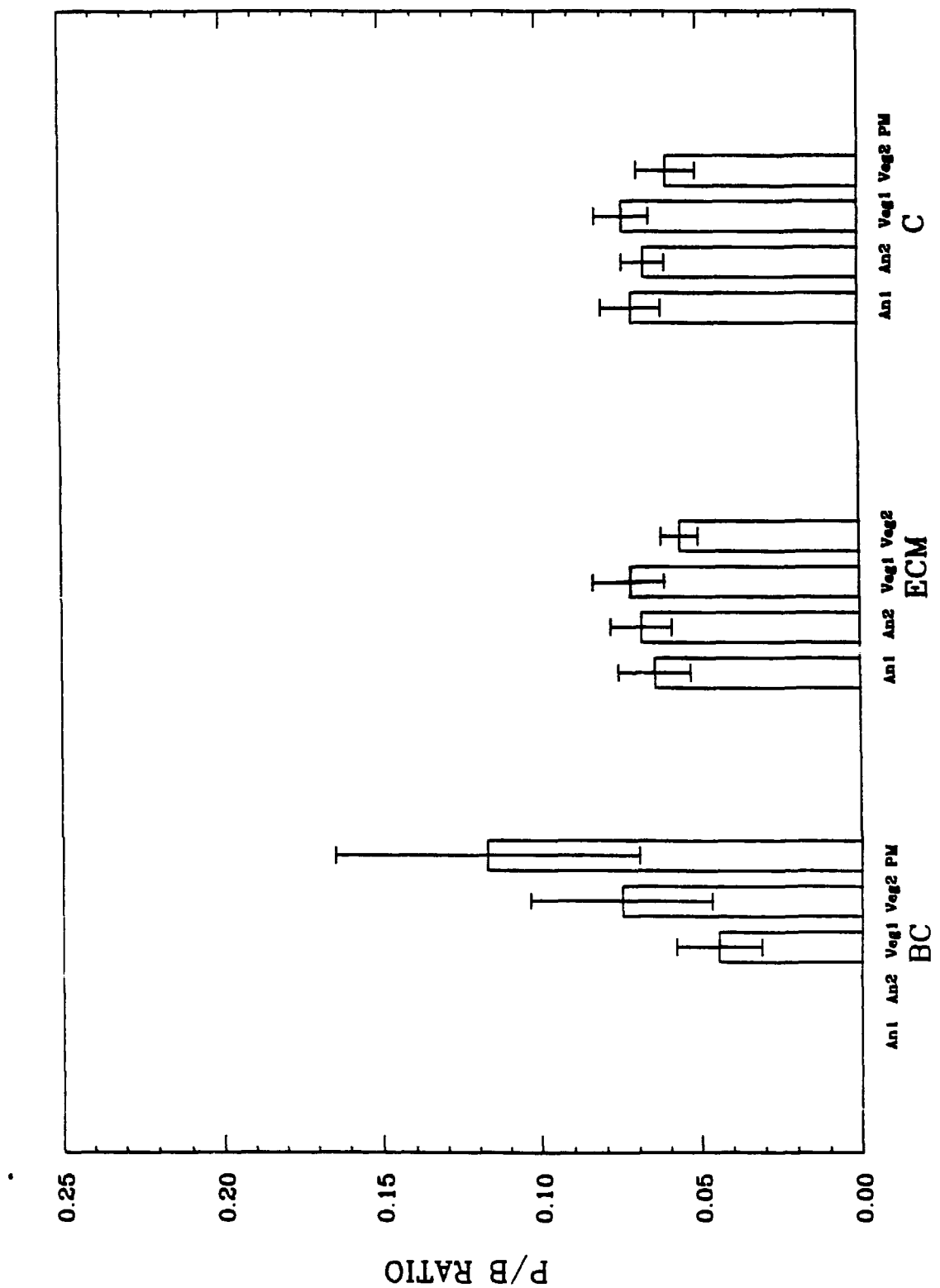
P/B RATIO
0.25
0.20
0.15
0.10
0.05
0.00
An1 An2 Veg1 Veg2 PM
BC
An1 An2 Veg1 Veg2
ECM
An1 An2 Veg1 Veg2 PM
C

Figure 37. Early gastrula P/B ratios at 2.3 KeV (S) as sampling circumscribes the embryo. Sampling volumes overlap the basal portion of the cell, basal lamina and blastocoel (BC), the cytosol of two adjacent cells and the intermediate ECM (ECM), and the cytosol of a single cell (C). Error bars = $\pm$ 1 sem.

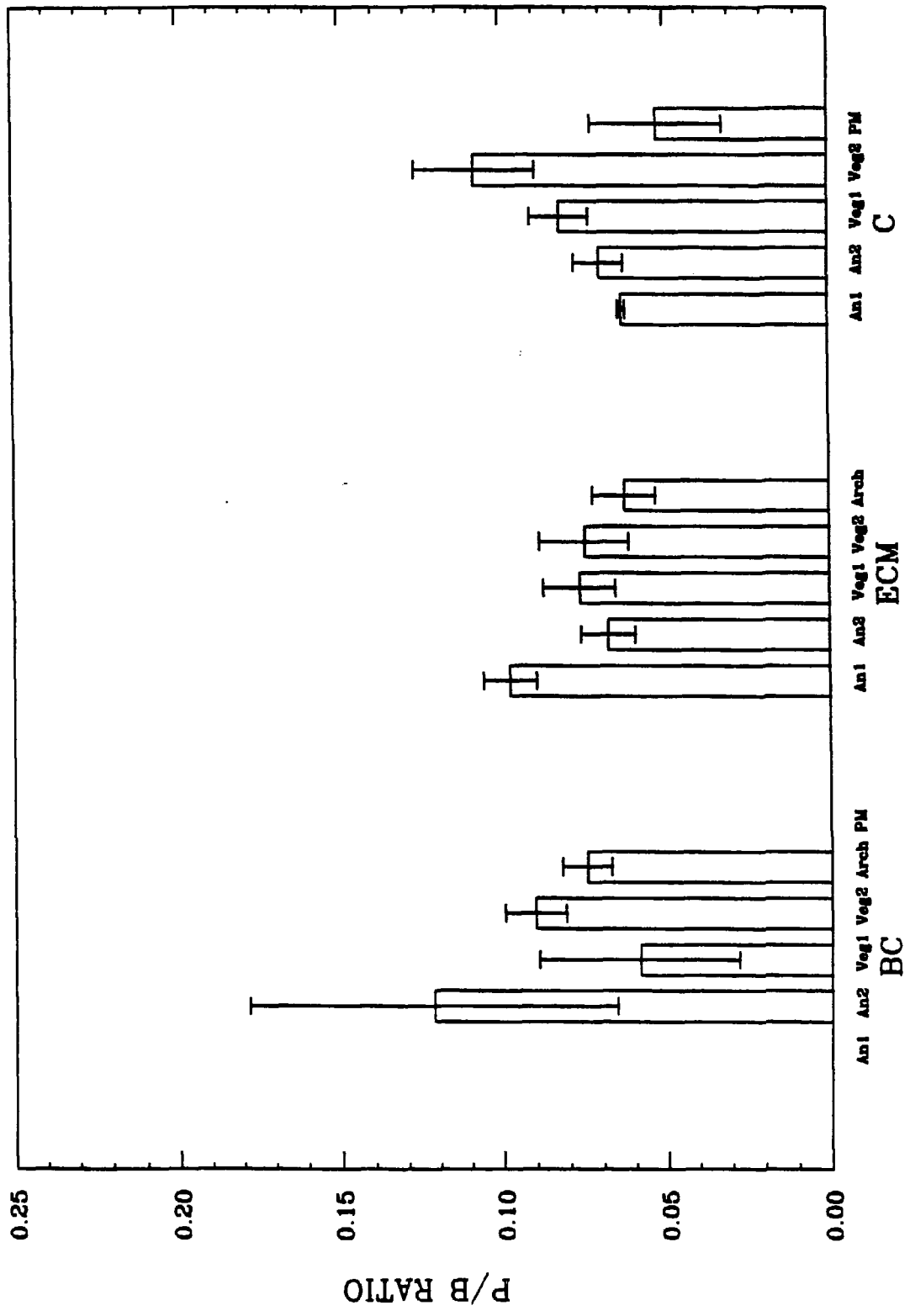
P/B RATIO
0.25
0.20
0.15
0.10
0.05
0.00
An1 An2 Veg1 Veg2 Arch PM
BC
An1 An2 Veg1 Veg2 Arch
ECM
An1 An2 Veg1 Veg2 PM
C

Figure 38. Mesenchyme blastula P/B ratios at 2.0 KeV (P) as sampling circumscribes the embryo. Sampling volumes overlap the basal portion of the cell, basal lamina and blastocoel (BC), the cytosol of two adjacent cells and the intermediate ECM (ECM), and the cytosol of a single cell (C). Error bars = $\pm$ 1 sem.

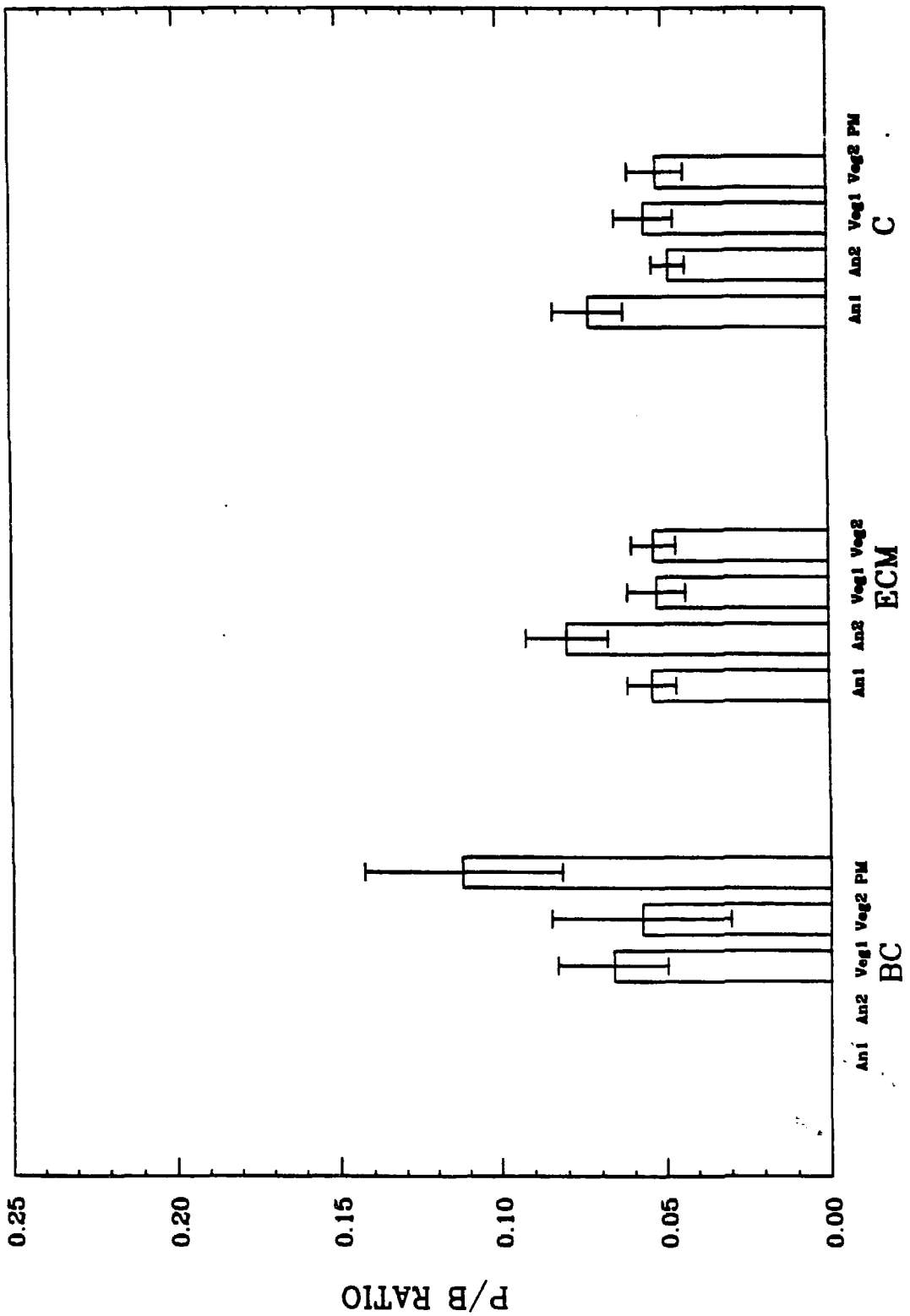
P/B RATIO
0.25
0.20
0.15
0.10
0.05
0.00
An1 An2 Veg1 Veg2 PM
BC
An1 An2 Veg1 Veg2
ECM
An1 An2 Veg1 Veg2 PM
C

Figure 39. Stereo pair images of a properly fractured bead (a) and an improperly fractured bead (b). The only embryos visible in the improperly fractured bead are located on a fractured surface sloping off to the left.

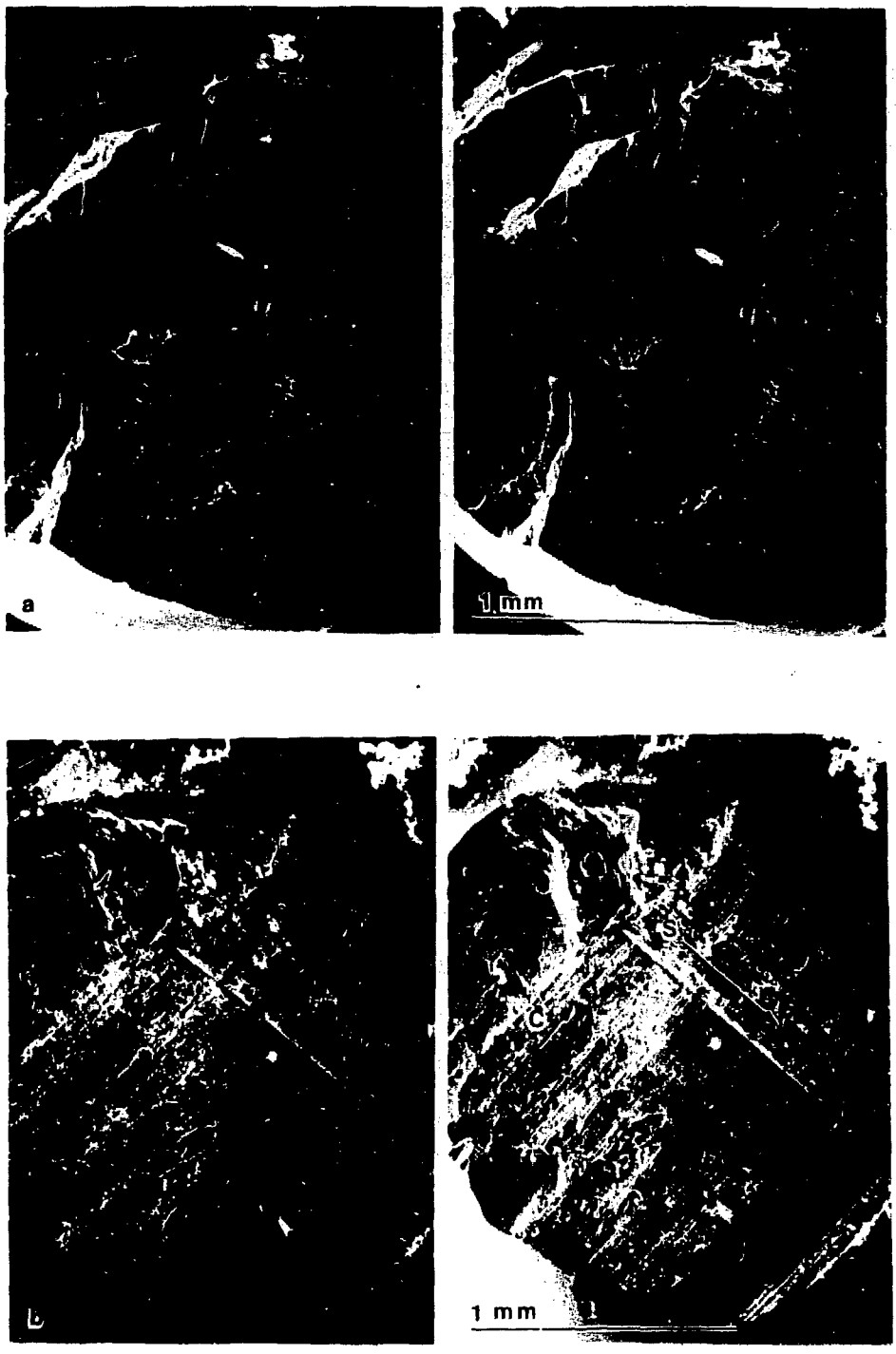

XBB 859-7635

Figure 40. Comparison of counts per second detected as the tissue dehydrated under the electron beam. The least squares slope indicates a linear correlation between collection duration and count rate (Pearson's R = 0.81106). Error bars = $\pm$ 1 sem.

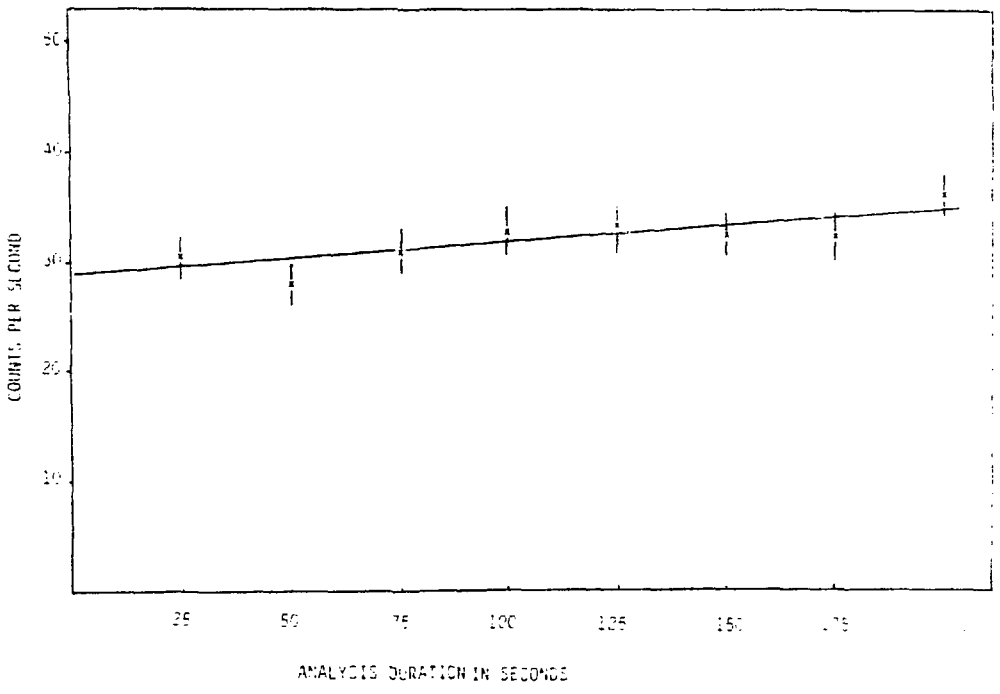
COUNTS PER SECOND
25
50
75
100
125
150
ANALYSIS DURATION IN SECONDS

Figure 41. Histogram illustrating the increase in P/B ratio for a 200 second analysis over a 100 second analysis. Cl and K energies are located on the smaller, negative slope and experience large background losses as dehydration occurs. Inset diagram shows location.

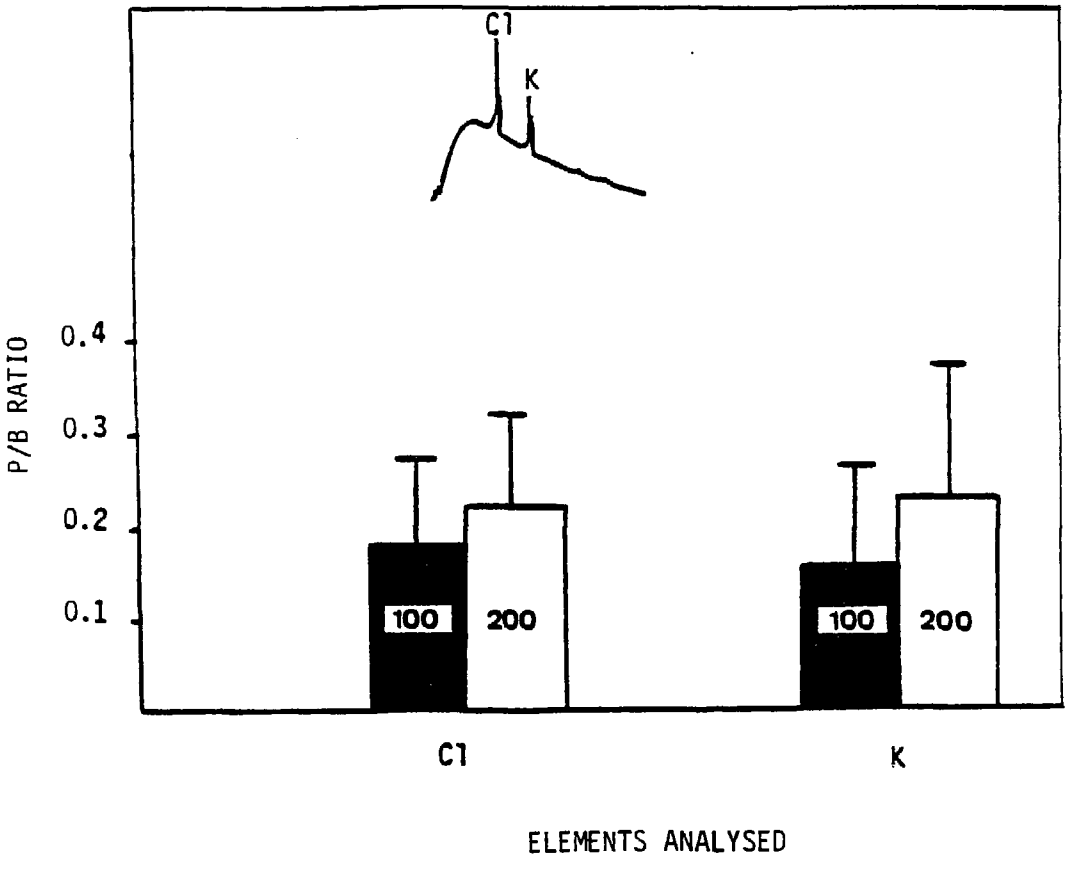
Cl
K
P/B RATIO
0.4
0.3
0.2
0.1
100
200
100
200
Cl
K
ELEMENTS ANALYSED

Figure 42. High magnification of 1 μm beads in partially hydrated blastocoel matrix. It is possible that these are the hydrated form of the 30 nm particles reported previously.

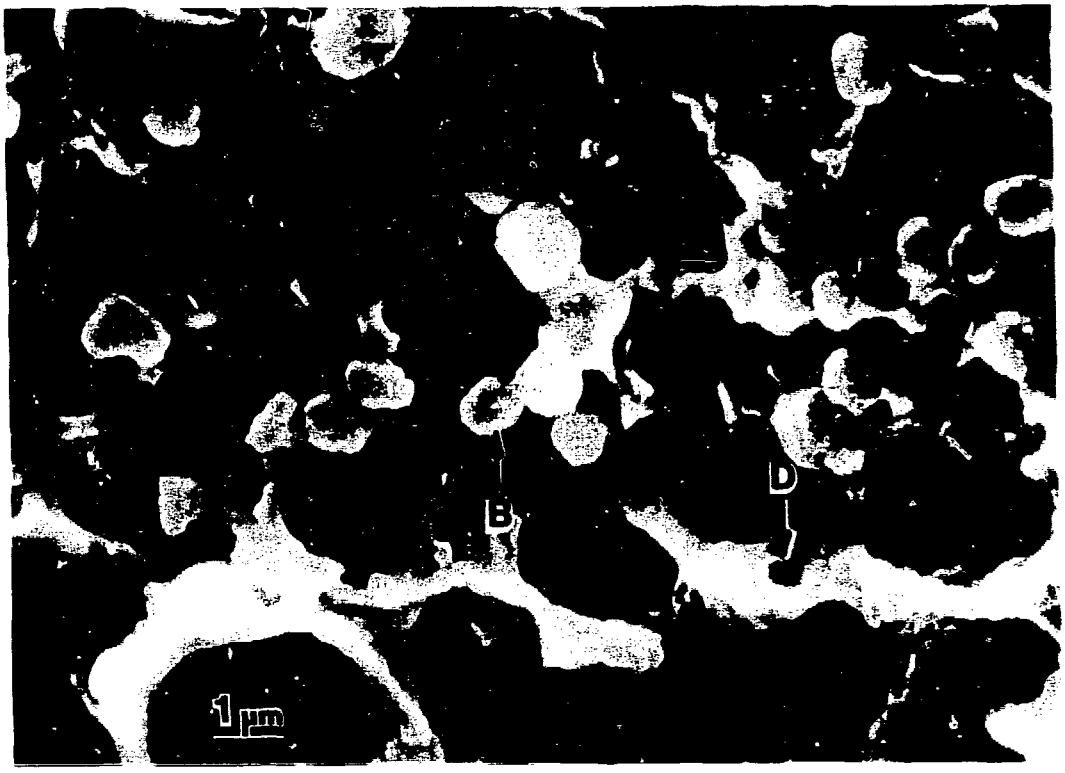

XBB 859-7636

Figure 43. Raster location map of mesenchyme blastula 303, showing data points 18-25. The raster locations are marked on the frozen hydrated image at the time of collection. The locations are transferred to the dried image via a double exposure print.

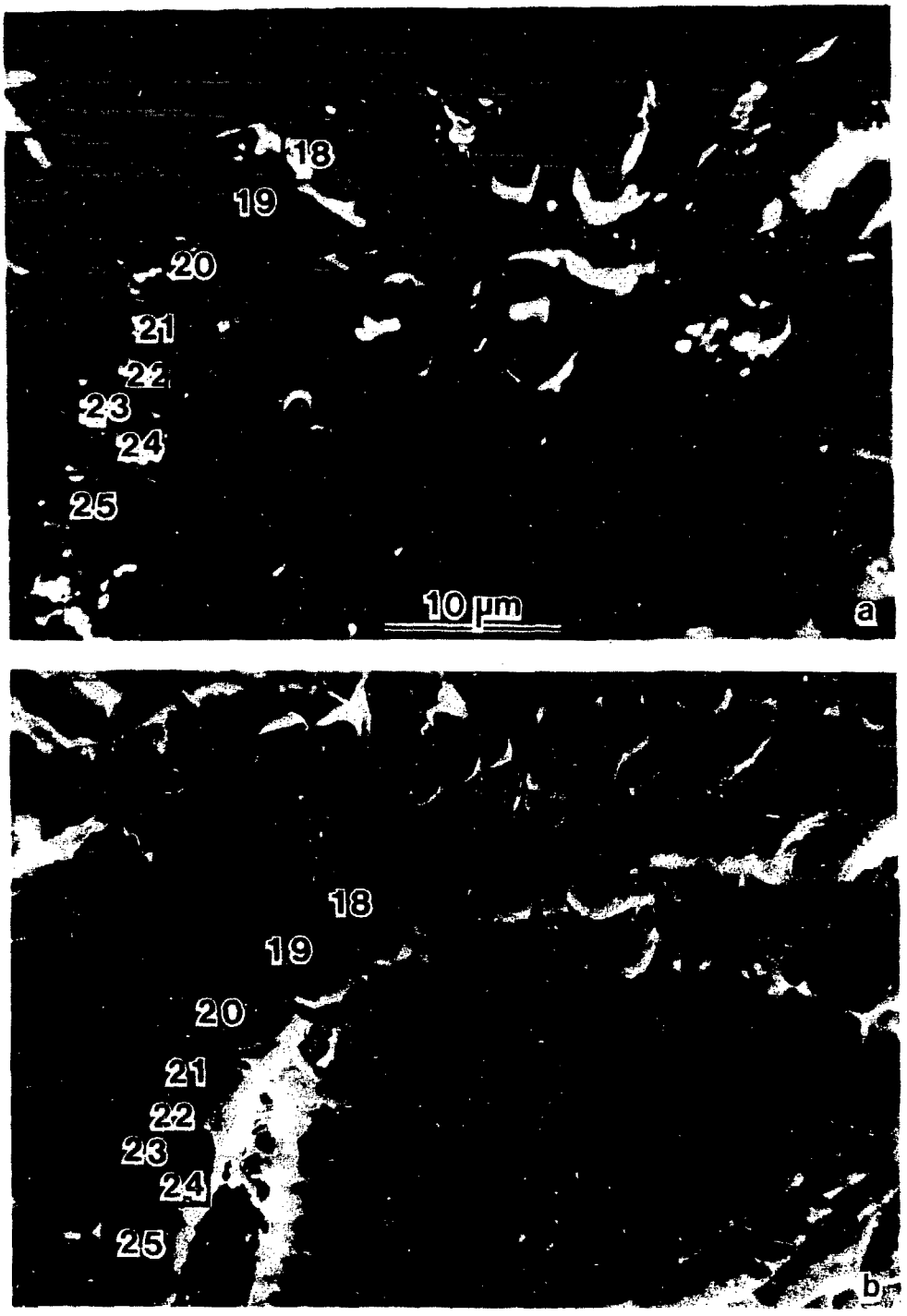

XBB 840-7876

Figure 44. Incompletely dried embryos. The presence of dark charging was typical. The sheath of blastocoel matrix (M) occurred in all embryos containing at least half of their original volume.

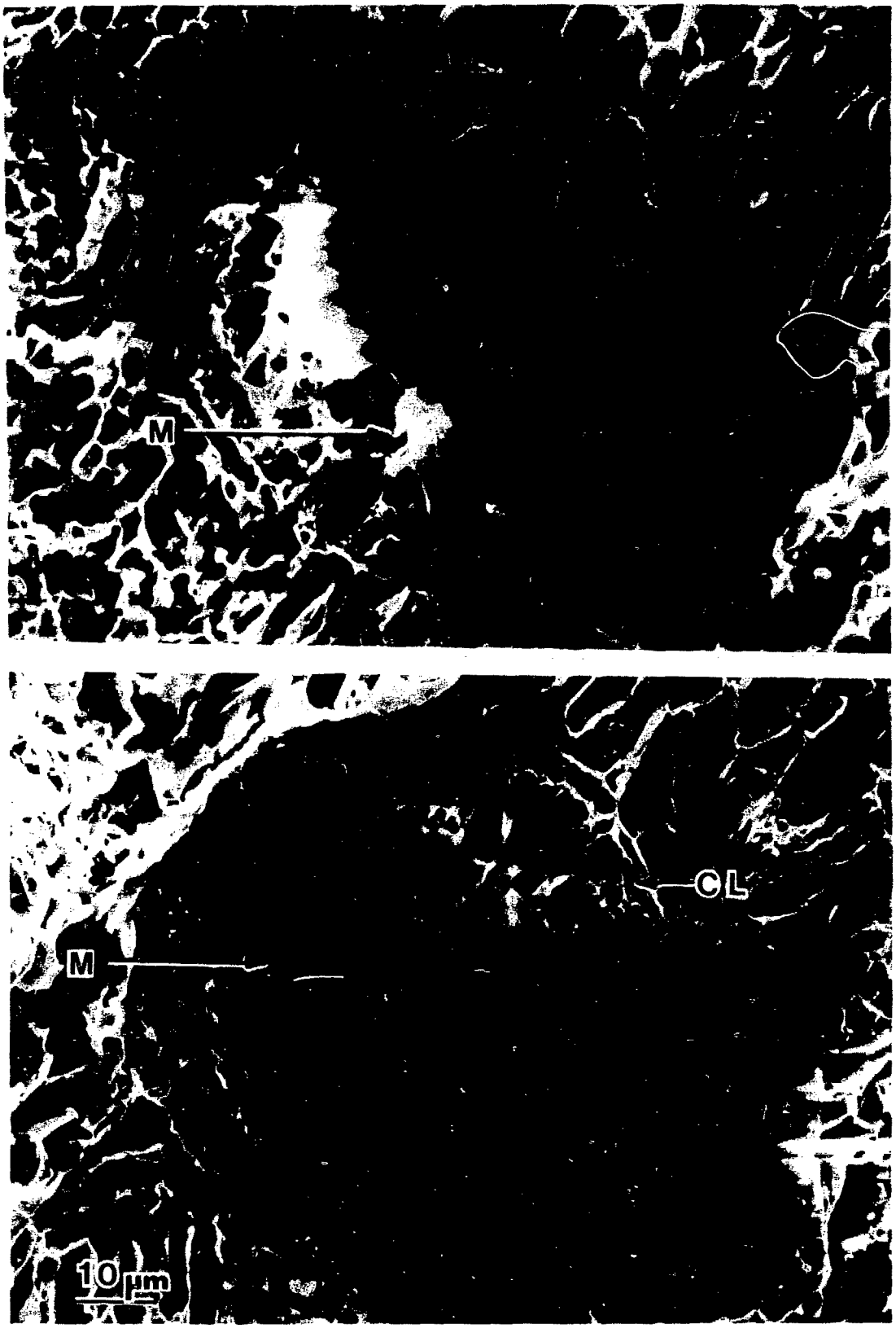

XBB 859-7637

Figure 45. Example of beam damage to the PM cells. The first micrograph (a) shows three PM cells which have been damaged during examination (arrows). The second micrograph (b) shows the subsequent data point (arrow). The interior of the cell has been exposed during analysis.

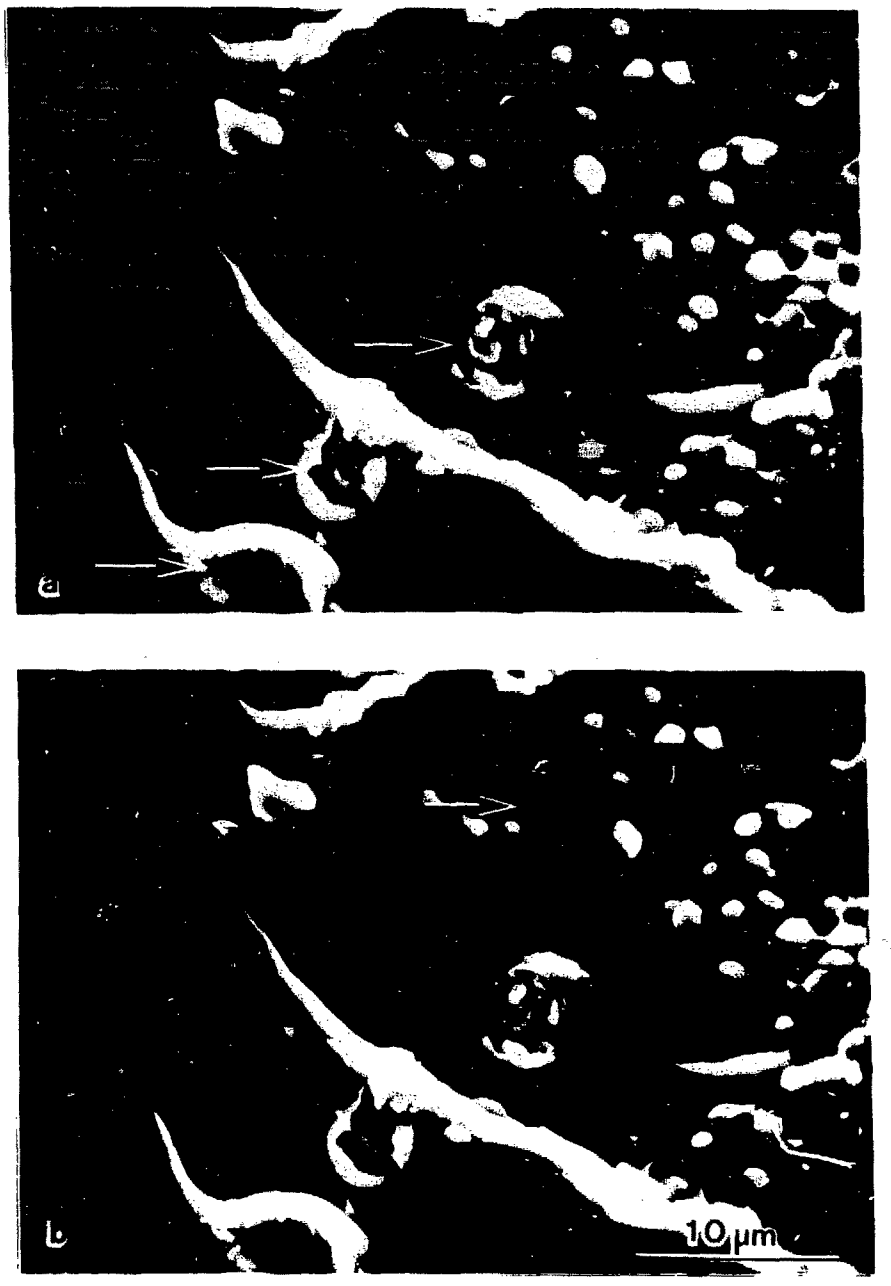

XBB 859-7638

Figure 46. Schematic illustration of electrical fields involved in the charging phenomena experienced in frozen hydrated material. Illustrated are a noncharging specimen (a), a specimen exhibiting increased secondary emission (b), dark charging (c), transient discharge (d), production of high Al P/B ratio (e), and reduced Bremstraahlung.

a.

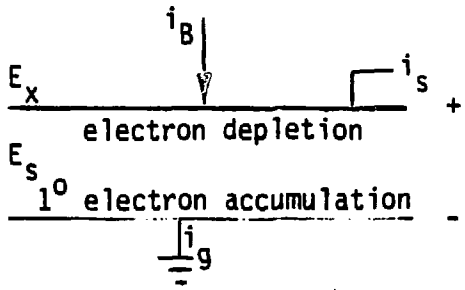

$E_x \simeq 0$

$i_s + i_g = i_B$

Conductor Model

b.

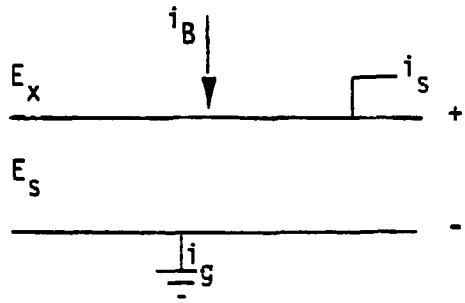

$E_x \geq 0$

$i_s \simeq i_B$

$i_g = \epsilon$

Semiconductor

Bright Charging

c.

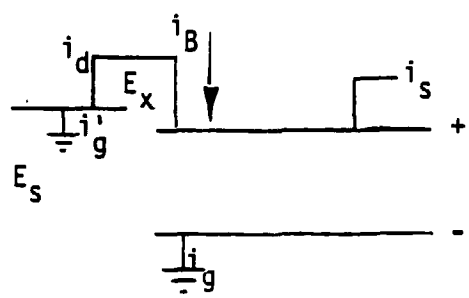

$E_x > 0$

$i_d \simeq i_B$

$i_s \simeq i_g = \epsilon$

Semiconductor

Dark Charging

d.

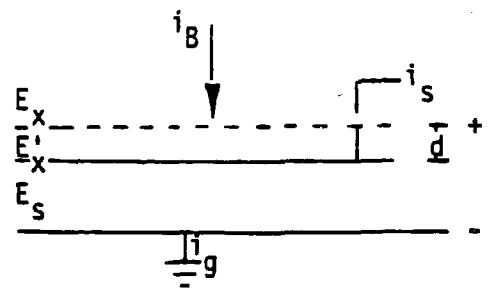

$E_x > 0$

$E'_x < 0$

$i_g = \epsilon$

$d = \epsilon$

Semiconductor

Flashing

e.

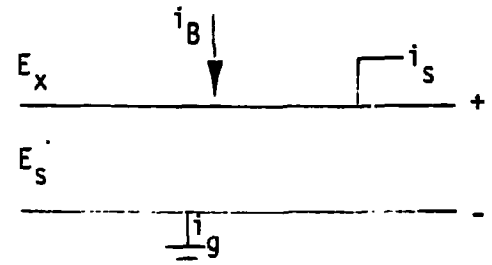

$|E_s| > |E_x|$

$i_g = \epsilon$

Semiconductor

Stray emission

f.

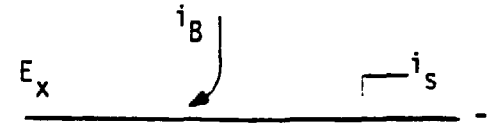

$E_x \gg 0$

Insulator

Beam Deflection

Figure 47. Least squares slope calculation for S from biological standards. Slope = the constant "f." Points represent the means of 20 P/B ratios collected from colloidal suspensions of C and $MgSO_4$.

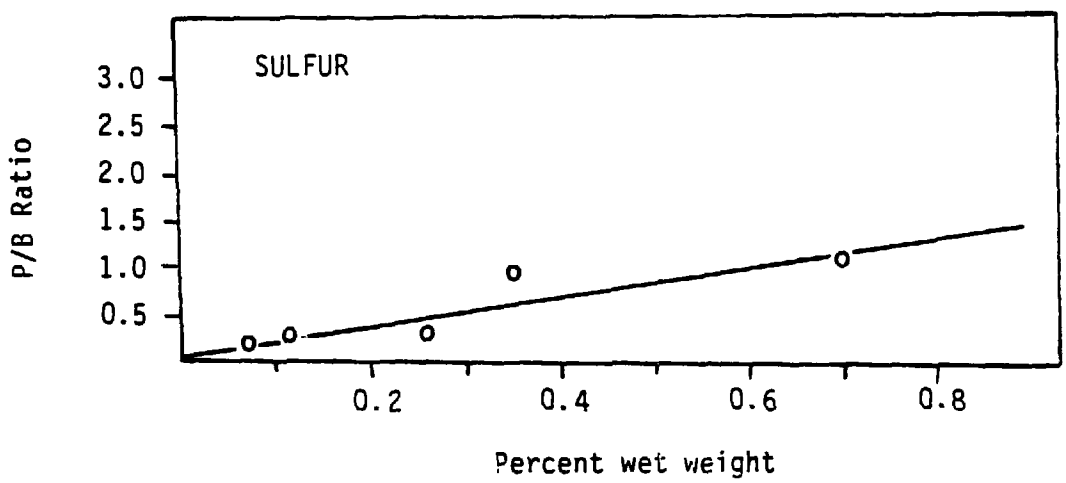
SULFUR
P/B Ratio
3.0
2.5
2.0
1.5
1.0
0.5
0.2
0.4
0.6
0.8
Percent wet weight

Figure 48. Least squares slope calculation for Mg from biological standards. Slope = the constant "f." Points represent the means of 20 P/E ratios collected from colloidal suspensions of C and $MgSO_4$.

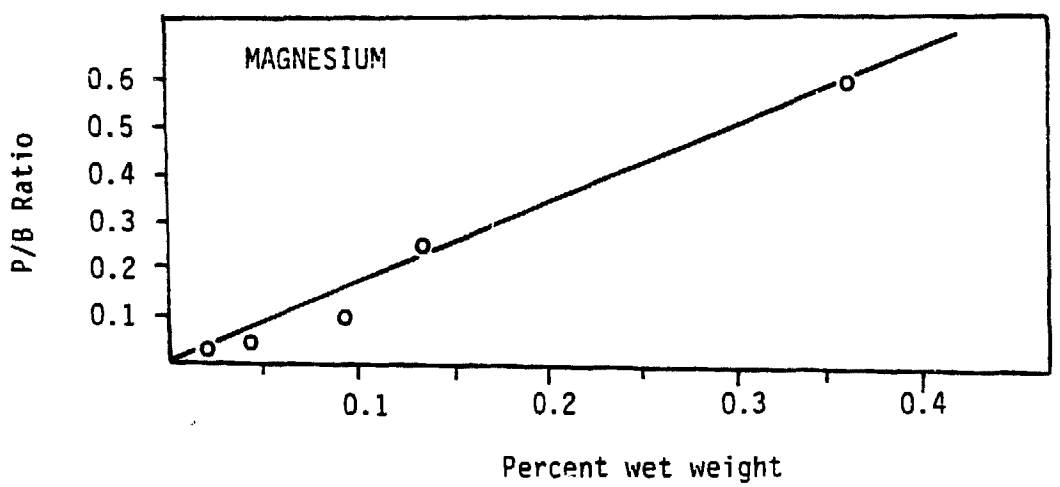
MAGNESIUM
P/B Ratio
0.6
0.5
0.4
0.3
0.2
0.1
0.1
0.2
0.3
0.4
Percent wet weight

Figure 49. Least squares slope calculation for P from biological standards. Slope = the constant "f." Points represent the means of 20 P/B ratios collected from colloidal suspensions of C, HES, and $Mg_3(PO_4)_2$.

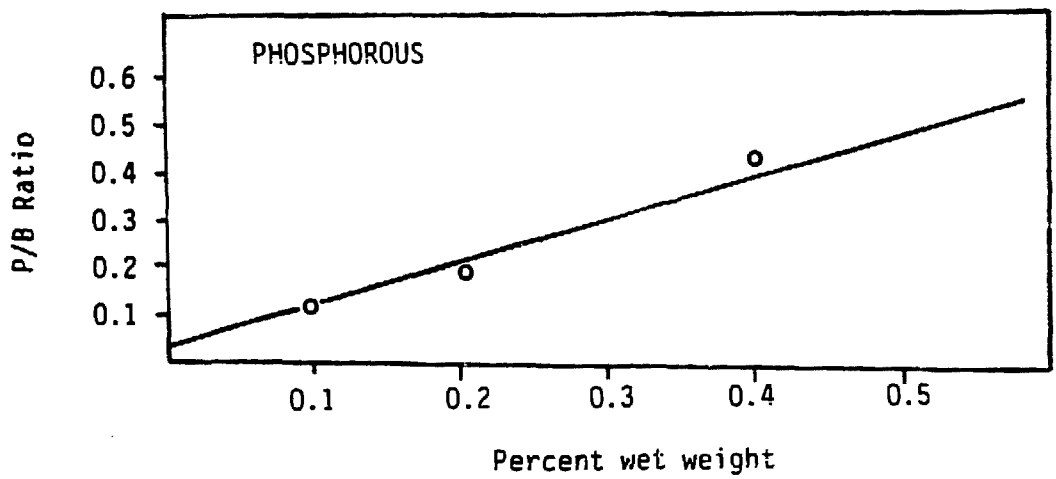
PHOSPHOROUS
P/B Ratio
0.6
0.5
0.4
0.3
0.2
0.1
0.1
0.2
0.3
0.4
0.5
Percent wet weight

Figure 50. Least squares slope calculation for K from biological standards. Slope = the constant "f." Points represent the means of 20 P/B ratios collected from colloidal suspensions of C, HES, and KCl.

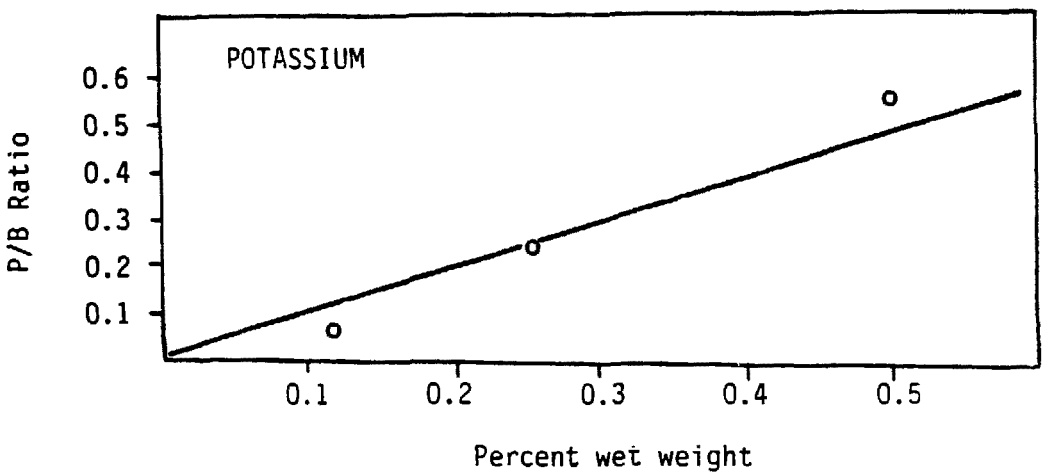
POTASSIUM
P/B Ratio
0.6
0.5
0.4
0.3
0.2
0.1
0.1
0.2
0.3
0.4
0.5
Percent wet weight

Table 1. Comparison of Standard Deviations From Mesenchyme Blastulae.

Data Point(s) - The averaging of all mesenchyme blastulae are denoted "300." The averaging of points within one mesenchyme blastula are denoted by 300 + the number of the embryo.

# of Embryos - A minimum of 3 points were collected for each embryo.

# of Points - Number of samples within the single embryo denoted.

% of $\bar{X}$ - Standard deviation expressed as a percent of the mean P/B.

ELEMENT	DATA POINT(S)	# EMBRYOS	S.D.	% of $\bar{X}$
P	An1C300	6	0.03479	47
S	An1C300	6	0.03070	43
P	An2C300	7	0.02303	48
S	An2C300	7	0.02966	44
P	An1ECM300	7	0.02276	42
S	An1ECM300	7	0.03391	53
		# POINTS		
P	An1C308	3	0.01431	17
S	An1C308	3	0.01928	17
P	An2C304	4	0.00691	10
S	An2C304	4	0.00790	8
P	An1ECM307	3	0.02355	37
S	An1ECM307	3	0.01690	18

Table 2. Correlations Between Various Cell Types Within Stages.

Cell Types - Cell classifications compared.

Correlation - Perfect correlation = 1.000. All correlations greater than 0.300 are listed.

	BLASTULAE		MESENCHYME BLASTULAE		GASTRULAE	
ELEMENT	CELL TYPES	CORRELATION	CELL TYPES	CORRELATION	CELL TYPES	CORRELATION
P	An1/Veg1	0.616	An1/Veg1	0.720	An1/PM	0.930
	An2/Veg2	0.393	Veg1/Veg2	0.658	An2/Veg1	0.511
			An1/Veg2	0.562		
S	Veg1/PM	0.411	Veg1/Veg2	0.705	An1/PM	0.930
			An1/Veg2	0.574	An2/Veg1	0.511
			An1/Veg1	0.548		
K	An1/PM	0.872	Veg1/Veg2	0.859	An1/PM	0.897
			An1/Veg2	0.591	An2/Veg1	0.577
			An1/Veg1	0.554	Veg2/PM	0.316
Ca	An1/Veg1	0.584	An1/Veg2	0.459	An2/PM	0.408
Mg	Veg2/PM	0.827	Veg2/PM	0.794		

Table 3. Conversion of the P/B Ratios to Concentration.

f Factor - Conversion factor derived from standards of known concentration.

P/B Ratio - errors = 12% of the ratio to represent maximum possible error due to topography.

Concentration - Errors = 12% of the concentration to represent maximum possible error due to topography.

ELEMENT	f FACTOR	CELL TYPE	P/B RATIO	% WET WEIGHT
Mg	1.75	B An1	0.035 ± 0.004	0.061 ± 0.007
		B Veg2	0.008 ± 0.001	0.014 ± 0.002
		B PM	0.030 ± 0.004	0.053 ± 0.006
		MB An1	0.020 ± 0.002	0.035 ± 0.004
		MB An2	0.012 ± 0.001	0.021 ± 0.003
		MB Veg1	0.004 ± 0.001	0.007 ± 0.001
		MB Veg2	0.011 ± 0.001	0.019 ± 0.002
		MB PM	0.001 ± 0.000	0.002 ± 0.000
		EG An1	0.014 ± 0.002	0.025 ± 0.003
		EG An2	0.007 ± 0.001	0.012 ± 0.001
		EG Veg1	0.013 ± 0.002	0.023 ± 0.003
		EG Veg2	0.010 ± 0.001	0.018 ± 0.002
		EG PM	0.019 ± 0.002	0.033 ± 0.004
P	1.04	B An1	0.022 ± 0.003	0.023 ± 0.003
		B Veg2	0.045 ± 0.005	0.047 ± 0.006
		B PM	0.053 ± 0.006	0.055 ± 0.007
		MB An1	0.073 ± 0.009	0.076 ± 0.009
		MB An2	0.048 ± 0.006	0.050 ± 0.006
		MB Veg1	0.056 ± 0.007	0.058 ± 0.007
		MB Veg2	0.052 ± 0.006	0.054 ± 0.006
		MB PM	0.032 ± 0.004	0.033 ± 0.004
		EG An1	0.065 ± 0.008	0.068 ± 0.008
		EG An2	0.071 ± 0.008	0.074 ± 0.009
		EG Veg1	0.075 ± 0.009	0.078 ± 0.009
		EG Veg2	0.060 ± 0.007	0.067 ± 0.007
		EG PM	0.058 ± 0.007	0.060 ± 0.007

ELEMENT	f FACTOR	CELL TYPE	P/B RATIO	% WET WEIGHT
S	1.68	B An1	0.029 ± 0.003	0.049 ± 0.006
		B Veg2	0.086 ± 0.010	0.114 ± 0.017
		B PM	0.095 ± 0.011	0.160 ± 0.019
		MB An1	0.071 ± 0.008	0.119 ± 0.014
		MB An2	0.067 ± 0.008	0.113 ± 0.014
		MB Veg1	0.074 ± 0.009	0.124 ± 0.015
		MB Veg2	0.060 ± 0.007	0.101 ± 0.012
		MB PM	0.021 ± 0.003	0.035 ± 0.004
		EG An1	0.063 ± 0.008	0.106 ± 0.013
		EG An2	0.070 ± 0.008	0.117 ± 0.014
		EG Veg1	0.082 ± 0.010	0.138 ± 0.016
		EG Veg2	0.108 ± 0.013	0.184 ± 0.022
		EG PM	0.052 ± 0.006	0.087 ± 0.010
K	1.29	B An1	0.088 ± 0.011	0.113 ± 0.014
		B Veg2	0.144 ± 0.017	0.186 ± 0.022
		B PM	0.077 ± 0.009	0.099 ± 0.012
		MB An1	0.206 ± 0.025	0.266 ± 0.032
		MB An2	0.180 ± 0.022	0.232 ± 0.028
		MB Veg1	0.219 ± 0.026	0.283 ± 0.034
		MB Veg2	0.188 ± 0.023	0.246 ± 0.295
		MB PM	0.139 ± 0.017	0.179 ± 0.021
		EG An1	0.165 ± 0.020	0.213 ± 0.026
		EG An2	0.198 ± 0.024	0.255 ± 0.031
		EG Veg1	0.241 ± 0.029	0.311 ± 0.037
		EG Veg2	0.252 ± 0.030	0.325 ± 0.039
		EG PM	0.227 ± 0.027	0.293 ± 0.035

REFERENCES

1. Agrell, I., "A Mitotic Gradient in Sea Urchin Embryo During Gastrulation," Arkiv. Zool. 6: 213-217, 1953.

2. Akasaka, K., Amemiya, S., Terayama, H., "Scanning Electron Microscopical Study of the Inside of Sea Urchin Embryos (Pseudocentrotus depressus)," Exp. Cell Res. 129: 1-13, 1980.

3. Akasaka, K., Terayama, H., "General Pattern, $^{35}SO_4$ Incorporation and Intracellular Localization of Glycans in Developing Sea Urchin (Anthocidaris) Embryos," Develop. Growth Differentiation 22: 749-762, 1980.

4. Akasaka, K., Terayama, H., "A Proteoglycan Fraction Isolated from the EDTA Extract of Sea Urchin (Hemicentrotus pulcherrimus) Gastrulae Stimulates Reaggrigation of Dissociated Embryonic Cells," Exp. Cell Res. 150: 226-233, 1984.

5. Altura, B.M., Altura, "Magnesium Ions and Contraction of Vascular Smooth Muscle: Relationship to Some Vascular Diseases," Fed. Proc. 40: 2672-2679, 1981.

6. Anderson, C.A., Hasler, M.F., "Extension of Electron Microprobe Techniques to Biochemistry by the Use of Long Wavelength X-ray," Proc. 4th Int. Congr. X-ray Optics and Microanalysis. Castaing, R., Deschampes, P., Philibert, J., eds. Herman, Paris, 310, 1966.

7. Balk, S.D., Polimeni, P.I., Hoon, B.S., LeStourgeon, D.N., Mitchell, R.S., "Proliferation of Rous Sarcoma Virus-Infected, but not of Normal, Chicken Fibroblasts in a Medium of Reduced Calcium and Magnesium Concentration," Proc. Natl. Acad. Sci. 76: 3913-3916, 1979.

8. Barnard, T., "Ultrastructure Effects of High Molecular Weight Cryoprotectants Dextran and Polyvinylpyrrolidone on Liver and Adipose Tissue," J. Microsc. 120: 93-104, 1980.

9. Bastacky, S.J., Hayes, T.L., von Schmidt, B., Klein, S.B., Barr, J., Finch, G.L., McCoon, M., Baskin, L., Hook, G.R., "Correlative Microscopy of Native Surfaces of Human Lung: Color Macrography, SEM, LM, TEM, HVEM, and Low Temperature Scanning Electron Microscopy," in Proc. 41st Annual Meeting EMSA, pp. 500-503, San Francisco Press, S. F., 1983. 10. Becker, F.F., ed, Cancer: A Comprehensive Treatsie, Plenum Press, N.Y., 1975.

11. Beckett, A., Porter, R., Read, N.D., "Low Temperature Scanning Electron Microscopy of Fungal Material," J. Microsc. 125: 193-200, 1982.

12. Bedard, P., Brandhorst, B.P., "Patterns of Protein Synthesis and Metabolism During Sea Urchin Embryogenesis," Dev. Biol. 96: 74-83, 1983.

13. Boekstein, A., "Quantitative Proceedures in X-ray Microanalysis of Biological Bulk Specimens," Proc. 3rd International Low Temperature Biological Microscopy and X-ray Microanalysis Meeting, RMS, 20: 8, 1985.

14. Bissell, M.J., Hall, H.G., Parry, G., "How Does the Extracellular Matrix Direct Gene Expression?," J. Theor. Biol. 99: 31-68, 1982.

15. Boekestein, A., van Kerkhof-Peters, E., Stadhouders, A.M., "The Use of Peak to Background Ratios in the Electron Probe X-ray Microanalysis of Biological Specimens," Proc. 9th Int. Conf. X-ray Optics and Microanalysis EUREM 80. Brederoo, P., Coslett, V.E., eds. Elsevier, N. Holland, 1980.

16. Bridges, K., Levenson, R., Housman, D., Cantley, L., "Calcium Regulates the Committment of Murine Erythroleukemia Cells to Terminal Erythroid Differentiation," J. Cell biol. 90: 542-544, 1981.

17. Brombach, J.D., "Electron Beam X-ray Microanalysis of Frozen Biological Bulk Specimens Below 130K, II. The Electrical Charging of the Sample in Quantitative Analysis," J. Microscopie Biol. Cell 22: 233, 1975.

18. Brooker, G., Harper, J.F., Terasaki, W.L., Moylan, R.D., "Radioimmunoassay of Cyclic AMP and Cyclic GMP," Adv. Cycl. Nucl. Res. 10: 1-33, 1979.

19. Bullock, G.R., Wilson, A.J., Harris, T.S., Robards, A.W., Manning, A.S., "Applications of Low Temperature Scanning Electron Microscopy to the Study of Ischaemic Heart," Proc. Roy. Microsc. Soc. 15: 18-19, 1980.

20. Carr, K.E., Hayes, T.L., McKoon, M.M., Sprague, M., Bastacky, S.J., "Low Temperature Scanning Electron Microscope Studies of Mouse Small Intestine," J. Microsc. 132: 209-217, 1983.

21. Carr, K.E., Hayes, T.L., Watt, A., Bastacky, S.J., Klein, S., Fife, M., "Specimen Handling and Data Interpretation in X-ray Microanalysis of Frozen Hydrated Etched Gastrointestinal Tract," submitted, J. Microsc. Tech., 1985.

22. Carr, K.E., Hayes, T.L., Watt, A., Klein, S., McKoon, M., Bastacky, S.J., Ellis, S., "Biological Variation in Cryo Microanalytical Data from Mouse Small Intestinal Villi," submitted, J. Microsc. Tech., 1985.

23. Cheung, W.Y., Calcium and Cell Function, Academic Press, N.Y., 1980.

24. Culp, L.A., Murray, B.A., Rollins, B.J., "Fibronectin and Proteoglycans as Determinants of Cell-Substratum Adhesion," J. Supramol.Struct. 11: 401-427, 1979.

25. Dan, K., "Cyto-Embryology of Echinoderms and Amphibia," Int. Rev. Cytol. 9: 321-367, 1960.

26. David, G., Bernfield, M.R., "Collagen Reduces GAG Degradation by Cultured Mammary Epithelial Cells: Possible Mechanism for Basal Lamina Formation," Proc. Natl. Acad. Sci. 76: 786-790, 1979.

27. Dorge, A., Rick, R., Gehring, K., Mason, J., Thurau, K., "Preparation and Applicability of Freeze-Dried Sections in the Microprobe Analyser of Biological Soft Tissue," J. Microsc. Biol. Cell 22: 205, 1975.

28. Dubochet, J., Lepault, J., Freeman, R., Berriman, J.A., Homo J.-C., "Electron Microscopy of Frozen Water and Aqueous Solutions," J. Microsc. 128: 219-238, 1982.

29. Echlin, P.E., "Low Temperature Scanning Electron Microscopy: A Review," J. Microsc. 112: 47-61, 1978.

30. Echlin, P., Burgess, A., "Cryofracturing and Low Temperature Microscopy of Plant Material," Proc. 10th Annual IITRI-SEM Symp. 1: 491, 1977.

31. Echlin, P., Hayes, T.L., McKoon, M., "Analytical Procedures for Bulk Frozen-Hydrated Biological Tissues," in Microbeam Analysis, Gooley, R., ed. San Francisco Press, S.F., 243-246, 1983.

32. Echlin, P., Lai, C.E., Hayes, T.L., "Low Temperature X-ray Microanalysis of the Differentiating Vascular Tissue in root Tips of Lemna minor L," J. Microsc. 126: 285-306, 1982.

33. Echlin, P.E., Pawley, J.B., Hayes, T.L., "Freeze Fracture SEM of Lemna minor L (Duckweed)," S.E.M. 1979/III, 69-76, 1979.

34. Echlin, P., Taylor, S.E., "Procedures for the Quantitative X-ray Microanalysis of Bulk Frozen Hydrated Plant Tissue," Proc. RMS 20: 8, 1985.

35. Ettensohn, C.A., "Primary Invagination of Vegetal Plate During Sea Urchin Gastrulation," Am. Zool. 24:571-588, 1984.

36. Everhart, T.E., "Reflections on Scanning Electron Microscopy," in Scanning Electron Microscopy, Johari, O., ed. ITT Research Institute, Chicago, IL, 3-12, 1968.

37. Everhart, T.E., Hayes, T.L., "The Scanning Electron Microscope," Sci. Amer. 226: 54-69, 1972.

38. Fibbi, G., Vannucci, S., Cavallini, P., Del Rosso, M., Pasquali, F., Cappelletti, R., Chiarugi, V., "Involvement of Chondroitin Sulfate in Preventing Adhesive Cellular Interactions," Biochim. Biophys. Acta. 762: 512-518, 1983.

39. Finch, G.L., "Electron Microscope Investigations of Lung Cell Response to Particulate Insult," Ph.D. Thesis: LBL-17218, 1984.

40. Fuchs, W., Brombach, J.D., Trosch, W., "Charging Effect in Electron Irradiated Ice," J. Microsc. 112: 63-74, 1978.

41. Fuchs, W., Fuchs, H., "The Use of Frozen Hydrated Bulk Specimens for X-ray Microanalysis," Scanning Electron Microsc. 1980/II: 371-382, 1980.

42. Fuchs, W., Lindermann, B., "Electron Beam X-ray Microanalysis of Frozen Biological Bulk Specimens Below 130K, I. Instrumentation and Specimen Preparation," J. Microsc. Biol. Cell 22: 227, 1975.

43. Furukawa, K., Bhavanandan, V.P., "Influences of Polysaccharides on DNA Synthesis in Isolated Nuclei and by DNA Polymerase α: Correlation of Observed Effects with Properties of the Polysaccharides," Biochim. Biophys. Acta. 740: 466-475, 1983.

44. Gardner, D.L., Oates, K., O'Connor, P., "Surface Structure of Mammalian Articular Cartilage: An Investigation by Low Temperature Scanning Electron Microscopy," Clin. Sci. 58: 31, 1979.

45. Gibbins, J.R., Tilney, L.G., Porter, K.R., "Microtubules in the Formation and Development of the Primary Mesenchyme in Arbacta punctulata, I. The Distribution of Microtubules," J. Cell Biol. 41: 201-226, 1969.

46. Glaeser, R.M., Taylor, K.A., "Radiation Damage Relative to Transmission Electron Microscopy of Biological Specimens at Low Temperature: A Review," J. Microsc. 112: 127-138, 1978.

47. Goldstein, J.I., Newbury, D.E., Echlin, P.E., Joy, D.C., Fiori, C., Lifshin, E., Scanning Electron Microscopy and X-Ray Microanalysis, Plenum Press, N.Y., 1981.

48. Grinnell, F., "Cellular Adhesiveness and Extracellular Substrata," Int. Rev. Cytol. 53: 64-144, 1978.

49. Gufstafson, T., Wolpert, L., "Cellular Movements and Contact in Sea Urchin Morphogenesis," Biol. Rev. 42: 442-498, 1967.

50. Gullasch, J., Kaufmann, R., "Energy Dispersive X-ray Microanalysis in Soft Biological Tissue: Relevance and Reproduciility of the Results as Depending on Specimen Preparation (Air Drying, Cryofixation, and Cool Stage Techniques)", in Microprobe Analysis as Applied to Cells and Tissues, Hall, T.A., Echlin, P., Kaufmann, R., eds., Academic Press, London, 1974.

51. Gupta, B.L., Hall, T.A., "The X-ray Microanalysis of Frozen-Hydrated Sections in Scanning Electron Microscopy: An Evaluation," Tissue and Cell 13: 623-643, 1981.

52. Gupta, B.L., Hall, T.A., Madrell, S.M.P., Moreton, R.B., "Distribution of Ions in a Fluid Transporting Epithelium Determined by Electron-Probe X-ray Microanalysis," Nature 264: 284-287, 1976.

53. Hall, T.A., Gupta, B.L., "Beam-Induced Loss of Organic Mass Under Electron-Microprobe Conditions," J. Microsc. 100: 177-188, 1973.

54. Harkey, M.A., Whiteley, A.H., "Isolation, Culture, and Differentiation of Echinoid Primary Mesenchyme Cells," Roux's Arch. Dev. Biol. 189: 111-122, 1980.

55. Hascall, V.C., Hascall, G.K., "Proteoglycans" in Cell Biology of Extracellualr Matrix, Hay, E.D., ed. Plenum Press, N.Y., 1981.

56. Hay, E.D., ed. Cell Biology of Extracellular Matrix, Plenum Press, N.Y., 1981.

57. Hayes, T.L., "Biophysical Aspects of Scanning Electron Microscopy, " S.E.M. 1980/I,: 1-10, 1980.

58. Heinrich, K.F.J., "Interrelationships of Sample Composition, Backscatter Coefficient, and Target Current Measurement," in Advances in X-ray Analysis, Proc. Twelfth Annual Conferences on Application of X-ray Analysis, Mueller, Mallett and Fay eds., pp. 325-339, Plenum Press, N.Y., 1963.

59. Hennings, H., Michael, D., Cheng, C., Steinert, P., Holbrook, K., Yuspa, S.H., "Calcium Regulation of Growth and Differentiation of Mouse Epidermal Cells in Culture," Cell 19: 245-254, 1980.

60. Hess, F.D., "Influence of Specimen Topography on Microanalysis," in X-ray Microanalysis in Biology, Hayat, M.A., ed. University Press, Baltimore, 1980.

61. Hobbs, P.V., Ice Physics, Clarendon Press, Oxford, 1974.

62. Hook, G., Lai, C., Bastacky, S.J., Hayes, T.L., "Conductive Coatings Studied on Inflated Lung in the Frozen Hydrated and Freeze Dried States," S.E.M. 1980/IV,: 27-32, 1980.

63. Horstadius, S., "The Mechanics of Sea Urchin Development, Studies By Operative Methods," Biol. Rev. 14: 132-179, 1939.

64. Inoue, S., "Cell Division and the Mitotic Spindle," J. Cell Biol. 91: 131s-147s, 1981.

65. Inoue, S., Okazaki, K., " Biocrystals," Sci. Amer. 236: 83-92, 1977.

66. Iwanczyk, J.S., Dabrowski, A.J., Hurth, G.C., Bradley, J.G., Conely, J.M. Albee, A.L., "First Use of Mercuric Iodide (HgI_2) Energy Dispersive X-ray Detector in a Scanning Electron Microscope," S.E.M. 1984/I: 9-14, 1984.

67. Iwata, M., Nakano, E., "Characterization of Sea Urchin Fibronectin," Biochem. J. 215: 205-208, 1983.

68. Iwata, M., Nakano, E., "Cell-to-Substratum Adhesion of Dissociated Emryonic Cells of the Sea Urchin Pseudocentrotus depressus," Roux's Arch. Dev. Biol. 193: 71-77, 1984.

69. Johnson, J.D., Epel, D., Paul, M., "Intracellular pH and Activation of Sea Urchin Eggs After Fertilization," Nature 262: 661-664, 1976.

70. Karp, G.C., Solursh, M., "Acid Mucopolysaccharide Metabolism, the Cell Surface and Primary Mesenchyme Cell Activity in the Sea Urchin Embryo," Dev. Biol. 41: 110-123, 1974.

71. Katow, H., Solursh, M., "Ultrastructure of Blastocoel Material in Blastulae and Gastrulae of the Sea Urchin Lytechinus pictus," J. Exp. Zool. 210: 561-567, 1979.

72. Katow, H., Solursh, M., "Ultrastructural and Time Lapse Studies of Primary Mesenchyme Cell Behavior in Normal and Sulfate Deprived Sea Urchin Embryos," Exp. Cell Res. 136: 233-245, 1981.

73. Katow, H., Solursh, M., "In Situ Distribution of Concanavalin A-Binding Sites in Mesnechyme Blastulae and Early Gastrulae of the Sea Urchin Lytechinus pictus," Exp. Cell Res. 139: 171-180, 1982.

74. Katow, H., Yamada, K.M., Solursh, M., "Occurrence of Fibronectin on the Primary Mesenchyme Cell Surface During Migration in the Sea Urchin Embryo," Differentiation 22: 120-124, 1982.

75. Kawabe, T.T., Armstrong, P.B., Pollock, E.G., "An Extracellular Fibrillar Matrix in Gastrulating Sea Urchin Embryos," Dev. Biol. 85: 509-515, 1981.

76. Kinoshita, S., Saiga, H., "The Role of Proteoglycan in the Development of Sea Urchins, I. Abnormal Development of Sea Urchin Embryos Caused by the Disturbance of Proteoglycan Synthesis," Exp. Cell Res. 123: 229-236, 1979.

77. Kinoshita, S., Yoshii, K., "The Role of Proteoglycan Synthesis in the Development of Sea Urchins, II. The Effect of Administration of Exogenous Proteoglycan," Exp. Cell Res. 124: 361-369, 1979.

78. Kleinman, H.K., Kleve, R.I., Martin, G.R., "Role of Collagenous Matrices in the Adhesion and Growth of Cells," J. Cell Biol. 88: 473-485, 1981.

79. Koch, G.R., "Preparation and Examination of Specimens at Low Temperatures," in Principles and Techniques of Scanning Electron Microscopy. Biological Applications, Vol. 4, Hayat, M.A., ed., Van Nostrand, N.Y., 1975.

80. Koch, K.S., Leffert, H.L., "Increased Sodium Ion Influx is Necessary to Initiate Rat Hepatocyte Proliferation," Cell 18: 153-163, 1979.

81. Kramer, R.H., Vogel, K.G., Nicholson, G.L., "Solubilization and Degredation of Subendothelial Matrix Glycoproteins and Proteoglycans by Metastatic Tumor Cells," J. Biol. Chem. 257: 2678-2686, 1982.

82. Kuijpers, G.A.J., Roomans, G.M., Effects of Polymeric Cryoprotectant Dextran on Fluid Secretion in the Isolated Rabbit Pancreas," J. Micros. 129 141-146, 1983.

83. Kujawa, M.J., Tepperman, K., "Culturing Chick Muscle Cells on Glycosaminoglycan Substrates: Attachment and Differentiation," Dev. Biol. 99: 277-286, 1983.

84. Kurth, R., Steymann, J., Tanaka, T., Lower, J., Frank, H. "Phosphorylating Proteins as Effectors in Malignant Cell Transformation" Adv. Cycl. Nucl. Res. 14: 443-462, 1981.

85. Lai, C.E., Hayes, T.L., "Calibration of SEM, Frozen-Hydrated Analyses Using Standard Salt Solutions and Peak to Background Measurements," Proc. 38th Ann. EMSA Meeting, San Francisco Press, San Francisco, 800, 1980.

86. Laterra, J., Silbert, J.E., Culp, L.A., "Cell Surface Heparin Sulfate Mediates Some Adhesive Responses to Glycosamino Binding Matrices, Including Fibronectin," J. Cell Biol. 96: 112-123, 1983.

87. Levenson, R., Housman, D., Cantley, L., "Amiloride Inhibits Murine Erythroleukemia Cell Differentiation: Evidence for a Ca^{2+} Requirement for Commitment," Proc. Natl. Acad. Sci. 77: 5948-5952, 1980.

88. Lewis, E.R., Pawley, J.B., "S.E.M. Freeze Fracture Studies of the Otoconial Membrane of the Frog Lagena," S.E.M. 1979/III, 955-962, 1979.

89. Marshall, A.T., "X-ray Microanalysis of Frozen Hydrated Biological Specimens: the Effect of Charging," Micron. 5: 275-280, 1975.

90. Marshall, A.T., "Frozen Hydrated Bulk Specimens," in X-ray Microanalysis in Biology, Hayat, M.A., ed., University Park Press, Baltimore, 1979.

91. Marshall, A.T., "Simultaneous Use of EDS, Windowless EDS, BE and SE Detectors and Digital Realtime Line Scanning for the X-ray Microanalysis of Frozen Hydrated Specimens," S.E.M. 2: 327-328, 1981.

92. Marshall, A.T., Carde, D., "Beryllium Coating For Biological X-ray Microanalysis," J. Microsc. 134: 113-116, 1984.

93. McCarthy, R.A., Spiegel, M., "Serum Effects on the In Vivo Differentiation of Sea Urchin Micromeres," Exp. Cell Res. 149: 433-441, 1983a.

94. McCarthy, R.A. Speigel, M., "Protein Composition of the Hyalin Layer of Sea Urchin Embryos and Reaggregating Cells," Cell Differ. 13: 93-102, 1983b.

95. McKay, K.G., in Advances in Electronics, Marton, L., ed., Academic Press Inc., New York, 1948.

96. Mendoza, S.A., Wigglesworth, N.M., Pohjanpelto, P., Rozengurt, E., "Na Entry and Na-K Pump Activity in Murine, Hampster, and Human Cells - Effect of Monesin, Serum, Platelet Extract, and Viral Transformation," J. Cell Physiol. 103: 17-27, 1980.

97. Mendoza, A.A., Wiggleswoth, N.M., Rozengurt, E., "Vasopressin Rapidly Stimulates Na Entry and Na-K Pump Activity in Quiescent Cultures of Mouse 3T3 Cells," J. Cell Physiol. 105: 153-162, 1980.

98. Metcalf, J.C., Pozzan, T., Smith, G.A., Hesketh, T.R., "A Calcium Hypothesis for the Control of Cell Growth," Biochem. Soc. Sym. 45: 1-26, 1980.

99. Mizoguchi, H., Yasumasu, I., "Archenteron Formation Induced by Ascorbate and Alpha-ketogluterate in Sea Urchin Embryos Kept in SO_4^{-2}-free Artificial Sea Water,"

100. Moolenaar, W.H., Mummery, C.L., van der Saag, P.T., de Laat, S.W., "Rapid Ionic Events and the Initiation of Growth in Serum-Stimulated Neuroblastoma Cells," Cell 23: 789-798, 1981.

101. Moore, A.R., Burt, A.S., "On the Locus and Nature of the Forces Causing Gastrulation in the Embryos of Dendraster excentricus" J. Exp. Zool. 82: 159-171.

102. Morishita, V., Akogyeram, C, Deu, B., Criss, W.E., "Regulation of Polyamine Responsive Protein Kinase by Certain Highly Specific Polyamines and Charges Carbohydrates," Biochim. Biophys. Acta. 22;755: 358-362, 1983.

103. Motomura, I., "Secretion of Mucosubstance in the Gastrula of the Sea Urchin Embryo," Bull. Mar. Biol. Asamushi 10: 159-169, 1960.

104. Nathanson, M.A., "Analysis of Cartilage Differentiation from Skeletal Muscle Grown on Bone Matrix III. Environmental Regulation of Glycosaminoglycan and Proteoglycan Synthesis," Dev. Biol. 96: 46-62, 1983.

105. Nei, T., "Cryotechniques," in Principles and Techniques of Scanning Electron Microscopy. Biological Applications, Vol. 1, Hayat, M.A., ed., Van Nostrand, New York, 1975.

106. Niedrig, H., "Physical Background of Backscattering," Scanning, 1: 17-34, 1978.

107. Ohtake, H., Suyemitsu, T., Koga, M., "Sea Urchin (Anthocidaris crassispina) Egg Zink-Binding Protein," Biochem. J. 211: 109-118, 1983.

108. Pawley, J.B., "Charging Artifacts in the Scanning Electron Microscope," S.E.M. 1972/I: 153-159, 1972.

109. Pawley, J.B., Hook, G., Hayes, T.L., Lai, C., "Direct Scanning Electron Microscopy of Frozen Hydrated Yeast," Scanning 3: 219-226, 1980.

110. Pawson, T., Guyden, J., Kung, T., Radke, K., Gilmore, T., Martin, S., "A Strain of Fujinami Sarcoma Virus which is Temperature-Sensitive in Protein Phosphorylation and Cellular Transformation," Cell 22: 767-775, 1980.

111. Perkins, M.E., Ji, T.H., Hynes, R.O., "Crosslinking of Fibronectin and Sulfated Proteoglycans at the Cell Surface," Cell 16: 941-952, 1979.

112. Pihakaski, L., Seveus, L., "High Polymeric Protective Additive in Cryomicrotomy in Plants, I. PVP Infusion of Fixed Plant Tissue," Cryoletters 1: 494, 1980.

113. Rappaport, R., "Reversal of Chemical Cleavage Inhibition in Echinoderm Eggs," J. Exp. Zool., 176: 249-255, 1971.

114. Read, N.D., Porter, R., Beckett, A., "A Comparison of Preparative Techniques for the Examination of the External Morphology of Fungal Material with the Scanning Electron Microscope," Can. J. Bot. 61: 2059-2078, 1983.

115. Reed, S.J.B., Electron Micorprobe Analysis, Cambridge University Press, Cambridge, 1975.

116. Remington, R.D., Schork, M.A., Statistics with Applications to the Biological Sciences, Prentice-Hall, Inc., Englewood Cliffs, New Jersey, 1970.

117. Revel, J., Yip, P., Chang, L.L., "Cell Junctions in Early Chick Embryo - A Freeze Etch Study," Dev. Biol. 35: 302-317, 1973.

118. Robards, A.W., Crosby, P., "A Comprehensive Freezing, Fracturing and Coating System for Low Temperature Scanning Electron Microscopy," Scanning Electron Micros. 2: 325-344, 1979.

119. Roberts, K., Hyams, J.S., Microtubules, Academic Press, New York, 1979.

120. Roff, C.F., Wozniak, R.W., Blenis, J., Wang., J.L., "The Effect of Mannose 6-Phosphate on the Turnover of Cell Surface Glycosaminoglycans," Exlp. Cell Res., 144: 333-344, 1983.

121. Roomans, G.M., "Problems in Quantitative X-ray Microanalysis of Biological Specimens," S.E.M. 1980/II: 309-320, 1980.

122. Rozengurt, E., Gelehrter, T.D., Legg, A., Pettican, P., "Melittin Stimulates Na Entry, Na-K Pump Activity and DNA Synthesis in Quiescent Cultures of Mouse Cells," Cell 23: 781-788, 1981.

123. Saubermann, A.J., "The Application of X-ray Microanalysis in Physiology," J. Microsc. Biol. Cell 22: 401, 1975.

124. Saubermann, A.J., Echlin. P., "The Preparation, Examination and Analysis of Frozen Hydrated Tissue Sections by Scanning Transmission Electron Micrscopy and X-ray Microanalysis," J. Micros., 105: 155-191, 1975.

125. Saubermann, A.J., Riley, W., Echlin, P., "Preparation of Frozen-Hydrated Tissue Sections for X-ray Microanalysis Using a Satelite Vacuum Coating and Transfer System," Proc 10th Ann. IITRI-SEM Symp. 1: 347-000, 1977.

126. Sawyer, S.T., Cohen, S., "Enhancement of Calcium Uptake and Phosphatidylinositol Turnover by Epidermal Growth Factor in A-431 Cells," Biochem. 20: 6280-6286, 1981.

127. Sekiguchi, K., Hakomori, S., Funahashi, M., Matsumoto, I., Seno, N., "Binding of Fibronectin and Its Proteolytic Fragments to Glycosaminoglycans," J. Biol. Chem. 258: 14359-14365, 1983.

128. Shaffner, T.J., Hearle, J.W.S., "Recent Adances in Understanding Specimen Charging," S.E.M. 1976/I: 61-70, 1976.

129. Small, J.A., Heinrich, K.F.J., Newbury, D.E., Myklebust, R.L., "Progress in the Development of the Peak to Background Method for the Quantitative Analysis of Single Particles with the Electron Probe," S.E.M. 1979/II: 807-816, 1979.

130. Solursh, M., Hardingham, T.E., Hascall, V.C., Kimura, J.H., "Separate Effects of Exogenous Haluronic Acid on Proteoglycan Synthesis and Deposition in Pericellular Matrix by Cultured Chick Embryo Limb Chondrocytes," Dev. Biol. 75: 121-129, 1980.

131. Spiegel, E., Burger, M., Spiegel, M., "Fibronectin in the Developing Sea Urchin Embryo," J. Cell Biol. 87: 309-313, 1980.

132. Spiegel, E., Burger, M., Spiegel, M., "Fibronectin and Laminin in the Extracellular Matrix and Basement Membrane of Sea Urchin Embryos," Exp. Cell Res. 144: 47-55, 1983.

133. Statham, P.J., "A Comparative Study of Techniques for Qualitative Analysis of the X-ray Spectra Obtained with a Si(Li) Detector," X-ray Spectrom 5: 16, 1976.

134. Statham, P.J., "Measurement and Use of Peak to Background Ratios in X-ray Microanalysis," Mikrochim. Acta, Suppl. 8: 229, 1979.

135. Statham, P.J., "X-ray Microanalysis with Si(Li) Detectors," J. Microsc. 123: 1-23, 1981.

136. Statham, P.J., Pawley, J.B., "A New Method for Particle X-ray Micro-Analysis Based on Peak to Background Measurements," S.E.M. 1978/I: 469-478, 1978.

137. Steinbrecht, R.A., "Recrystallization and Ice Crystal Growth in a Biological Specimen," Proc. RMS 20: 5-6, 1985.

138. Steinhardt, R.A., Zucker, R., Schatten, G., "Intracellular Calcium Release at Fertilization in the Sea Urchin Egg," Dev. Biol. 58: 185-196, 1977.

139. Sugiyama, K., "Occurrence of Mucopolysaccharides in the Early Development of the Sea Urchin Embryo and Its Role in Gastrulation," Dev. Growth Differ. 14: 63-73, 1972.

140. Takata, K., Yamamoto, K.Y., Ozawa, R., "Use of Lectins as Probes for Analyzing Embryonic Induction," Roux's Archiv. 190: 92-96, 1981.

141. Taylor, S.E., Echlin, P., "Quantitative Low Temperature X-ray Microanalysis of Tobacco Leaf Tissue," Proc. 3rd International Low Temperature Biological Microscopy and X-ray Microanalysis Meeting, RMS 20: 9, 1985.

142. Teng, A.S., Schwarz, R.I., Bissell, M.J., "Collagen Fiber Formation by Isolated Avian Tendon Cells in Culture," J. Cell Biol. 75: 156a, 1977.

143. Tilney, L.G., Gibbins, J.R., "Microtubules in the Formation and Development of the Primary Mesenchyme in Arbacta punctulata, II. an Experimental Analysis of Their Role in Development and Maintenance of Cell Shape," J. Cell Biol. 41: 227-250, 1969.

144. Toole, B.P., "Glycosaminoglycans in Morphogenesis" in Cell Biology of Extracellular Matrix, Hay, E.D., ed., Plenum Press, N.Y., 1981.

145. Van Veld, R.D., Shaffner, T.J., "Charging Effects" in Scanning Electron Microscopy, Johari, O., ed., ITT Research Institute, Chicago, IL, 17-24, 1971.

146. Weeds, A., "Actin Binding Proteins - Regulators of Cell Architecture and Motility," Nature 296: 811-816, 1981.

147. Weitzenkamp, L.A., "Measurement of Fibre Potentials in a Scanning Electron Microscope," J. Phys. E: Sci. Instrum. 2: 561-564, 1969.

148. Wells, O., Scanning Electron Microscopy, McGraw-Hill, N.Y., 1974.

149. Whitecross, M.I., Price, G.D., Preston, J.S., "Use of Colloidal Graphite in Frozen Hydrated Standard Solutions for X-ray Microanalysis," J. Microsc. 128: RP3-RP4, 1982.

150. Winkler, M.M., Steinhardt, R.A., Grainger, J.L, Minning, L., "Dual Ionic Controls for the Activation of Protein Synthesis at Fertilization," Nature 287: 558-559, 1980.

151. Yamada, K.M., Kennedy, D.W., Kiwata, K., Pratt, R.M., "Characterization of Fibronectin Interactions with Glycosaminoglycans and Identification of Active Proteolytic Fragments," 255: 6055-6063, 1980.